POLITECNICO DI MILANO
School of Industrial and Information Engineering
Master of Science Degree in Mechanical Engineering

A STUDY ON MONITORING FATIGUE CRACK PROPAGATION BY SOURCE LOCALIZATION OF ACOUSTIC EMISSION EVENTS

Dipartimento di Meccanica del Politecnico di Milano

Supervisor: Prof. Michele CARBONI

Candidate:
Stefano Milan, matr. 899883

Academic Year 2018-2019

A chi ha dedicato la propria vita alla ricerca

Ringraziamenti

Ringrazio il Prof. Carboni per avermi dato l'opportunità di svolgere questo lavoro di tesi con lui, facendomi da guida e dandomi la possibilità di apprendere molto dalla sua esperienza.

Ringrazio i miei genitori per avermi dato l'opportunità di studiare al Politecnico di Milano, sostenendomi in ogni momento.

Ringrazio i miei compagni di corso con i quali ho condiviso molte fatiche e hanno saputo alleggerire i periodi più critici.

Ringrazio i tecnici del C4, sono sempre stati disponibili e pazienti, soddisfando tutte le mie esigenze pratiche per condurre questo lavoro.

Ringrazio tutte le persone, sia quelle che ho visto spesso sia quelle che sono riuscito a vedere un po' meno, che hanno saputo regalarmi un sorriso nei momenti più difficili.

Contents

List of Figures

List of Tables

Abstract

This work concerns the monitoring of fatigue cracks through Structural Health Monitoring (SHM) with the aim of measuring the size of the damage present in a piece. Among the various existing SHM, Acoustic Emission (AE) was the most suitable for this type of problem. The purpose of this thesis is to locate via AE, the position of a fatigue crack tip in a component, exploiting the phenomenon of acoustic emission. When a crack propagates in the piece, the stored energy is released as acoustic waves. Through a network of PZT sensors applied on the surface of the component, these acoustic waves, that propagate in the material, can be recorded. Knowing therefore, the flight times of the signals and the position of the sensors, it is possible to locate the position of the acoustic source.

The first phase of the work concerns the research for the best sensor layout, to maximize the accuracy of the location. These preliminary analysis were carried out on an aluminum sheet, artificially simulating acoustic events. Once the specimen was chosen (steel beam with H section), the experimental test setup was designed and the specimen was sensorized and prepared for the fatigue test.

The raw data provided by the Vallen Systeme (commercial package used for the AE) were not satisfactory enough and signals were analyzed during post processing. Various algorithms have been implemented to identify the correct arrival time of the acoustic wave. The results of the various methods were analyzed, comparing how the localization of the crack tip improved.

Sommario

Questo lavoro riguarda il monitoraggio di cricche da fatica tramite Structural Health Monitoring (SHM) con l'obiettivo di misurare la dimensione del danneggiamento presente in un pezzo. Tra i vari SHM esistenti, l'Emissione Acustica (AE) era quello più adatto a questa tipologia di problema. Lo scopo di questa tesi è localizzare tramite AE, la posizione dell'apice di una cricca di fatica in un componente, sfruttando il fenomeno dell'emissione acustica. Quando una cricca propaga nel pezzo, l'energia accumulata viene rilasciata come onde acustiche. Tramite una rete di sensori PZT applicati sulla superficie del componente, queste onde acustiche che propagano nel materiale, possono essere registrate. Sapendo quindi, i tempi di volo dei segnali e la posizione dei sensori, si può risalire alla posizione della sorgente acustica.

La prima fase del lavoro riguarda la ricerca del miglior layout dei sensori, per massimizzare la precisione della localizzazione. Queste analisi preliminari sono state svolte su una lamiera di alluminio, simulando artificialmente degli eventi acustici. Una volta scelto il provino (trave in acciaio con sezione ad H), è stato progettato il setup della prova sperimentale e il provino è stato sensorizzato e preparato per il test a fatica.

I dati grezzi forniti dal Vallen Systeme (pacchetto commerciale usato per l'AE) non sono stati abbastanza soddisfacenti e i segnali sono stati rielaborati durante il post processing. Sono stati implementati diversi algoritmi per individuare il corretto tempo di arrivo dell'onda acustica. I risultati dei vari metodi sono stati analizzati, confrontando come migliorava la localizzazione dell'apice della cricca.

Chapter 1

Introduction

"The task to which we must work is not to reach safety,
but to tolerate insecurity"

Erich Fromm

There are no perfect components. There are always defects created in the production process: inclusions, cracks, excessive roughness... A production free of defects, both physically and economically, is not feasible. If these defects are small enough not to be detected, they are inevitably formed during their working life. The degard and aging of a component is natural. The difference between theory, in which everything is described by laws and physical principles, and reality, is to take into account all the aspects and characteristics that a component has and that deviate from its theoretical model.

Engineers and technicians have the task and responsibility to ensure that the component is still able to perform its function. It cannot be guaranteed that the piece is perfectly intact, but it can be guaranteed that it is in a safety zone such as to tolerate its damage for a specific in-service time. Hence, the need to monitor structures and mechanical components to understand their state of health.

1.1 General Overview

This work is about monitoring crack propagation with Structural Health Monitoring (SHM) in order to find and measure damage's dimension and product's integrity. Acousting Emission Testing (abbreviated: AE or AT)

is a SHM already used in industrial field to monitor degradation and damage of mechanical component and structures. For this reason, AE was chosen to monitor the position of a crack tip in a steel beam, during a fatigue test. The purpose of this thesis, is to locate the position of a crack tip in real time, through a network of PZT sensors and understand the degree of reliability of this system.

1.2   Short Work Description

This study was born from the need to monitor the position of a crack tip by means of acoustic emission. Some physical phenomena such as plasticization, crack propagation ... emit acoustic waves that propagate in the material. The idea is to record these waves through a network of PZT sensors, and knowing the flight times and the position of sensors, triangulate the signal and locate the acoustic source.

Before, preliminary tests were carried out on an aluminum sheet to understand how the measurement system worked and to find the best layout of the sensor network: how many sensors to use? What distance between them? ... Subsequently, the test was designed: taking into account the constraints of the problem, the test setup was designed: choice of crack mode, applied forces, type of constraints and states of stress produced.

Later, the sensors'layout was adapted to the beam specimen and prepared for the test: a notch was produced to facilitate the nucleation of the crack, drilled to be fastened with bolts ... The fatigue test was then carried out, recording the acoustic events.

To improve the results provided by the Vallen Systeme (commercial monitoring package used), the data was analyzed and manipulated by us in Matlab during the post processing. The accuracy of the location strongly depends on the accuracy of identifying the arrival time of the acoustic waves. Different algorithms for calculating the arrival time have been implemented to improve the localization of the crack tip.

1.3   Thesis Structure

The thesis is structured as follows:

Chapter 1 contains the introduction of the thesis, explaining the area

in which the work is carried out, the purpose of this study and a brief summary of the work performed. It is used to introduce the reader into the monitoring environment and to give him an overview of the problem.

Chapter 2 contains the state of art: all the theory and knowledge acquired until now in this field, are in this chapter. It is important to understand the physical phenomena underlying the acoustic emission, on which this work is based; without understanding it, it is impossible to follow the reasoning and the concepts which will then be illustrated.

Chapter 3 contains preliminary analysis to understand how the measurement system works. It is the starting point of the work in which the best sensor layout is sought, to be adapted to the specimen.

Chapter 4 contains the test setup and shows how it was designed. Then it is shown how the specimen was prepared and adapted for the test. Finally it shows the raw results obtained.

Chapter 5 contains post processing data. The registered transient signals have been handeld in Matlab with different algorithms to improve the identification of the arrival time of acoustic waves. The final results obtained are shown and the different methods compared with each other, showing how localization improves.

Appendix A shows the technical drawings of the various components designed and used for the test setup. Finally, it shows their assembly.

Chapter 2

State of Art

To locate a crack tip through AE, it is necessary to achieve a specimen in laboratory that reproduces a crack, equivalent to that of a real situation. Therefore, it is necessary to understand what type of specimen use and study how to carry out the fatigue test to induce and propagate a crack. Once has been chosen AE as SHM, it is needed to study the physical phenomenon to understand what acoustic waves are formed and their characteristics. It is necessary to study how to configure the measurement system to optimize data acquisition and understand problems related to AE. Finally it is necessary to identify which parameters are important and which must be analyzed during data post processing.

2.1 Fatigue in Materials and Fatigue Crack Growth

Fracture is a problem that society has faced for as long as there have been man-made structures. The problem may actually be worse today than in the previous centuries, because more is the level of technological complexity achieved by our society. Fortunatley, advances in the field of fracture mechanics have helped to offset some of the potential dangers posed by increasing technological complexity. Our understanding of how materials fail and our ability to prevent such failures have increased considerably. Much remains to be learned, however, and existing knowledge of fracture mechanics can be improved.

Components of machines, vehicles, and structures are frequently subjected to repeated loads, and the resulting cyclic stresses can lead to microscopic physical damage to the materials involved. Even at stresses well below a given material's ultimate strength, this microscopic damage can accumulate with continued cycling until it develops into a crack or other macroscopic damage that leads to failure of the component. This process of damage and failure due to cyclic loading is called *fatigue*. Use of this term arose because it appeared to early investigators that cyclic stresses caused a gradual, but not readily observable, change in the ability of the material to resist stress (Cf. [1]).

At present, there are three major approaches to analyzing and designing against fatigue failures:

- The traditional *stress-based approach* was developed to essentially its present form by 1955. Here, analysis is based on the nominal (average) stresses in the affected region of the engineering component. The nominal stress that can be resisted under cyclic loading is determinated by considering mean stresses and by adjusting for the effects of stress raisers, such as grooves, holes, fillets, and kayways;

- *Strain-based approach* involves more detailed analysis of the localized yielding that may occur at stresses raisers during cyclic loading;

- *Fracture mechanics approach* treats specifically growing cracks by the methods of fracture mechanics.

This work concerns the latter point. In the component subjected to fatigue, an already present crack and its propagation must be monitored.

The presence of a crack can significantly reduce the strength of an engineering component due to brittle fracture.

Crack growth can be caused by cyclic loading, a behavior called *fatigue crack growth*. Otherwise, if a hostile chemical environment is present, even a steady load can cause *environmental crack growth*. Both types of crack growth can occur if cyclic loads are applied in the presence of a hostile environment, especially if the cycling is slow or if there are periods of steady load interrupting the cycling.
Engineering analysis of crack growth is often required and can be done with the *Stress Intensity Factor* (K) of fracture mechanics. K quantifies the severity of a crack situation. It depends on the combination of crack length, loading and geometry given by

$$K = F\sigma\sqrt{\pi a}$$

where a is crack length, σ is nominal stress, and F is an adimensional function of geometry and the relative crack length.

Later in the text, it will be explained that the specimen used is very similar to a compact specimen, as can be seen in Fig. 2.1. Only in this case, the coefficient F is defined as $\alpha = a/b$. Dimensions a and b will therefore be useful for calculating the necessary load to propagate the crack (Cf. [2]).
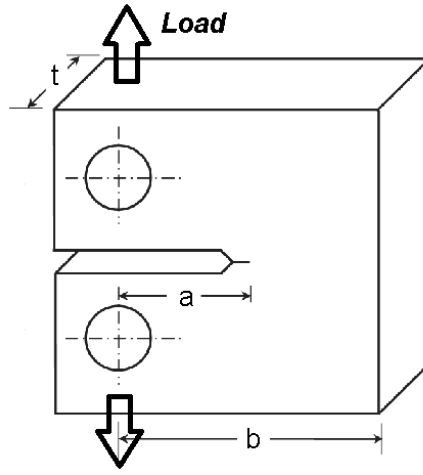
Figure 2.1: Geometry of compact tension specimen for a fatigue test, mode I fracture (opening mode): a is the length between crack tip and load axle; b is the length beteween specimen's side and load axis

The rate of fatigue crack growth is controlled by K. Hence, the dependece of K on a and F causes cracks to accelerate as they grow, Cf. [3]. The variation of crack length with cycles is thus similar to Fig. 2.2.

2.2   Structural Health Monitoring

Structural Health Monitoring (SHM) is a very recent area of *Experimental Mechanics* and now is spreading quickly because it allows:

- Increase safety in operation;

- Increase reliability in operation;

- Decrease operation costs.
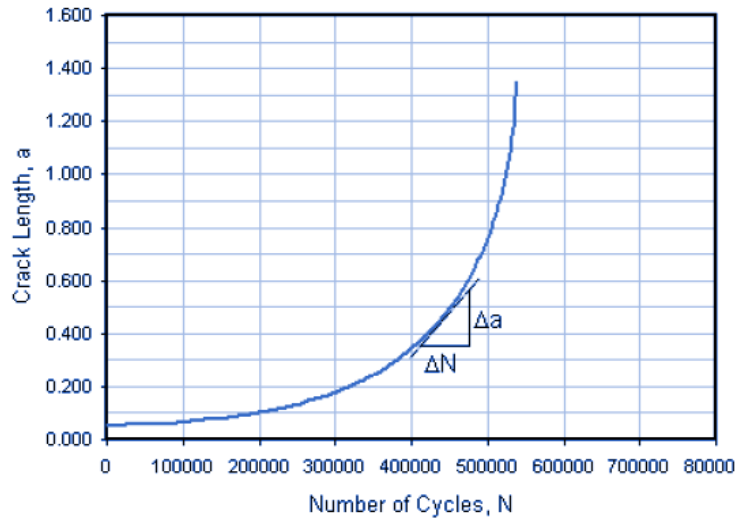
Figure 2.2: Growth of a crack from minimum detectable length a_d until critical length a_c where failure occurs

This is possible because SHM is able to provide, in real-time or on-demand, a diagnosis of the status of a given structure in every service moment. Furthermore, SHM keeps track of the previous history of the structure allowing also the prognosis (estimate of the evolution of the damage, residual life, ...).

SHM helps prevent catastrophic disasters by identifying and monitoring developmental damage before they degenerate into failure. In this way safety and reliability of systems are increased. In particular, the state of the structure, monitored by SHM, must always remain within the functional domain defined in the design context, while it undergoes, during the service, an natural "aging" due to the use, the action of the environment, to accidental events. . . Today, the monitoring of fatigue crack growth has assumed major importance for large engineered items, especially where safety is paramount: the areas of application of SHM are aerospace, civil, oil & gas, railway, power generation and military.

Nowadays, maintenance and repair of safety components represent a large part of the operating costs. SHM has shown the possibility to significantly reduce the overall costs of traditional Non-Destructive Testing (NDT), because it allows to replace the planned service interruptions with a targeted maintenance based on the real conditions of the structure instant

by instant.

SHM was born from the meeting of different technical-scientific fields and presents a common basis with the NDT. From this point of view, it can be considered a new and improved version of the NDT even if there are some differences, because SHM requires:

- Sensorization of the structure;

- Use of "smart" materials;

- Data transmission;

Furthermore, the structure itself requires dedicated planning and management.
Other advantages are the possibility of having more useful data for diagnosis, monitoring the service in a continuous or on-demand way, and the decrease of the influence of the "human factor", because the monitoring takes place automatically.

There are various SHM methods which differ in substantial characteristics and which make them very different from each other. They can be distinguished in:

- *Passive Monitoring*: it simply consists of "observing" and recording the behavior of the structure using sensors.

- *Active Monitoring*: it interacts with the structure using actuators to perturb it and sensors to read its response. The structure's response can only be recorded if it is stimulated from the outside. Actuators and sensors can be of the same or different nature. Certain types of transducers can perform both functions simultaneously.

Fig. 2.3 illustrates the concept behind the terms "active" and "passive" in SHM. In essence, the source emitting the waves is generally applied to the material in active methods (Fig. 2.3, top) using for example scanning techniques, whereas, in the passive methods, the sources are within the material (Fig. 2.3, bottom); they almost "produce" the test signal by themselves.

Another distinction concerns the way sensors are applied to the structure:
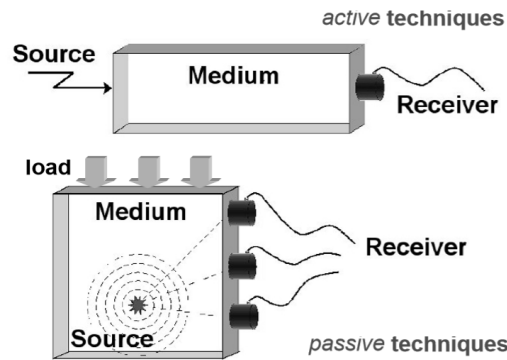
Figure 2.3: Comparison of SHM principles using active or passive techniques.

- *Applied*: sensors are applied to existing structures, or in any case after production and assembly, and which are then put into operation or perturbed.

- *Embedded*: sensors are placed in the structure during production, creating the so called "integrated systems".

The advantages of SHM embedded are sensor protection, better sensor-material interaction, monitoring in inaccessible areas. However, not all materials allow this option and if the sensor is damaged, all the component that contains it, must be replaced. Applied SHM have opposite advantages and disadvantages than embedded ones.

The SHM mainly used today are five:

- *Modal-Data-Based (eigen-frequency, mode shape and curvature, damping properties...)*
  Based on the fact that presence of structural damage reduces structural stiffness, and changes frequency response function and mode shapes. It's simple and low cost; particulary effective for detecting large damage in large infrastructure or rotating machinery. It's insensitive to small damage or damage growth and diffcult to excite high frequencies. It needs a large number of measurement points and is hypersensitive to boundary and environmental changes.

- *Electro-Mechanical-Impedance-Based*
  Based on the fact that the composition of a system contributes a certain amount to its total electrical-mechanical impedance of the

system, and presence of damage modifies the impedance in a high frequency range, normally higher than 30 KHz. It's simple for implementation and low cost. It's particulary effective for detecting defects in planar structures. However, it's unable to detect damage distant from sensors; accurate only for large damage.

- *Static-Parameter-Based (displacement, strain...)*
  Based on the observation that presence of damage causes changes in displacement and strain distribution in comparison with benchmark. It's locally sensitive to defects, simple and cost-effective. However, it's relatively insensitive to undersized damage or the evolution of deterioration.

- *Elastic-Wave-Based*
  Based on the fact that structural damage causes unique wave scattering phenomena and mode conversion, whereby quantitative evaluation of damage can be achieved by scrutinising the wave signals scattered by damage. It's fast, repeatable and cost-effective. It's able to inspect a large structure in a short time and is sensitive to small damage. It's able to detect both surface and internal damage. However, it needs a sophisticated signal processing due to complex appearance of waves signals and multiple waves modes available simultaneously. It's difficult to simulate wave propagation in complex structures. It has a strong dependance on prior models or bechmark signals.

- *Acoustic Emission*
  Based on the fact that rapid release of strain energy generates transient waves, whereby presence or growth of damage can be evaluated by capturing damage-emitted acoustic waves. It's able to triangulate damage in different modalities including matrix crack, fibre fracture, delamination, welding flaw and corrosion. It can predict damage growth. Sensors are mounted on surface and it has a good coverage.

The latter method SHM, Acoustic Emission, is the one of our interest and in the next paragraphs it will be explained in detail.

2.3 Acoustic Emission

Acoustic Emission (AE) is one of the SHM used to monitor and check component's integrity. AE measurement is a technique for detecting an elastic wave that is generated by the occurrence of microscale defects. Phenomena resulting from microscale defects can thus be readily detected by AE.

Traditionally, the usefulness of such techniques for predicting rockfalls has been known in mines worldwide. Later, AE testing was standardized as a structural health monitoring for detecting defects in pressure vessels, tanks, reactors and piping systems during elevated pressurization. This became the motivation for current AE testing. In recent years, applications of AE measurements have been extended from the fields of metal and mechanical engineering to those of civil and chemical engineering, resulting in the establishment of practical inspection in many fields.

Because of its capability to detect defects right at the moment of their growth, the AE testing method may also be used as a real-time monitoring and warning system to avoid a failure of the structure under test with possibly disastrous consequences.

AE testing is a passive, receptive technique analyzing the ultrasond pulses emitted by a defect at the moment of its occurrence. AE doesn't measure the response to an artificial and repeatable acoustic excitation of the test object, but the sound signals produced by defects at every growth's step, that are unique event and cannot be exactly reproduced again. Being an entire passive non-destructive test method, AE testing is very well suited for a large number of applications, particulary for those, which are not accessible by other testing methods.

2.3.1 Principles of the AE Method

When an external force is applied to a solid material, the material deforms. In the case of low stress due to a small external force, the deformed material elastically recovers to its original shape upon unloading. Such deformation is called elastic deformation. In the elastic range, the external force leads to accumulation of energy inside the material as strain energy. There is a limit for energy accumulation in the solid material. If the strain energy stored in the material due to the external force reaches the limit, it is released and results in plastic deformation. That is, even when the external force is unloaded, the material cannot recover its original

shape.

If even larger external force is applied, cracking usually occurs in the material. In this case, the strain energy accumulated inside the material is consumed by the generation and growth of cracks. When the solid material is deformed or cracked, it consumes strain energy. Thus, most of the strain energy is released. Simultaneously, remaining energy is consumed to generate sound and heat. A phenomenon in which sound is generated by the energy release is referred to as acoustic emission (AE).

Because of cracking inside the material, elastic waves are generated and propagate through the material. The phenomenon is analogous to an earthquake. In other words, AE can be referred to as a "micro-earthquake" in a solid material (Cf. [4]).

In summary, AE is defined as a phenomenon in which strain energy accumulated in a solid is released because of deformation or cracking, and thus generates elastic waves. Elastic waves generated by cracking propagate through the material and are detected by an AE sensor (vibration-to-electrical signal conversion element) placed on the surface.

2.3.2 AE sources

Cracks, plasticization, crack nucleation... are well known as AE sources. Furthermore, AE waves are generated by rust formation and friction caused by rust. Differently, in the case of a composite material, delamination and fiber fracture occur in the material.

Therefore, AE is caused by a complicated combination of these events. Next, the detection of abnormal noise for acoustic diagnosis has been carried out to monitor the safety of equipment and determine when the equipment must be replaced. Furthermore, this method can detect the existence of broken pieces and fragments of parts (loose parts) that have slipped into the insides of pipes in a reactor, Cf.[5].

Some of the materials reported so far do not generate AE upon their failure. This is considered to be due to the minimum energy of failure or ultra-highspeed failure. This does not mean that AE waves are not generated; rather, they cannot be as easily detected as in AE events.

AE waves are essentially generated by failure phenomena and can be mostly attributed to the formation of microcracks. This type of AE is sometimes called primary AE. On the other hand, AE generated by rust formation and friction caused by inclusions and particles is called secondary AE. Typical mechanisms that generate AE waves are conceptually illustrated in Fig. 2.4.
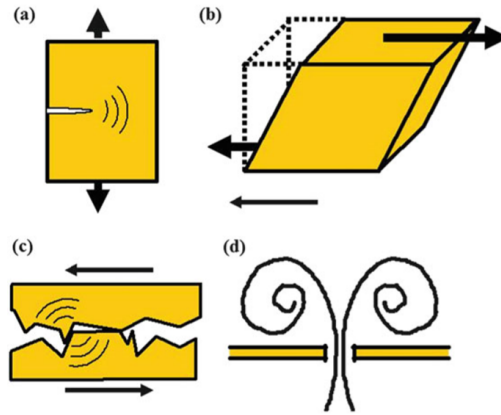
Figure 2.4: Examples of sources of AE waves. (a) Cracking. (b) Deformation and transformation. (c) Sliding or slip. (d) Leakage

Basically, there are two types of AE signals, transient and contiuous signals. With transient AE signals, also called brusts, start and end points deviate clearly from background noise. With continuous AE signals, we can see amplitude and frequency variations but the signals never ends. In Fig. 2.5 an example of both types of AE signals are shown.
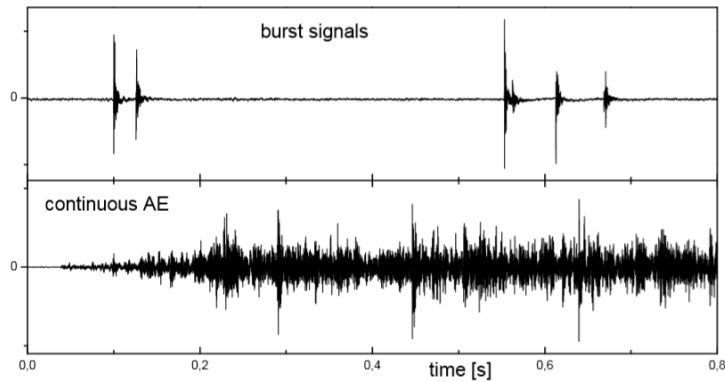
Figure 2.5: Example of burst signals compared to a continuous emission of acoustic waves

The useful signals for AE testing are burst type signals, e.g. originating from fracture or crack growth. Contiuous signals are mostly unwanted (noise) signals such as friction or flow noise. At best the background noise is just the electronic noise of the preamplifier or the sensor.

2.3.3 AE waves

An AE wave is defined as an elastic wave generated at an AE source. Wave motion is a phenomenon in which particle motions are dynamically transferred to adjacent particles, as each particle only vibrates at its own position and does not move. However, wave motion itself propagates with its characteristic velocity. Wave motions are defined on the basis of orientations of particle motions and directions of propagations (Cf. [5]). AE waves are classified as longitudinal, transverse and other waves (see Fig. 2.6):

- *Longitudinal wave (P-wave, Primary wave)*
  In longitudinal waves, particles vibrate along the direction in which the wave propagates. This kind of is wave the fastest and with small amplitude wave.

- *Transverse wave (S-wave, Secondary wave)*
  In the case of transverse waves, particles vibrate perpendicular to the direction in which the wave propagates. It's slower than longitudinal wave but oscillation amplitude is larger.

- *Rayleigh and Lamb wave*
  When longitudinal and transverse waves, generated inside the elastic solid, reach the surface other waves are generated.

  In Rayleigh wave, also konwn as surface waves, particles near the surface move elliptically and motion decreases with depth.

  Instead, Lamb waves are generated in a thin plate, as the plate vibrates. The Lamb wave has a symmetrical mode (S mode) in which the plate vibrates symmetrically and an anti-symmetrical mode (A mode) in which the plate vibrates asymmetrically.

On flat surfaces, the wave propagates in the terms of concentric circles around its source and can be detected by one or more sensors. Signal intensity is not constant, but attenuation occurs in time (viscous damping) and in space (distance attenuation). The maximum distance, where an AE event can still be detected depends on various parameters, e.g. on the material properties, the geometry of the test object, its content and environment, . . . So it becomes necessary to determine the proper positions and number of AE sensors, depending on sensor-to-sensor distances, otherwise not all signals can be detected and localized.
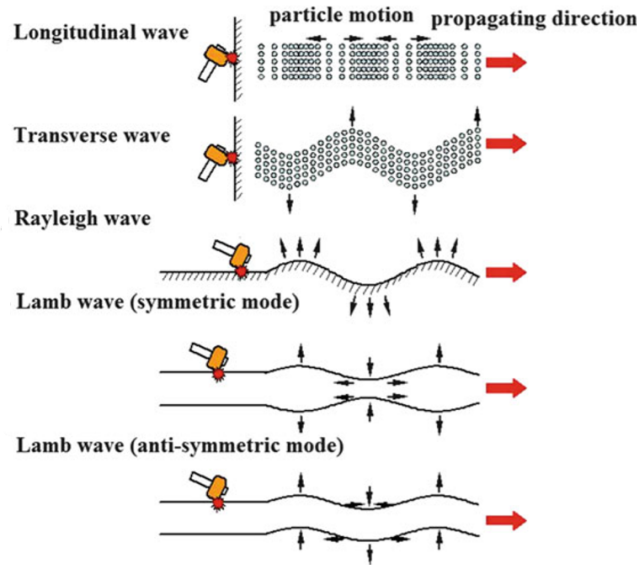
Figure 2.6: Types of wave motion

On flat or cylindrical metal surfaces, events can still be detected at a distance of several meters, which is one of the great advantages of this technique.

2.3.4   Waveform Parameters

A wave generated in one AE event comprises a block of various wave components such as longitudinal, transverse, or surface waves. Because of the difference in the propagation velocities of different wave components, these components successively reach the AE sensor placed far from the AE source with a time lag. The wave packets[1] of the AE signal, corresponding to the AE waves released from a certain source, are separated and extracted from signals that are continuously output by the AE sensor. This signal processing is called discrimination, Cf. [5].

AE signal include information on an AE event and on source generating the wave. AE sensros don't interact directly with the signal source, but record an acoustic wave produced by it. Therefore, information on AE events and physical phenomena is generally inferred indirectly, by calculat-

---

[1]A series of pulses

ing waveform parameters representing the characteristics of a waveform of the discriminated AE signal.

In very few cases, AE testing is based on only a few brusts. In general, some hundreds or thousands of brusts are recorded for statistical evaluation. Statistical evaluation of the waveforms themselves is difficult, but certain features of waveforms can be evaluated statistically. One has to determine the most important parameters of esch waveform in order to compare the results of the structure under test with those of a defect-free test object and with those of a defective test object.

The most commonly used features are:

- *AE signal (peak) amplitude*
  The maximum voltage in an AE signal detected between the start and end of the AE signal discriminated on the basis of a given measured threshold. The voltage value of the AE signal can be expressed as a common logarithm on the basis of a reference value of $1\mu V$.

$$AE \text{ signal peak amplitude } [dB_{AE}] = 20 \text{ } log_{10}(A1/A0)$$

  $A0 = 1\mu V$, which is the output from the AE sensor without any amplification, and A1 is the measured maximum voltage of the AE signal.

- *AE count (ring-down count)*
  Number of measured voltage of the AE discriminated signal exceeds the threshold of one polarity. The count result per unit time is called the AE count rate.

- *AE energy*
  The AE signal energy is determined as the integral of the square of the instantaneous amplitude of the AE discriminated signal over a certain duration.

- *AE signal duration*
  Time that has elapsed between the start and end of the AE discriminated signal, measured as interval between first and last threshold crossing.

- *Arrival time*
  Absolute time of first threshold crossing.

- *AE signal rise time*
  Time that has elapsed between the start of the AE discriminated signal and the time at which the AE signal peak amplitude is attained.

- *Ratio of rise time to amplitude*
  The ratio of the AE signal peak amplitude to the AE signal rise time.

- *AE root-mean-square (RMS) value*
  The root-mean-square of an AE signal represents the energy level of the AE signal and also enables us to evaluate the rate of occurrence of AE.
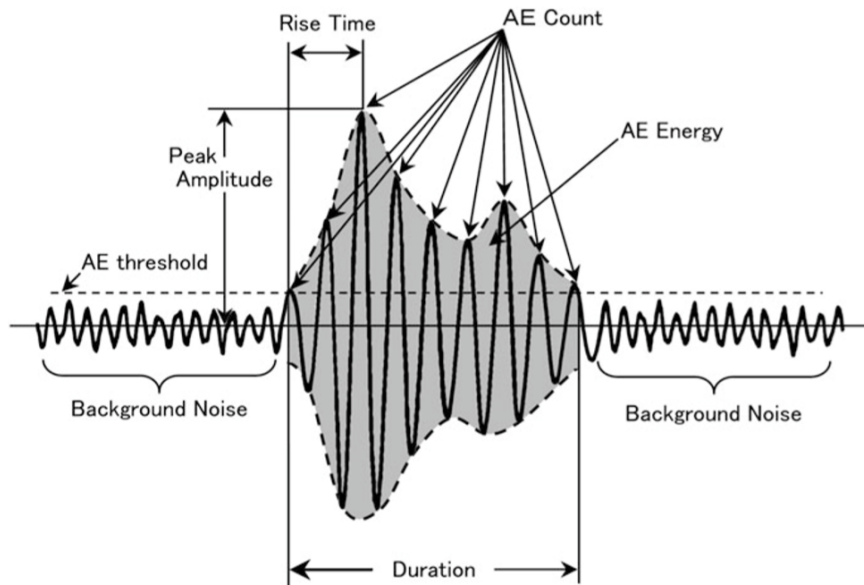
Figure 2.7: AE threshold and AE parameters

2.3.5 Kaiser Effect

The Kaiser effect is a well-known phenomenon in AE-studies. The Kaiser effect, which was first investigated by Wilhelm Kaiser in 1950, describes the phenomenon where a material under load emits acoustic waves only after a primary load level is exceeded, Cf. [4]. He discovered with repeated loading of tensile specimens that metals retain a memory of the previously applied stress. During reloading, these materials behave elastically before the previous maximum load level is reached. If the Kaiser effect is permanent for these materials, little or no AE will be recorded before the previous maximum stress level is achieved. In other words, Kaiser effect can be defined as the absence of acoustic emission at stress levels below the previously applied maximum stress.

The effect is illustrated in Fig. 2.8 in an experiment where a specimen, subject to compression, was tested under a cyclic load. The figure shows the AE rate versus time, and the applied load versus time.
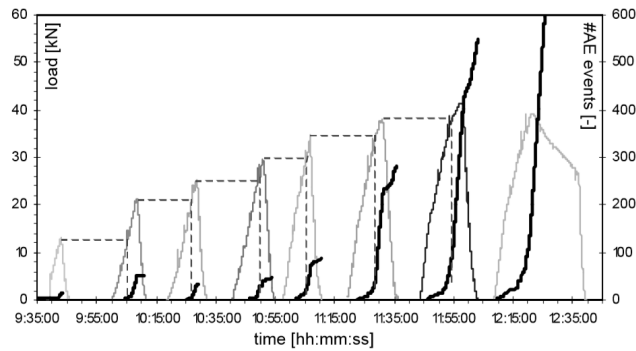
Figure 2.8: Example of the Kaiser effect occurred in a cyclically loaded concrete specimen. Thick black lines represents the AE activity, thin lines the load and the dashed lines indicate the Kaiser effect

This phenomenon is very important because if an AE is not registered for a given stress level, this response is lost forever. It will be necessary to introduce a higher level of stress with respect to the previous one, in order to have another emission of AE, but in this way the defect propagates and the structure is lead into a more critical condition.

2.4   Determination of the Arrival Time

One of the very important task of an AE system is to convert the AE bursts into compact data sets and to eliminate the background noise (which is more or less continuous).

For this, modern AE systems use detection thresholds. The threshold has to be set to the right value by the user. If the AE signal exceeds the threshold in either positive or negative direction, this means the start of a hit (a hit is a detected burst).

The time of the first threshold crossing is called "arrival time of the burst" and is needed for location calculation. Waveforms diplayed by the software are produced by joining many single points called "samples". They correspond to single measurements at constant time intervals.

Digital system has sampled the AE signal every $0.2\,\mu s$, which means 5 milion times a second. Having an high sampling rate means having a high temporal resolution and therefore also a better precision in measuring the arrival time. On the contrary, it means having a lot of data to store and a huge amount of memory required for a single burst.

A sufficient high sampling rate must be chosen, to be sure not to have aliasing, but not too high if not necessary. For a good balance, a correct value must be set before starting to acquire.

2.4.1   Sound Velocity

Different types of elastic waves, travel at different speeds in the material, as explained in Cf. [4]. The velocity of the longitudinal wave, $C_L\,[m/s]$, is expressed in terms of Young's modulus E, Poisson's ratio ν and the density ρ of the material through which the wave propagates:

$$C_L = \sqrt{\frac{(1-\nu)E}{(1+\nu)(1-2\nu)\rho}}$$

On the other hand, the velocity of the transverse wave, $C_T\,[\mathrm{m/s}]$, is expressed as:

$$C_T = \sqrt{\frac{E}{2(1+\nu)\rho}}$$

The velocities of the longitudinal and transverse waves propagating through

typical materials are listed in Tab. 3.1. The velocity of the Rayleigh wave is approximately 90 % of that of the transverse wave. The velocity of the Lamb wave varies with the plate thickness, frequency, and mode.

Medium	Density (Kg/m^3)	Velocity of longitudinal wave (m/s)	Velocity of transversal wave (m/s)
Alluminium	2700	6350	3130
Steel	7800	5900	3200
Concrete	2500	4000	2600
Water	1000	1430	-
Water	1.2	330	-

Table 2.1: Velocities of typical materials (rapresentative values)

The wavelength is defind as the distance of one cycle in the sinusoidal motion of a wave. The time interval between successive motions of one cycle is defined as the period and expressed as T [s]. The number of cycles per second is defined as the frequency and expressed as f [Hz], which is equivalent to cycles per second. In the case that the wave propagates with velocity C [m/s], the wavelength is expressed as λ [m] eith the relation:

$$\lambda = \frac{C}{f}$$

When motion is repeated at f cycles per second, a wave with wavelength λ travels a distance of $f \cdot \lambda$ per second, which is equal to the velocity C.

2.5 AE Source Location

A great advantage of the AE method is that the location of an AE source can be determined relatively easily. It is not necessary to scan the whole object using a probe for determining the position of damage in the object, but it's sufficient use fixed sensors. Two main methods are used and are distinguished by range of coverage and accuracy. Both are illustrated below just for illustrative purposes, even if, only the Planar Location Method will be used, Cf. [5].

2.5.1   Zonal Location Method

The simplest way to locate the source of AE is the so-called "zone location method". The exact source coordinates are not determined, but the defect is located within a radius of the sensor's sensitivity range. The zone location method is frequently used to monitor large structures such as buildings, pipes, vessels, etc. Sensors are distributed over a wide area on the surface of the structure and/or concentrated at the most critical locations. In case of a large object or a weak generated signal, all AE signals cannot be recorded in all measured channels because of signal attenuation. In this case, it is impossible to locate the AE source with accuracy. The AE channel that firstly records tha AE signal, correspond to the sensor nearest to the AE source; this enables approximate location of the AE source.

The graph in Fig. 2.9 clearly shows that the AE source is in the neighborhood of sensor 2, but it is not possible to know the exact position. Fig. 2.10 shows an example of a sensor configuration used to monitor leaks in pipes. The leak or failure must be within the detection range of the sensor, to allow the AE to be detected. If AE is recorded by a particular sensor, the technician should inspect the neighborhood of this sensor for leaks or cracks.
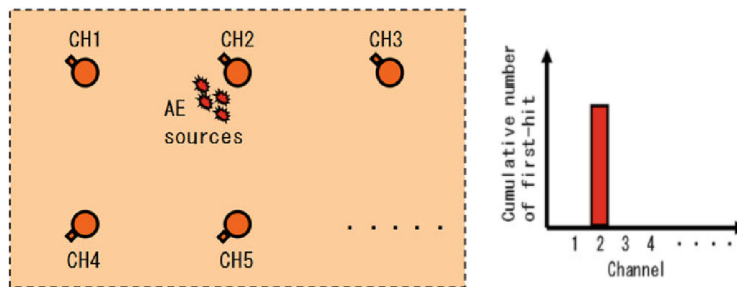
Figure 2.9: Zone location on a plate
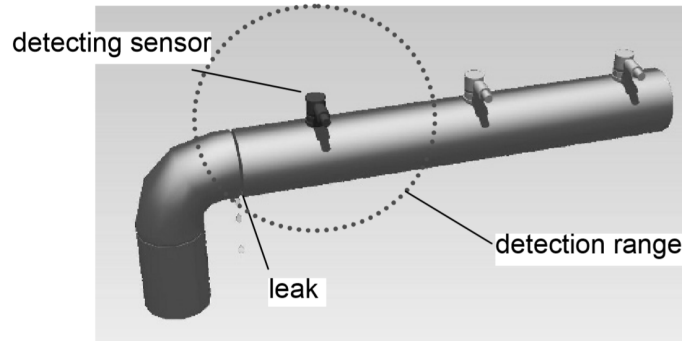
Figure 2.10: Example of the zonal monitoring of leakages in a pipe using AE testing

2.5.2 Planar/2D and 3D Location Method

This method is a localization technique to extract the source coordinates of the acoustic emission events as accurately as possible. Source location determination is an inverse problem. Due to the arrival time differences of the elastic wave emitted by the fracture and recorded at each sensor, the source location can be calculated. The acoustic emission source location is defined by the origin time (start of the rupture) and the source position in Cartesian coordinates (x_0, y_0, z_0). The computed location corresponds to the point in space and time where the fracture initiated.
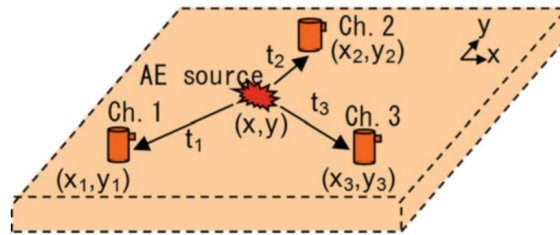
Figure 2.11: Planar source location

The planar localization technique is applied to 2-D structures, where the thickness is small compared to the extent of the object, and the source coordinates are only required in two directions. In case of waves having wavelengths longer than the thickness of the structure/plate, Lamb waves have to be used and their group velocities considered. The 2-D method to determine acoustic emission sources is usually applied when the accuracy

of zone technique is insufficient.

The distance differences between a source (defect) and different sensors are equal to *Arrival Time Difference · Sound Velocity*. Location caculation is based on the evaluation of arrival time differences of the AE signal propagating from its source to different sensors. An AE wave propagates in concentric circles from its source and arrives at different sensors with certain delays. The delay is proportional to the distance between the sensor and the source.
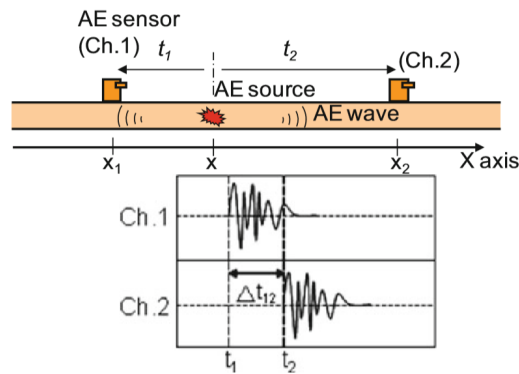
Figure 2.12: Linear source location

Assuming constant velocity and three measured arrival times t_1, t_2 and t_3 of the compressional wave, at three different sensors, the epicenter can be calculated by the hyperbola method. The epicenter must be located on a curve for which the arrival time difference between two sensors e.g. $t_2 - t_1$ is constant, as can been seen in Fig. 2.13. Such a curve is a hyperbola with the corresponding sensor coordinates of sensor 1 and sensor 2 as foci.

Due to the fact that generally one arrival time is greater than the other e.g. $t_2 > t_1$ the epicenter location is limited to one branch of the hyperbola. The hyperbolas of the other station pairs (t_1, t_3 and t_2, t_3) are calculated in a similar way. The epicenter is the intersection point of the 3 hyperbolas.

Due to measurement errors the three hyperbolas may not intersect at one point. For such a case, using more than 3 sensors should improve the localization accuracy and statistical methods must be applied.

For Vallen System AMSY-6, when more sensors than needed are available, the problem is over-determined and the calculation is performed using an iteration algorithm, where the coordinates are estimated by minimizing the errors of the unknown parameters. The more recordings, the more over-determined the system, and the more reliable the evaluation will be.
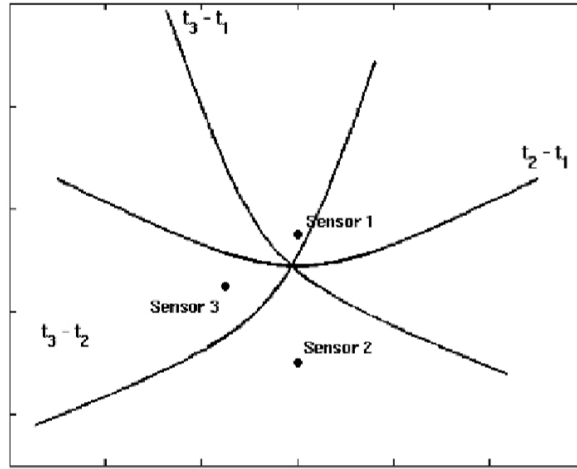
Figure 2.13: 2-dimensional localization using the hyperbola method. t_1, t_3 and t_2, t_3 are the arrival times of the compressional wave at the corresponding sensors

The general rule is that for localization in n-D space dimensions, n+1 sensors are required. So, at least 3 sensors are needed for a 2D localization. The 3D localization, compared to the 2D one, requires at least one more sensor (if the problem is not oversized) and different types of waves can be generated (compression, transversal) instead of just those of Lamb.

The most common approach is to use an iterative localization algorithm, which requires the linearization of the problem. To do this, a "first guess" or trial hypocenter (x_0, y_0, z_0, t_0) is required. The travel time residuals r_i of the first guess hypocenter are then a linear function of the correction in hypocentral distance. Due to the first guess hypocenter being a trial solution, the calculated travel times differ from the measured ones. A correction $(\Delta x, \Delta y, \Delta z, \Delta t)$ of the first guess hypocenter is needed to minimize the travel time residuals. If the necessary corrections are relatively small, the travel time function can be linearized. A corretiction vector must be calculated and applied to the next step in order to be minimized iteratively. Convergence criteria can be set for terminating the iteration when a particular desired accuracy has been reached, or if the procedure is diverging.

2.6   Localization Errors

An error analysis is necessary for assessing the accuracy and reliability of any localization result. There are different sources of errors that are not clearly separated. Uncertainties in the determination of the arrival times generally depend on data quality, and how impulsive onsets are. In the presence of noise, low amplitude onsets are easily overlooked. Moreover, the widely used assumption of a homogeneous behavior of the wave propagation may not be correct for a tested structure. All these errors are intrinsic and difficult to eliminate.

Another component of error, that can be improved, and is much more influential in the accuracy of the localization, is the geometrical relationships between source location and sensor distribution, expalined in Cf. [4]. In the case that AE are expected to occur in certain regions of the test object, it generally can be considered whether a given sensor arrangement is suitable for an accurate localization of these AE sources or where additional sensors should be placed. Localization accuracy is highest for events that have a good azimuthal coverage by the sensors. This can be illustrated by the following theoretical example where four sensors, arranged in a square are used to localize AE sources in two dimensions.

In a theoretical case, starting from the arrival times detected at each sensor, the hyperbolas perfectly intersect in one point, identifying exactly the AE source location as depicted in left part of Fig. 2.14. Top left shows a source within and bottom left a source outside the sensor array, without any differences in accuracy.

In real applications the arrival times contain an uncertainty and the hyperbola will not intersect in one point but rather an area. In the present example this is simulated by adding random errors of time delays to the calculated arrival times. Fig. 2.14 right part demonstrates the effect of the sensor arrangement on the localization result. In the diagram below, where the AE source is outside the sensor array, the hyperbolas intersect in a much larger area then in the case, with respect the AE source is within the sensor array.

This example clearly shows the great importance of the correct choice of geometrical sensors' position and how much it's crucial for the final location error.

The effects of all the errors overlap determining the final precision of the location of the AE source process. In practical application the value of standard deviation σ, corresponding to *Geometrical Distribution of Location Error*, proves to be the best indicator to distinguish reliable from erroneous localization results. Inaccurate localization results, due
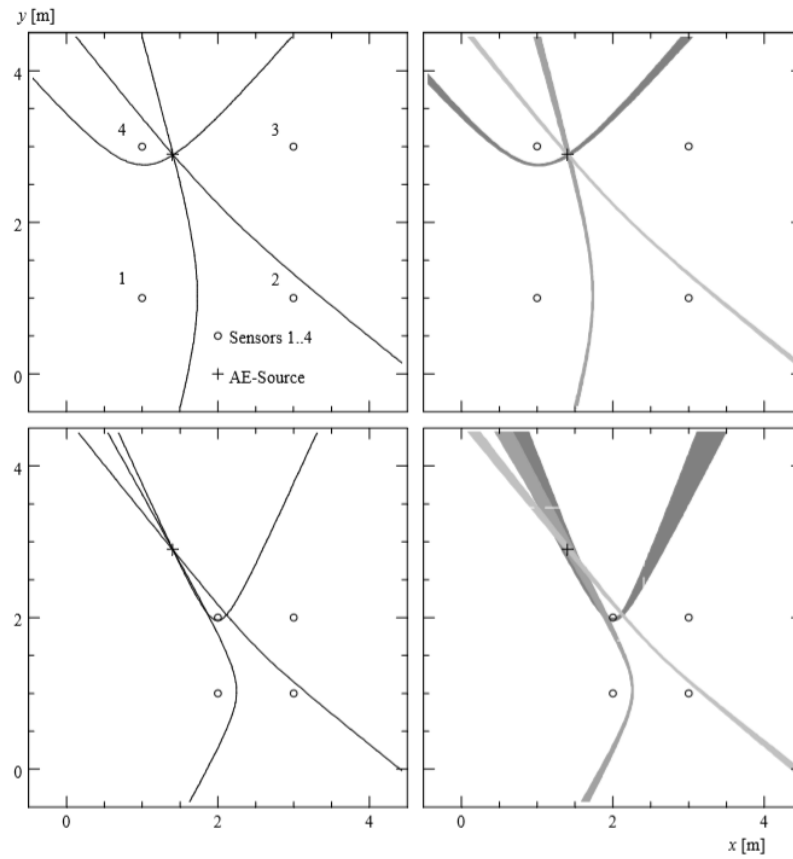
Figure 2.14: Theoretical example to demonstrate the effect of the sensor arrangement on the localization accuracy. *Top*: AE-source within sensor array; *Bottom*: AEsource outside. *Left*: accurate arrival times; *Right*: arrival times with an error of time delays

to erroneous arrival time determinations or sensor locations, are well recognized by high values of σ.

It is possible to estimate the component of σ due to time delays with a computer by simulating an artificial delay on the various sensors and compare the position provided by the algorithm with the real one. In this way it is possible to understand a priori how robust the chosen sensor layout is and how the accuracy varies according to the position of the AE source.

The following figures show how σ varies with a 3 and 5 sensor configuration. σ can also change a lot in relatively close areas and for this reason we cannot speak of localization precision of a configuration at general level but of *"Sensitivity Maps"*, Cf. [6].
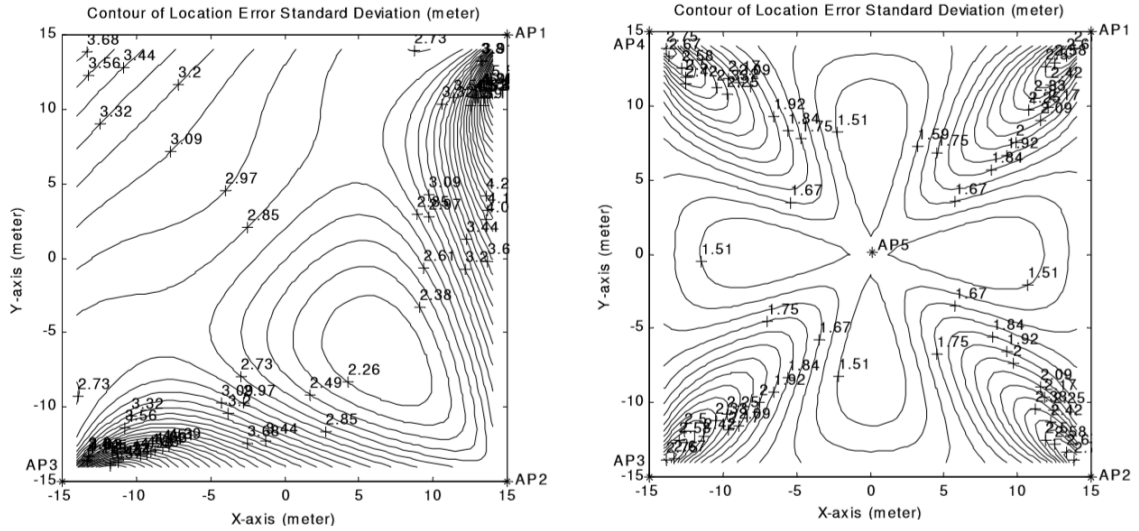
Figure 2.15: Geometrical distribution of location error (AP=sensor position). *Left*: 3 sensors. *Right*: 5 sensors.

The first step of the work so, is the research what is the position and the best number of sensors to maximize the accuracy of localization. The ideal, is to find a more or less constant sensitivity map throughout the monitoring area, with the lowest possible σ value.

Chapter 3

Preliminary Analysis for the Definition of Sensors Layout

Now that, the Acoustic Emission basic physical principle has been explained, we can proceed to describe the real problem that this work has faced.

A load-bearing beam of a structure, operating in a marine environment, has a fatigue crack which compromises its integrity. It propagates along the core of the beam, whose section is H-shaped. We do not know the loads to which it is subjected, nor the speed of propagation. The only data concern the shape and material of the beam (see chapter 4.1). It is necessary to monitor its propagation carefully to understand when the beam will no longer be in safe conditions and a maintenance stop will be necessary. It is wanted to monitor the position of the crack tip, exploiting the acoustic waves emitted by it during propagation. The SHM based on acoustic waves is Acoustic Emission Testing (AE).

AE testing is a well-established and reliable SHM for crack monitoring, used for years and therefore a "mature system", so much so that it is used in many different industrial sectors. This paper deals with the monitoring AE testing, describing steps, problems, operational solutions and results.

Once it was decided to use AE tests as SHM, it is needed to understand how to apply this monitoring method. How many sensors use? Where place them? What acquire? Which optimal input parameters select for data acquisition? What are the best waveform features to use? What numerical indices extract from data processing? What meaning attribute to numerical results? . . .

It is easy to understand that the problem is more complicated than it appears. It is not enough to apply the sensors to the structure and record, because what it is get, is illegible and useless.

Before moving on to the experimental test, which requires time and resources, it is necessary to find the best layout for AE testing for this application. The first tests have been carried out on a 3 mm thick aluminum plate in a laboratory environment. The plate is suspended with rubber pads on the bench, to isolate it as much as possible from the vibrations transmitted by it. At its edges, modelling clay was applied to dampen and absorb the elastic waves generated in the plate and prevent them from reflecting back due to the edges.

This aluminum plate, Fig. 3.1, is a test object very different from the steel beam then used in the test. It was used because initially we didn't know the specifications of the final specimen (section, material, thickness. . .). It was a material that was already available to us and could reproduce a 2-D location problem. In any case, the first tests were used to understand how the instrumentation worked, to find a general sensors'layout from which to start, to then be adapted and refined to the final specimen test.

Figure 3.1: Al-plate with PZT sensors applyed, used for preliminary tests

First of all, it is necessary to describe the instrumentation used for this specific case, as it determines the precision and quality of the measurements, as well as the repeatability.

3.1 AE Measurement Chain

The AE sensor is not directly applied to the material specimen but through a coupling agent. The sensor converts the wave picked up into an eletric AE-signal that is then amplified and transferred through a cable until to the acquisition unit. There, the signal is processed into a signal data set and then transferred to a computer which stores, analyses and displays the data (see Fig. 3.2 and 3.3).
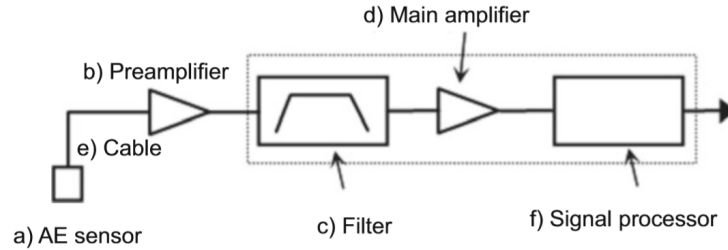
Figure 3.2: Main AE channel parts

For this work, it was used an AE measurement system provided by the *Vallen Systeme*. This company supplies all the measurement tools in a single package to the customer. In this way, it can test the entire measurement chain, certifying its effectiveness and accuracy.

Below, each component will be described and its function explained.

3.1.1 Sensor

The sensor's function is convert the mechanical wave into an electrical AE signal. Piezoeletric sensors have proved to be most appropriate for AE testing. They are robust and more sensitive than other sensor techniques, e.g. capacitive, electro-dynamic, or laser-optical sensors.

AE sensors can be mainly classified as either resonance models or broadbandwidth models. Usually, the widely used resonance-type AE sensors have been employed. When an AE wave reaches a piezoelectric ceramic
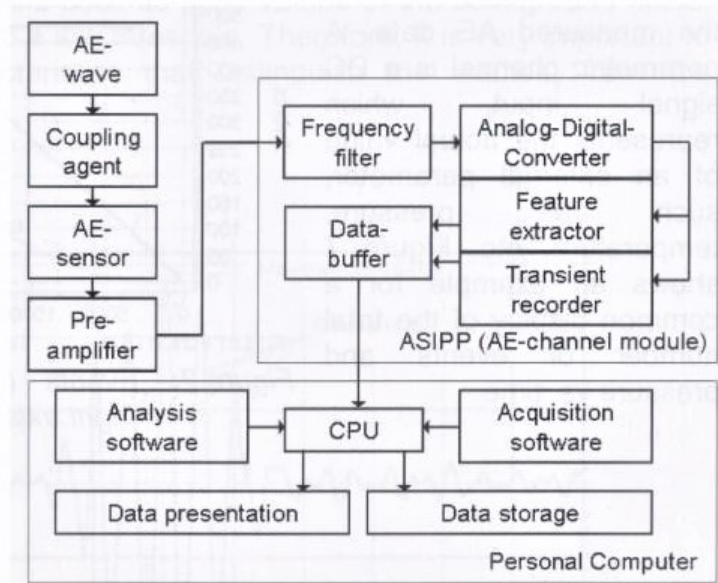
Figure 3.3: AE measurement chain

through the detection face, the AE wave is repeatedly reflected within the piezoelectric ceramic (i.e., transfer element). During this reflection, the AE wave with the resonance frequency is emphasized and remains within the transfer element. In contrast, other components are attenuated quickly within the transfer element. Accordingly, the AE sensor achieves high sensitivity by taking advantage of the resonance provided by the transfer element.

Instead, a broadband AE sensor having a flat frequency response is used to confirm the frequency component and/or waveform analysis of AE waves. The two different sensor type areshown in Fig. 3.4.

When testing metal structures for integrity, frequencies between 100 and 300 KHz are usually most interestng. Phenomena that are sources of acoustic waves, such as crack propagation, plasticization. . . are found in this frequency range. For this reason, sensors used for AE testing have a resonance of about 150 KHz and cover the range of 100-300 KHz with a a variation of sensitivity of approximately 6 dB. In this way, high frequency noise or low frequency oscillations, which disturb the frequency range of interest, are attenuated quickly. In this way, a "cleaner" signal is obtained, which contains mainly the acoustic information that we need.

Piezoeletric sensors used in this work are VS150-M model, as in Fig. 3.5, are resonant type and their sensitivity can reach values of up to $1000\,V/\mu$m.
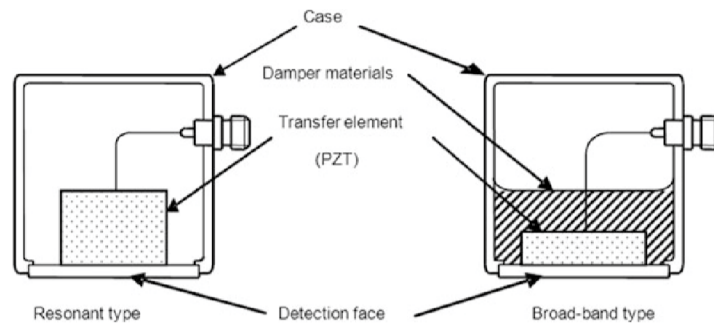
Figure 3.4: Schematic structures of resonant-type and broad-band type AE sensors

Figure 3.5: Piezo-eletric Sensor, VS150-M Vallen Systeme

3.1.2 Acquisition Unit

It's composed by:

- *Frequency Filter:* used to elimintae unwanted frequency ranges (noise sources) and matches the measurement chain to the requirements of the application (100-300 KHz for integrity testing metallic components).

- *A/D Converter:* used to digitize and discretize the AE signal that has passed the frequency filter. A huge measurement dynamic is required, as very strong bursts from nearby produce much higher amplitudes than weak ones from a large distance. A dynamic range and data processing speed are characteristics that identify a good acquisition unit. Given that acoustic waves of interest are placed in 100-300 KHz range, this requires a sample rate of 5-10 MHz.

The model used can beseen in Fig. 3.6.

Figure 3.6: Acqusition Unit AMSY-6, Model MB6 Vallen Systeme

3.1.3 Coupling Agent

The coupling agent is crucial to the quality of the sensor coupling. It provides a good acoustic contact between the sensor and the surface of the test object. It should be selected the appropiate couplant, which does not corrode the test object's surface, and which fits to the given temperature. Usually, silicone grease (high vacuum grease), oil or glue can be used.

The coupler's function is to transmit the vibrations from the component to the sensor, and to eliminate the air between the two parts. Being a gas, air does not transmit acoustic waves and acts as a barrier to the signal. If air were present between the piece and sensor, this latter would not record any signal.

It has been used a multi-silicone grease, as in Fig. 3.7. After attaching the sensors, the quality of the coupling must be verified (pencil lead break, automatic coupling test). If required, the coupling procedure must be repeated.

Figure 3.7: Multi-Silicone Grease, 1110 OKS

3.1.4   Hsu-Nielsen-Source

The pencil lead break (also termed as Hsu-Nielsen-Source or HSN-Source) is a frequently used artificial acoustic source, which produces well reproducible acoustic events, Fig. 3.8. A pencil lead (2H hardness, 0.35 mm diameter) is broken against the structure under a defined angle, Cf. [7]. A special shoe (specified e.g. in ASTM standard E976) aids in breaking the lead consistently, Fig 3.9. The Hsu-Nielsen-Source is used e.g. to verify the sensor coupling or to determine the acoustic attenuation of the structure.

Figure 3.8: Hsu-Nielsen-Sourc 0.35 mm (ASTM E976) Vallen Systeme
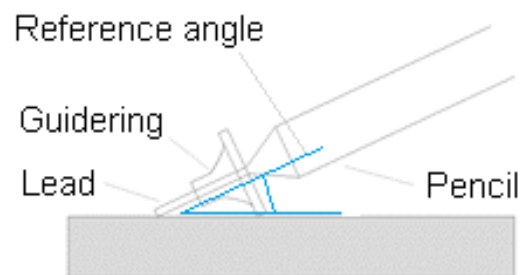
Figure 3.9: Hsu-Nielsen-Sourc: diameter 0.35 mm, hardness 2H, lead length 3 mm

3.1.5 Magnetic Holders

Usually, AE sensors are attached to the test object using magnetic holders if the structure is ferromagnetic, Fig. 3.10. In this way, a costant hold-down force is ensured during the whole measurement. With non-magnetic objects, elastic ties, tape, clamps, glue. . . are used.

Figure 3.10: Magnetic Holders, two magnets are placed next to a cylindrical cavity in which the sensor is inserted

3.1.6 Sensor to Preamplifier Cable

A special coaxial low-noise cable, Fig. 3.11, is used to connect the sensor to the pre-amplifier. It should not be longer than 1.2 m because of capacitive load on the sensor. Furthermore, the signal coming from the sensor is weak (order of mV) and must be amplified by the pre-amplifier as soon as possible. Also for this reason, this cable must be short. Usually it is very sensitive and thin because of miniaturized sensor connectors. It must not be bent sharply or strained, neither applied tensile load, especially to the connectors otherwise the cable generates electrostatic noise.

3.1.7 AE Pre-Aamplifier

The AE pre-amplifier can be either a separate device or is integrated into the sensor. The pre-amplifier amplifies the output signal from the sensor and drives the cable to the main amplifier. The preamplifier is necessary because the amplitude of the AE sensor output signal is small and the impedance of the signal source is high, such that the signal from

Figure 3.11: Sensor Cable, 1.2 m Vallen Systeme

the AE sensor is not suitable for driving a long cable and is susceptible to noise. The model used in this wrok is AEP5, as can be seen in Fig. 3.12.

Figure 3.12: Preamplifier, AEP5 Vallen Systeme

3.1.8 Pre-amplifier to System Cable

The length of the cable that connects the output of the preamplifier to the input of the acquisition unit (a coaxial cable in most cases) may exceed 100 m in some cases. The cable length in this case is no a problem, as can be seen in Fig. 3.13, because the signal has already been amplified by the pre-amplifier.

Figure 3.13: System Coaxial Cable, 50 Ω Vallen Systeme

3.1.9 Software

The Vallen System AMSY-6 use a contiuous sampling rate, until 10 MHz. This implies the huge amount of 10 milion measurement values per second per channel, which has to be processed in real-time. Therefore, a dedicated software (Fig. 3.14) with an appropriate calculation power is required. Result of these calculations is the feature extraction that is providing the above mentioned features (maximum amplitude, duration, rise-time . . .) for every hit in each channel.

Tasks of PC are: data acquisition and storage, data analysis, logical filetring, location calculations and clustering[1], statistics, and display the results (graphically and numerically).
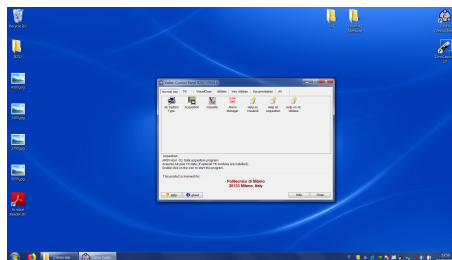
Figure 3.14: Vallen AE Software, Vallen Systeme

---

[1]highlight areas of high location density

3.2 Determination of Sound Velocity of Specimen's Material

Once all the measuring instruments have been installed, the first thing to do is to calculate the sound speed of the material of interest. As explained above, the phenomenon that must be measured concerns different elastic waves which can propagates through a solid. Their speed depends on the material properties (elastic and inertial characteristics) and also on the type of wave.

Sometimes, the wavelength becomes greater than the plate thickness. In this case, dominant motions of AE waves result in Lamb waves, instead of longitudinal and traverse waves. Therefore, it is necessary to pay a particular attention to selecting the correct velocity for locating AE sources.

Although the theory provides us a law to calculate the speed of sound for each material, this usually does not exactly correspond to the real one. In fact, C also depends on other factors: environmental conditions (temperatures...), exact chemical composition (pure substances are used only for research, not in the industrial field), chemical imperfections (grain structure...) and geometric, measurement uncertainty...For these reasons it is always necessary to measure and verify the real speed of sound in a given component in order to have precise measurements.

To calculate the speed of sound, it is sufficient to apply two piezoelectric sensors: one in transmission mode, generates a pulse that is recorded by the other sensor in reception mode. Knowing the distance between the two sensors and the time delay of the impulse's arrival, the speed of sound in that material is equal to $C = space/time$.

The acquisition unit is able to generate an electrical pulse. Such a pulse can be used to excite the piezo element in the sensor, which will induce a surface displacement leading to excitation of a surface wave. The pulse is generated with a peak frequency around 180 KHz and since the speed of sound in aluminum is around 6350 m/s, it is obtained that wavelength λ is about 35 mm. Since the aluminum plate is 3 mm thick, the waves generated by the piezoelectric sensor are just Lamb waves; volume waves can't be generated. This result must be compared with the relative velocity of Lamb waves through *phase dispersion curves* for an aluminum plate, as illustred in Fig. 3.16. Blue curves labeled S0, S1, S2,... and A0, A1, A2,... represent the symmetric and anti-symmetric mode dispersion curves respectively, Cf. [8]. A symmetric wave mode is often described as "compressional",

showing thickness bulging and contracting; and an antisymmetric mode is known as "flexural", presenting constant-thickness flexing. Anyway, both modes present in-plane and out-of-plane displacement's components, with different magnitude dependenig of mode's type, frequency and thickness of plate.
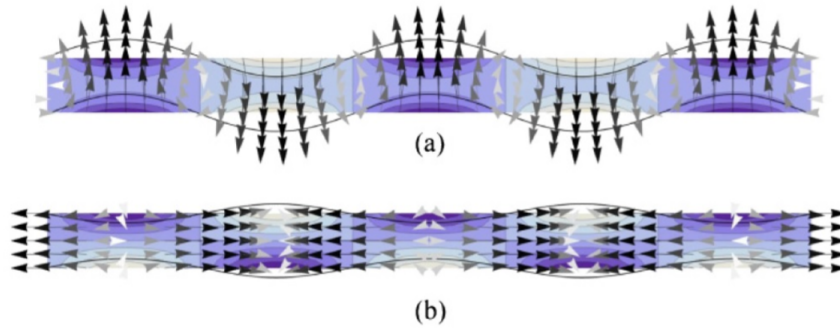
Figure 3.15: Illustration of the deformed plate, particle displacement and electrical potential for: (a) anti-symmetrical Lamb wave mode (A0) and (b) symmetrical Lamb wave mode (S0)

For the frequencies and thickness of the plate used, only the waves of order "0" are generated, while those of higher order do not appear. This makes the analysis of sensor responses easier because there are only two modes to overlap. The time delay between impulse and response is taken at the arrival of the first wave, that is S0 which is faster than the A0.

Several different tests were performed in different areas, with different sensors and different distances. This because sometimes, calculated C could be slightly different. By averaging the results we get the specific sound speed for the plate we use and it is $5485\,m/s$. This result corresponds to the velocity of the waves of Lamb "S0", which agrees to its phase dispersion curve, as can be seen from the graph above, in Fig. 3.16.

In this way, in addition to calculating the speed of sound, which is indispensable for the following phases, it is tested the sensors work properly in both modes (even if, from here until the end, only the reception mode will be used).
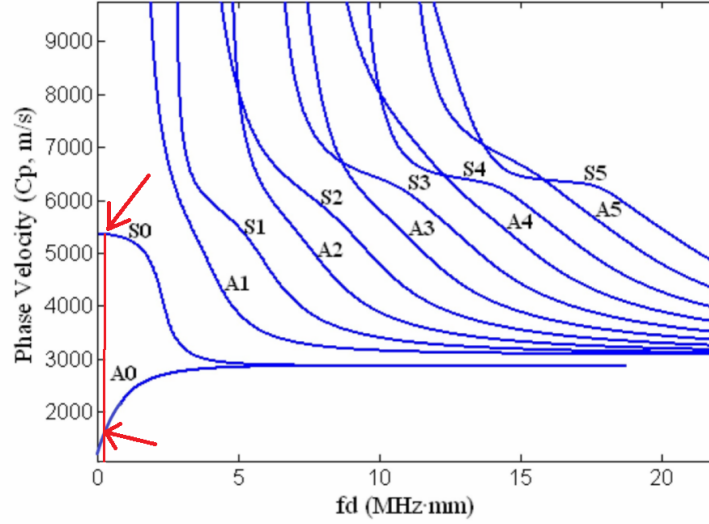
Figure 3.16: Phase velocity (C_P) dispersion curves for an aluminum plate. fd
is the product of ultrasonic frequency and plate thickness

3.3   Sensor Layout

Now that the location of an AE source has been shown and how impor-
tant it is to find the best possible setup, it is illustrated how the final setup
was achieved and then applied to the real piece during the experimental test.

It was decided to monitor crack propagation for a assumed length of
300 mm. A square (300 mm side) has been drawn on the plate, with
piezoelectric sensors positioned at the apexes. Along the two axes (per-
pendicular to the sides) two millimeter scales with a 5 mm step, have been
drawn, for a total of 61 points each. At each point of the millimeter scale,
an acoustic emission has been simulated with the pencil lead break. Since
the layout is symmetrical, the same procedure has been repeated for both
axes (expecting the same answer).

Not knowing if it is better to use 3 or 4 sensors to monitor, for each
acoustic event two *"virtual sensor networks"* will be created to locate the
source: 4 sensor square layout and 3 sensor right triangle layout. All 4
sensors are turned on and record, but for each configuration it has been
decided which responses use for localization. In this way, the simulated
event was the same for both and the localization error was only due to
the two different types of layout and not to all the other disturbance
phenomena or random noise. So, comparing the two localization results,
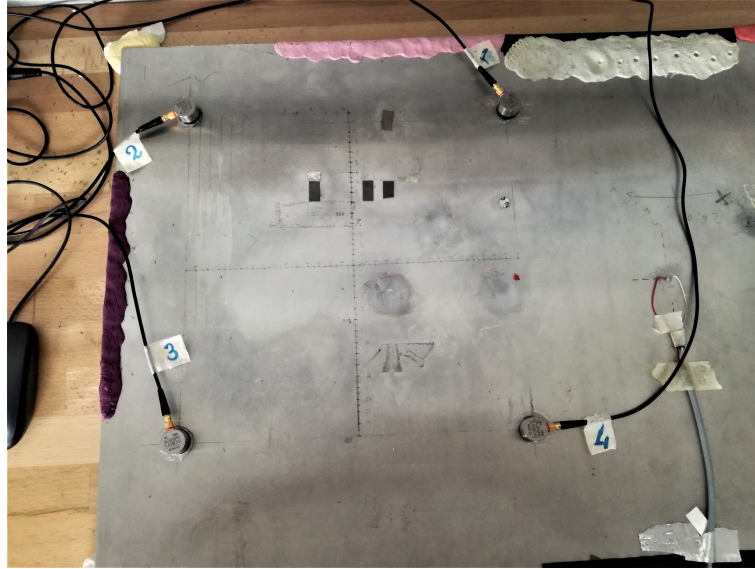
Figure 3.17: Sensors layout for AE simulation of best setting

it's easy understand clearly which layout is better.

Points located by the software have been saved and exported in Matlab for data analysis. In fact, knowing for each point the exact coordinates of the simulated acoustic source (with the pencil lead break) and those reconstructed by the software, it is possible to know the location error for each point, calculating it just as distance between the two points. Four complete tests for each axis were performed for a total of 488 points for each layout. This amount of data is sufficient to extract reliable statistical parameters that quantify the error numerically.

As mentioned in the previous section, the accuracy is different in every point of the monitored area. We do not need to know the localization error at any point with extreme accuracy because, even being in the laboratory, some disturbing factors are still present, influencing the measurement in addition to the measurement uncertainties, and many more data would also be needed. For this reason, it was decided to divide the monitored length into three parts, extracting statistical error parameters only for each zone.

As has been explained in the state of the art, the localization error changes from point to point. Calculating the error at each point, means performing several tests. To give a considerable meaning to statistical

results, it's needed to have a sufficient number of samples. In addition to a huge waste of test time, it is also useless to try to achieve such high precision. As will be seen in the next chapters, other factors will be equally influent on the localization. It is therefore, sufficient to divide the monitored area into three parts: two lateral and one central. This is a good balance between tests to be performed and localization precision.

Fig. 3.18 and Fig. 3.19 show results of one of the tests carried out (test $N°3$ on the horizontal axis) with the different localized points of the same event, the three zones in which the monitoring area was divided with the related parameters of mean μ and standard deviation σ.
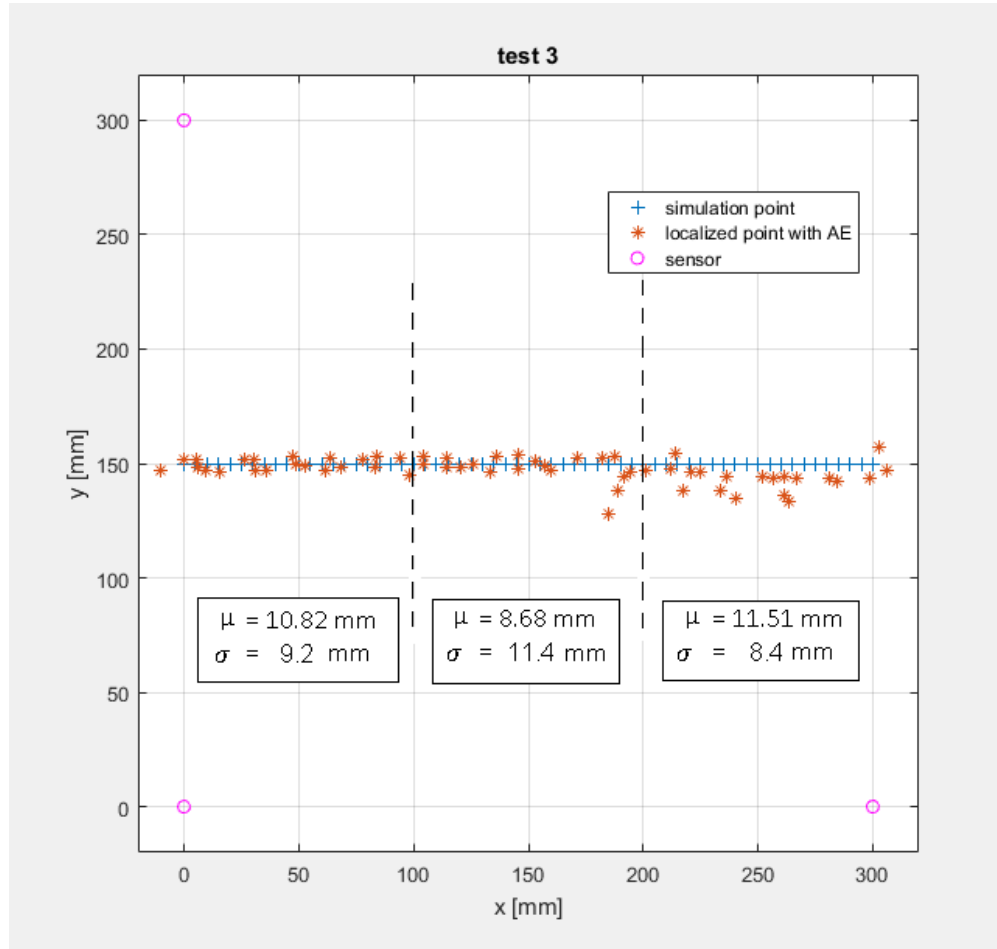
Figure 3.18: Results test 3-sensor layout, 300 mm x 300 mm monitored area

The left and central part of the graphs of both layouts show similar results: the μ values are very close even if the 4-sensors layout seems to be
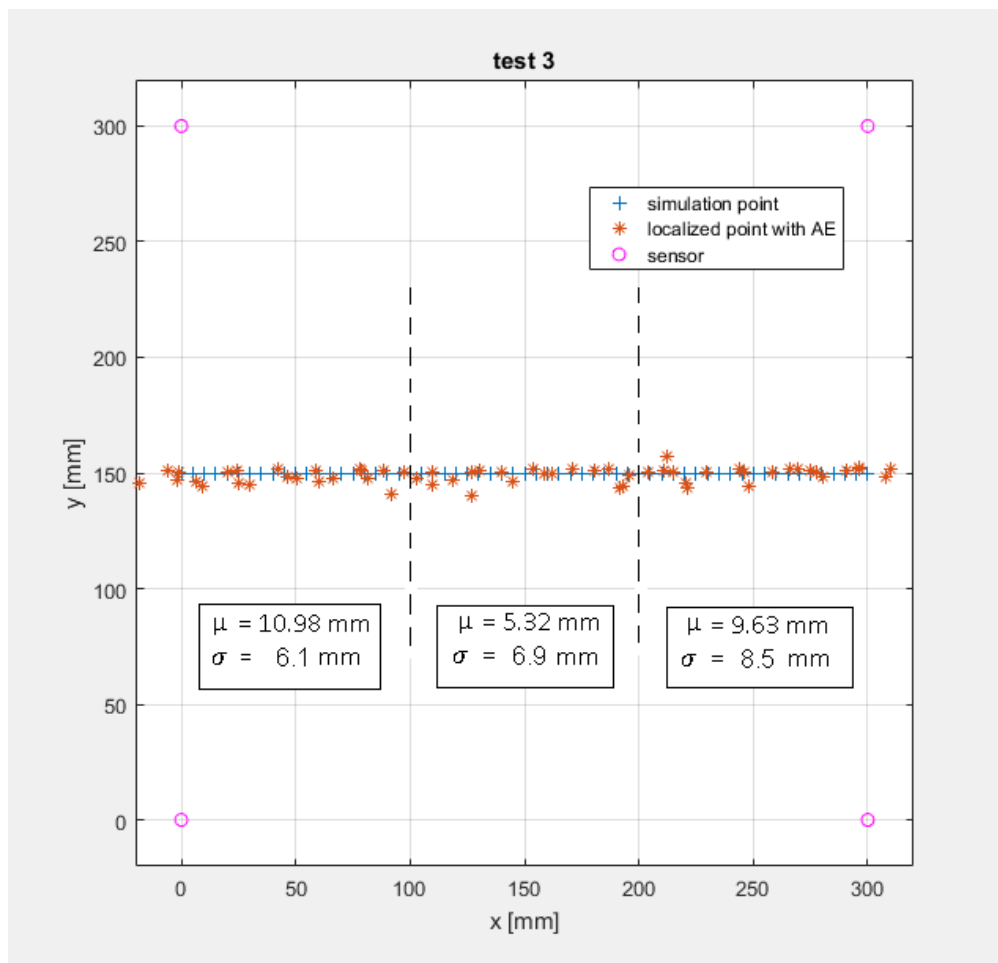
Figure 3.19: Results test 4-sensor layout, 300 mm x 300 mm monitored area

the best one, as confirmed by the numerical data, while the central sector appears as the most accurate one.

The right area in the 3-sensor layout instead, where the fourth sensor is missing, clearly shows that the points located by the software are much less accurate and precise. The μ of the localization error is 11.51 mm against 9.63 mm with four sensors.

Using a fourth sensor gives slightly better results, but especially a constant precision along the entire length of the crack, even in the *"termianl tail"* of the monitoring area.

The results of the 4-sensor layout are symmetrical, this is because the problem, differently from the 3-sensor layout, is symmetrical, providing positive feedback on the reliability of the results and how the measurements were made.

Tab. 3.1 summarizes the total value of μ for the two different layouts, showing a first impression that the 4-sensor layout is the best.

Parameter	3 sensors	4 sensors
μ **[mm]**	10.36	9.18
σ **[mm]**	9.7	7.2

Table 3.1: Error Localization μ, 300 mm x 300 mm monitored area

Once the necessary number of sensors has been established and the latter configuration is the best for our situation, we have worked on changing another parameter: the size of the square to be monitored.

It was decided to halve the size of the square'side (Fig. 3.20) to see how precision in localization changes. Being sensors closer to the AE source, we expect they record the acoustic waves better and, being the geometric distances between the sensors smaller, the areas of the hyperboles used to locate the source are narrower, resulting in a better localization. At this point, the side of the monitored square is 150 mm and the same test procedure has been repeated.

Even if it has already been understood that the configuration with 4 sensors is the best, also in this test, with sensors closer, the same analysis have been performed with both 3 and 4 sensor layouts to confirm the previous data. Below in Fig. 3.21 and i Fig. 3.22, are shown one of the tests performed with the related statistical parameters.

In this configuration, with closer sensors, it can be seen that the localization improves a lot in general in both layouts. This means that, if sensors are closer, the location is more accurate.
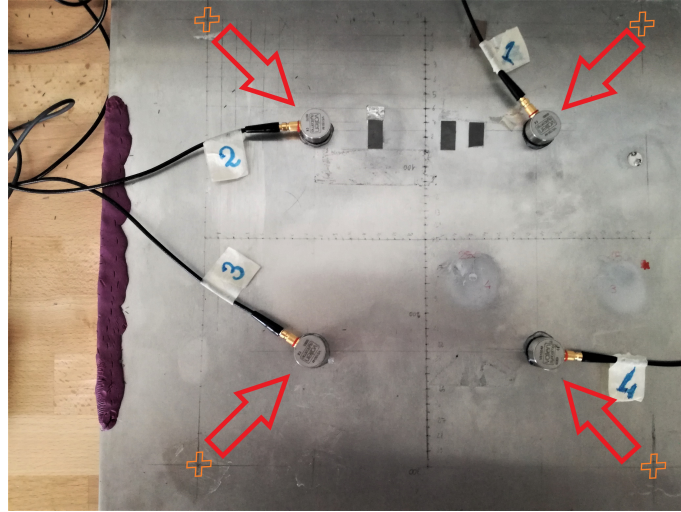
Figure 3.20: Sensors layout with halved monitoring distance

Parameter	3 sensors	4 sensors
μ [mm]	5.92	3.82
σ [mm]	4.7	3.1

Table 3.2: Error Localization μ, 150 mm x 150 mm monitored area
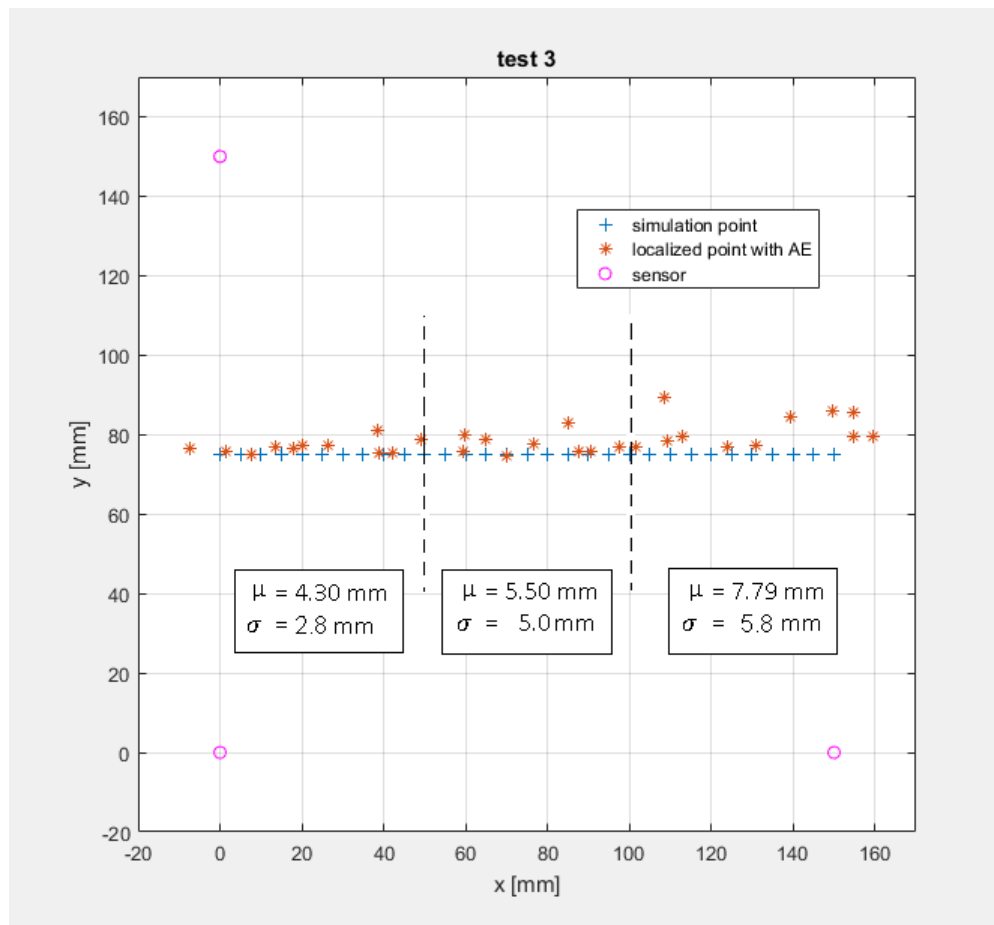
Figure 3.21: Results test 3-sensor layout, 150 mm x 150 mml monitored area
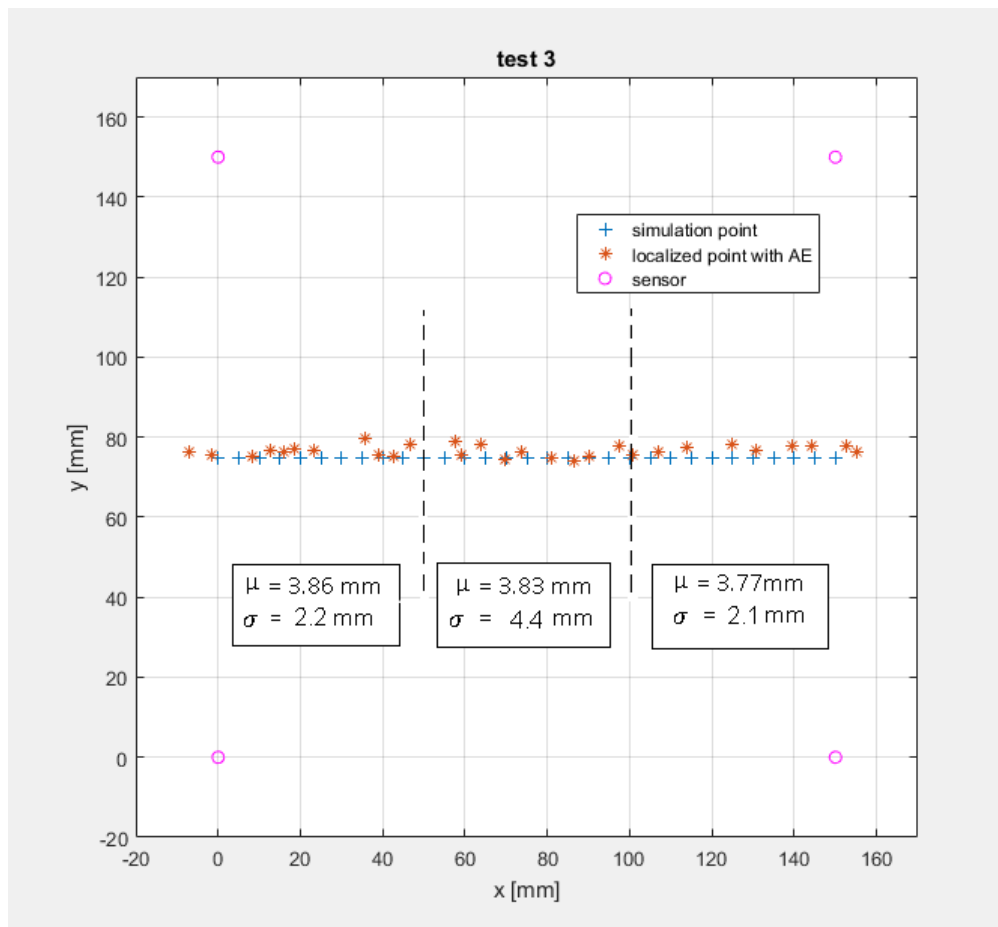
Figure 3.22: Results test 3-sensor layout, 150 mm x 150 mm monitored area

It can be noted that in the 3-sensor layout the same behavior always occurs: in the lateral sector, where one of the sensors is missing, the data are more dispersed. Instead in the 4-sensor layout, the error is more or less constant along all the length and remains more precise in the central sector. This confirms the results obtained with the 300 mm x 300 mm configuration.

Fig. 3.23 shows how the location error varies, point by point, in the 3-sensor layout for the 4 tests performed. It can be clearly seen that in the first part (on the left), where two nearby sensors are present, the error is contained and constant, never exceeding 10 mm. This means that the location is accurate. As the source approaches the opposite side (right), where only a nearby sensor is present, the trend of the error becomes increasingly irregular, with peaks even beyond 20 mm. In this area therefore, the location becomes less accurate and localized points have a greater dispersion.
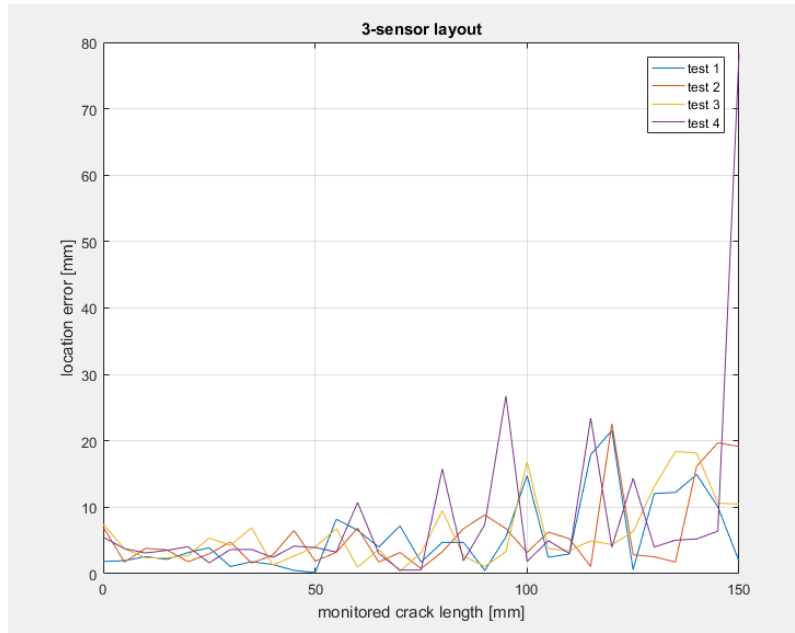
Figure 3.23: Location error along monitored crack length, 3-sensor layout

The Fig. 3.24 shows the same graph as the previous one but for 4-sensor layout. It can be seen how the error, for all the tests performed remains constant during the monitored length. Its width never exceeds 10 mm, remaining flattened on the x axis, which means low error and good localization accuracy. The few peaks present, which plenty exceed 50 mm,

are indications that the software localizes but it can be understood to be *"not relevant indications"*. It is clear they cannot be attributed to the real position of the source because they are too far away, and so they are easily eliminated with a distance filter. These peaks are erased from the data that are then analyzed, thus not affecting final results.
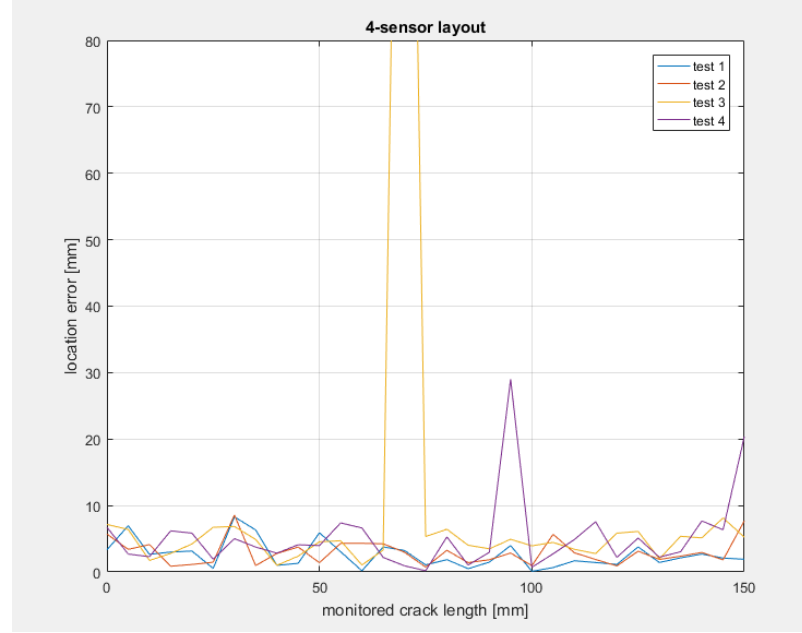
Figure 3.24: Location error along monitored crack length, 4-sensor layout

Fig. 3.25 compares the distribution of the error in locating both layouts. The graph shows the number of samples correlated with the size of the location error. A good localization system is identified with a distribution curve that has a sharp peak and is squeezed to the left in the graph. This means having lots of samples with a low error in a test. In Fig. 3.25 we note that the 4-sensor layout error distribution curve shows an evident peak on the left where the localization error is low, while the 3-sensor layout shows a more irregular trend. This graph shows in a different way, that the 4-sensor layout is the best.

Comparing results from error distribution along crack monitored length and Tab 3.2 with Tab 3.3 , it can therefore be definitively affirmed that the 4-sensor layout is better than that of 3-sensor one. Furthermore, the localization error obtained of 3.82 mm with 150 mm x 150 mm configuration can be considered sufficient for our application. This latter will be the starting configuration applied on the real beam for the fatigue test.
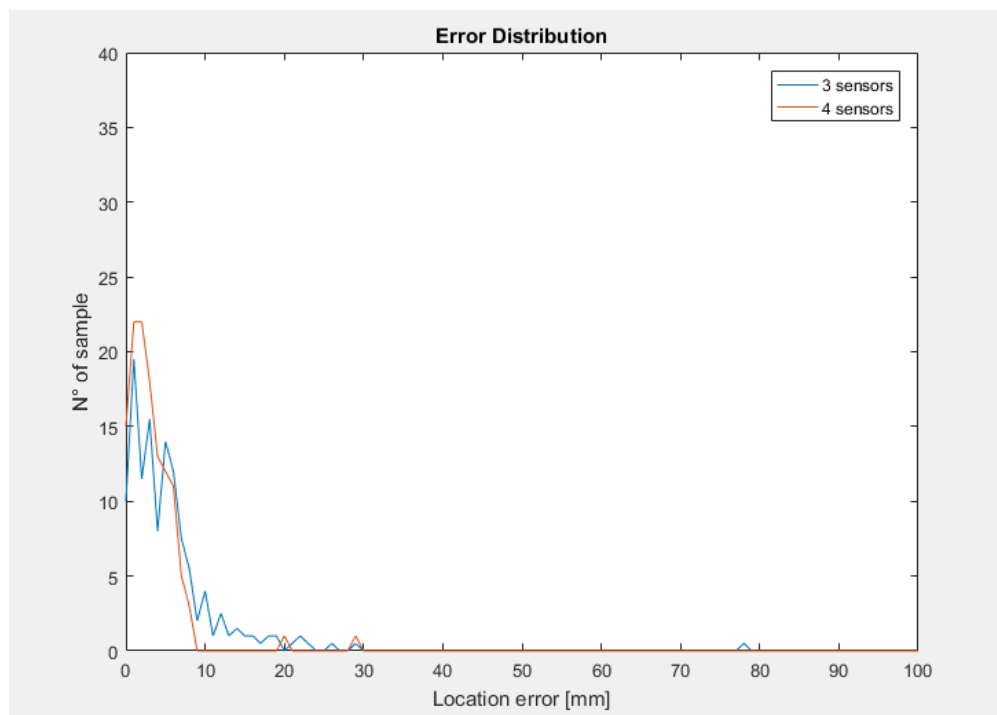
Figure 3.25: Location error ditribution, both layout, 150 mmx 150 mm configuration

Chapter 4

Fatigue Test

4.1 Test Specimen

The beam used in the laboratory must be as faithful as possible to that present in the field. The only information provided to us concerns the type of H section, indicative position of the crack in the beam, 15 mm thickness of the beam in that point, material of the beam composed of carbon steel with an external zinc coating (to protect it from external factors in the marine environment).

Among the various types of carbon steels available, an externally galvanized S355[1] / Fe510[2]/ A572 [3] (same material but different nomenclature) was chosen as required. Since the crack propagates along the core of the H-beam, the first type of beam with a core thickness of 15 mm was chosen from the catalog: HEM200 (geometry section can be seen in Fig 4.1).

Once the section and the material had been established, the length has to be chosen. For localization it is not important how long the crack is, it is sufficient sensors are close to the tip. In fact, only the tip of a crack emits acoustic waves, and therefore the entire previous part of the already cracked piece is not necessary. It should be chosen a significant length, sufficient to be monitored during crack propagation but not too long because it is useless. For this reason it has been decided to use 500 mm long samples.

---

[1]in accordance to EN 10025 : 1993 (new UNI standard)
[2]in accordance to EN 10025 : 1990 and UNI 7070 (old UNI standard)
[3]USA ASTM
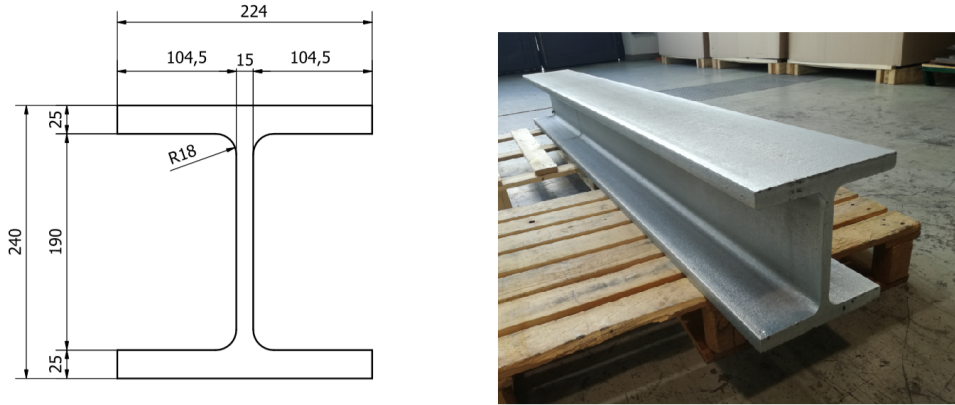
Figure 4.1: Section of HEM200 beam

4.2 Fatigue Test Description and Project Setup

4.2.1 Crack Mode

Now that the measurement system with AE has been defined, it has proceeded with the preparation of the fatigue test. First it has been decided how nuclear and propagate a fatigue crack in the HEM200 beam. There are three ways of applying a force to enable a crack to propagate:

- *Mode I fracture*
  When the load is applied in normal direction to the crack plane (opening mode)

- *Mode II fracture*
  When the applied load is an in-plane shear load (shear mode)

- *Mode III fracture*
  When the applied load is an out-of-plane shear load (tearing mode)

It has been chosen to use the mode I because it is the one that requires a lower load applied for the same value of Stress Intesity Factor K produced. Furthermore, mode I is the easiest to physically achieve, in terms of joints, frame and beam-actuator connection, since physical limits of the available
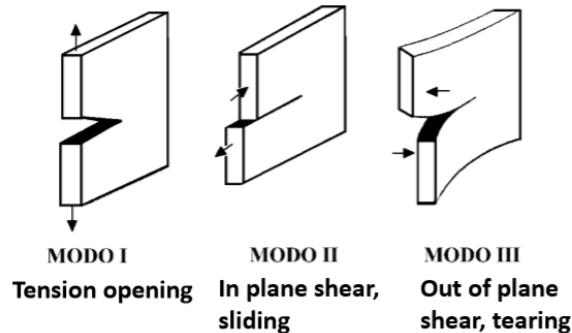
Figure 4.2: Fracture Mode of a specimen

supplies must be taken into account.

For the type of opening mode, there are several possible configurations that have different characteristics. Mainly they can be divided into two main categories:

- *Single edge notched*
  Crack started by the edge of the specimen, so there is only one crack tip that propagates in the piece.

- *Double edge notched*
  Crack can be inside the specimen or there are two cracks at the edge, in any case there are two crack tips.

The latter case is more complicated for monitoring the crack propagation because the two tips can propagate differently with different speeds. If double edge notched were used, the measurement system would mount only on a tip that probably will not propagate constantly during the test, due to the presence of the other twin tip. Choosing a single edge notched is the most reasoned and simple choice, since we have no particular need to use a double edge notched. In addition, a doubled edge notched requires the preparation, with machining, of two tips to be ready for the pre-cracking phase, and therefore requires more resources in terms of time. The management of two crack tips is more complicated, so the single edge notched has been chosen.

The idea is to create a specimen with the beam as similar as possible to the compact specimen. A notch is produced on one side in the core, to

facilitate the nucleation of the crack. On the same side, grips are designed to pull the traction beam perpendicular to the crack. PZT sensors for monitoring via AE will be applied on one side of the core.

4.2.2   Test Force and Components

To calculate the required force, laws of fracture mechanics must be used. The stress intensity factor K quantifies the severity of the crack situation. If the force is pulsating, to propagate the crack it must be:

$$\Delta K = \Delta K_{TH}$$

Where ΔK can be defined as:

$$\Delta K = F\Delta\sigma\sqrt{\pi \cdot a_0}$$

or as in Cf. [1] :

$$\Delta K = \frac{\Delta P}{t \cdot \sqrt{b}} \cdot f \tag{4.1}$$

where P is the tensile load applied, t is the thickness, b is the specimen length and f is the adimensional parameter (see Fig 2.1 in chapter 2). For our dimension compact specimen $f = 3.15$ (Cf. [1]).

In Cf. [9] are contained for S355 carbon steel:

- $\Delta K_{TH} = 22\,MPa\sqrt{m}$

- $\Delta K_{IC} = 108\,MPa\sqrt{m}$

So, from Eq. 4.1, it is get $\Delta P = 80\,KN$. It is always recommended to keep the test specimen during the test, without ever unloading it at 0 KN. So, an $R = \sigma_{min}/\sigma_{max} = 0.1$ has been used. For precautionary reasons, a project force of $100\,KN$ (equal to $\Delta K = 31MPa\sqrt{m}$) has been adopted, and all components of the test have been designed and verified to fatigue for this load value. So considering R value chosen, the applied tension force will be a sinusoid with maximum of 100 KN and a minimum of 10 KN.

Paris law has been used to calculate the time of test run:

$$\frac{da}{dN} = C\Delta K^m \tag{4.2}$$

Where a is the crack length, N the number of cycles, ΔK is $K_{max} - K_{min}$ applied, C and m are material parameter. In Cf. [9] are contained for S355 carbon steel:

- $C = 1.27 \cdot 10^{-12}$

- $m = 3.29$

From Eq. 4.2 is obtained 731772 cycles necessary to reach failure, with these load conditions. As it will be seen in the next chapter, this value will not be reached in any case.

An MTS actuator capable of generating the required dynamic force was used. The maximum force capable of exercising is $250\,KN$, much greater than that required. It is always advisable to have a large margin of available force greater than what you plan to use. It is always an estimate and, due to various uncertainties, may be required a greater force than what was initially assumed. Once the required power has been chosen, the actuator is chosen from the catalog: model number 244.31.
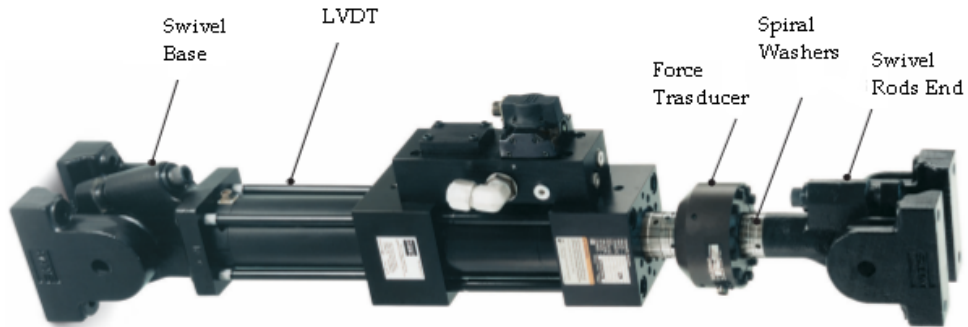
Figure 4.3: MTS 244.31 actuator's parts

Consequently, the holes in its pedestal base for bolting are standard and represent a constraint for the project, as seen in Fig. 4.4.

The best thing, would be to make the same holes on the HEM200 upper plate in order to bolt the pedestal base of the actuator directly to the beam. However, the HEM200 beam is too narrow to be drilled in the same points as the base of the actuator: the holes would be too close to the edge. It was decided to use an interface plate between the beam and the actuator (see Plate 2 in the appendix).
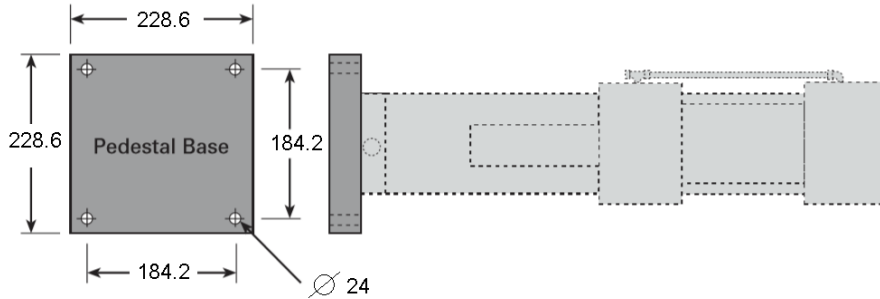
Figure 4.4: MTS 244.31 actuator's pedestal base geometry

On the other side of the beam, a joint must be positioned which allows to exchange only tensile forces between the beam and the actuator and not bending or cutting components. This is because the crack propagates perpendicularly to the main major stress. By exchanging only the traction component, the crack axis remains perpendicular to the direction of the actuator force, ensuring stable propagation along the beam axis. Model 249xx.M340 joint was used, capable of supporting $340\,KN$ (see Joint in appendix). The pitch of the joint holes represents a constraint for the project. Furthermore, joints need to be applied symmetrically if it want to avoid introducing cutting or bending actions into the HEM200 beam: therefore it is needed 4 joints. The two central joints cannot be fixed to the beam because they require drilling the beam too close to the core. The two external joints can be fixed directly to the HEM200 beam because the platband is sufficiently large. So it's not needed an interface plate here.

The beams that compose the external frame are HEB300 reinforced with ribs and holes with 150 mm pitch. To secure the two central joints with the HEB300 beam, a dedicated plate has been created (see Plate 1 in the appendix).

Joints are coupled with an externally hardened and grinded pin with a diameter of 60 mm. In Fig. 4.5 it can be seen the various pieces just described, still disassembled.

To prevent joints, attached to the two different components, from slipping along the axis of the pin, two 2 mm thick bushings were inserted between them. In the appendix it can be seen the setup assembly.

In Fig. 4.6 it can be seen the rendering of the test project, instead in Fig. 4.7 the test mounted in the laboratory.
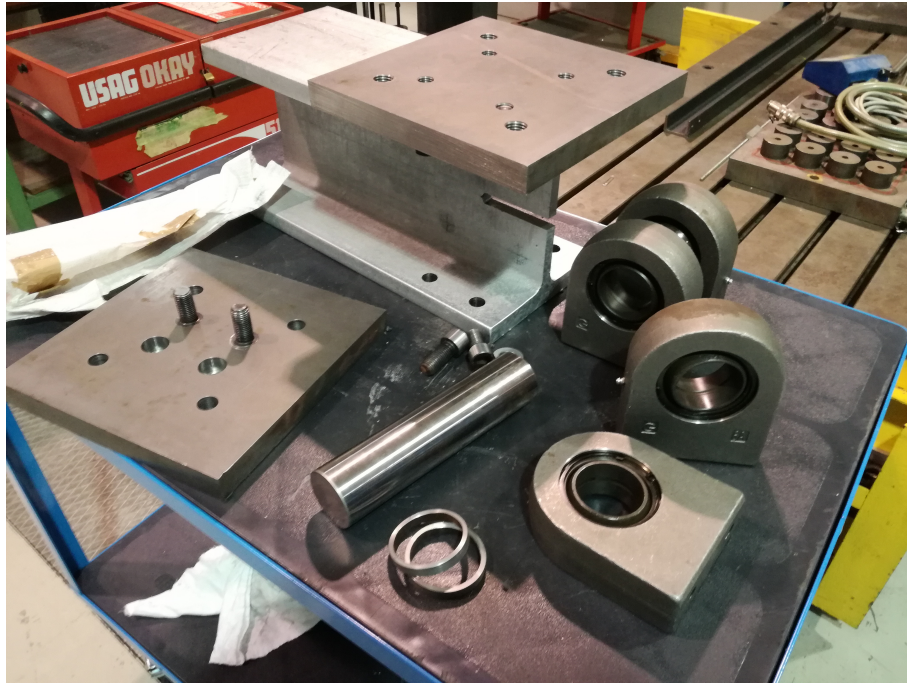
Figure 4.5: MTS 244.31 actuator's pedestal base geometry
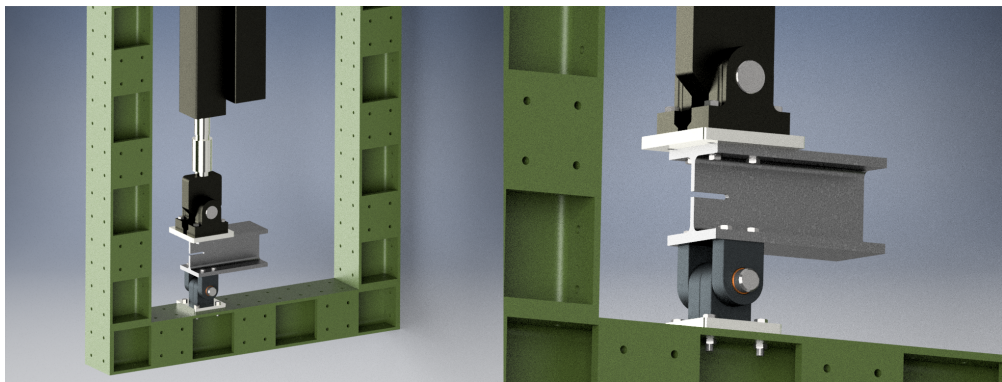
Figure 4.6: Render of test setup

Figure 4.7: Test setup

4.3   Preparation of the Specimen for Fatigue Test and AE Sensorization

As can be seen from Fig. 4.1, the plane face of the core is 15 mm thick. Considering that sensors have a diameter of 20 mm and that they cannot be applied exactly next to the fillet radius, a monitoring area of 150 mm x 150 mm cannot be applied for physical reasons. An area of 120 mm x 120 mm was used which is the largest possible.

This square area, which will be called the "monitoring cell", constitutes the basic unit of what will be a sensors'net (Fig. 4.8). When the crack is in the first cell (left), only the sensors that compose it (sens. 1-2-3-4) record the signals that will be used for localization. The other sensors (sens. 5 and 6) can be turned off or in any case do not contribute to the localization in this cell. As the crack advances and overpasses the cell, entering the next one (right), the sensors (sens. 2-4-5-6) of this one will record, while the others (sens. 1-3) will be turned off. There are two options: apply a network of sensors and turn on/off the sensors related to the cell of crack tip, or use only 4 sensors and move the monitoring cell following the crack.
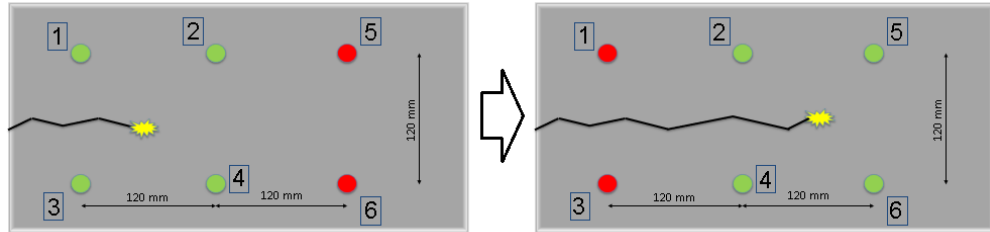
Figure 4.8: Monitoring sensors'net on/off mechanism: green turned on, red turned off

The data referring to the location obtained until this moment, refer to tests carried out with the pencil lead break on an aluminum plate. Before proceeding with the real fatigue test, it is necessary to verify a correspondence of these data on the HEM200 beam. In fact, some boundary conditions have changed: the material, the thickness and the distance between the sensors are different. The sensors were applied to the beam as shown in Fig. 4.9.

As long as the surface with the sensors remains horizontal, there are no problems. When the beam is placed on one of the flange (as it should

Figure 4.9: Sensor layout on HEM200 beam

be in the real test), the sensors, fixed with grease, slide down due to their weight. Since the material is steel, and therefore ferromagnetic, magnetic holders, specially supplied by Vallen Systeme, can be used to hold the sensors in place. This solution easily solves this problem, because they exert a considerable and constant force on the sensor, keeping it in position in any situation. In Fig. 4.10 it can be seen one of the uncovered sensors and the others on which the magnetic holders are applied. In Fig. 4.11 the final configuration of how the sensors will be applied to the beam can be seen.
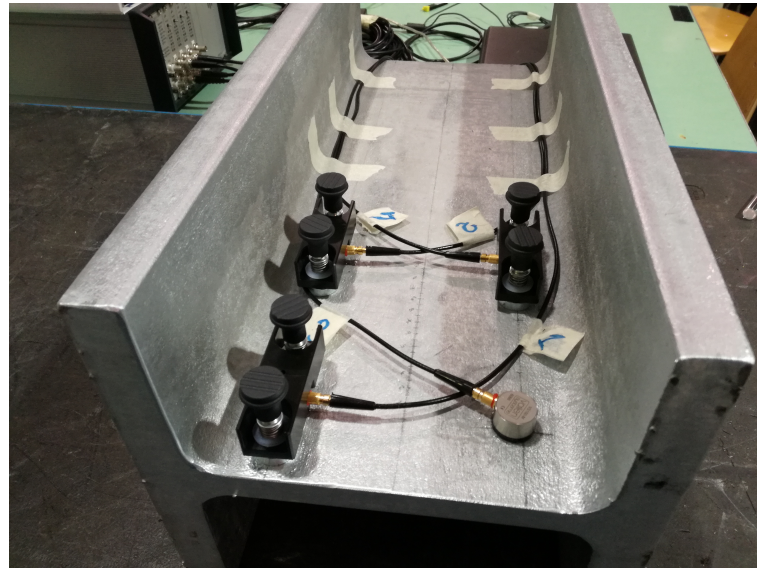
Figure 4.10: Sensors with magnetic holders applied on HEM200 beam

First we need to measure the speed of S0 waves in this carbon steel. After averaging measurements made at different points, a speed of 5420 m/s was obtained. Proceed by repeating the procedure done on the aluminium plate, positioning sensors, drawing a millimeter scale (this time on one axis is sufficient), artificial AE waves are simulated with the pencil lead break, responses are recorded with sensors and the position located by the software is compared with the one where the event was simulated, evaluating the error.

Figure 4.11: Final sensor layout on HEM200 beam for the fatigue test

4.3.1 Sensor Layout Check on HEM200 Beam Sensors'Side

Fig. 4.12 shows one of the tests conducted on the HEM200 beam. At first sight, it is clear that the location is very good; localized points are aligned along the axis distributed on a regular mode and very close to those where the event was simulated.

Tab. 4.1 shows the average location error is 1.74 mm in this configuration. The accuracy is excellent and allows for a very accurate and precise fatigue test.

Parameter	sensors'side
μ **[mm]**	1.74
σ **[mm]**	1.4

Table 4.1: Error Localization μ, 120 mm x 120 mm monitored area, sensors'side

The graph of the localization error distribution in Fig. 4.13 also clearly shows the high accuracy of this configuration. The peak is extremely sharp and flattened to the left axis and therefore, means almost all the localized points have a very low error.

Since up until now, there has been talk of 2-D localization on a flat surface, it must be kept in consideration that the problem is actually in
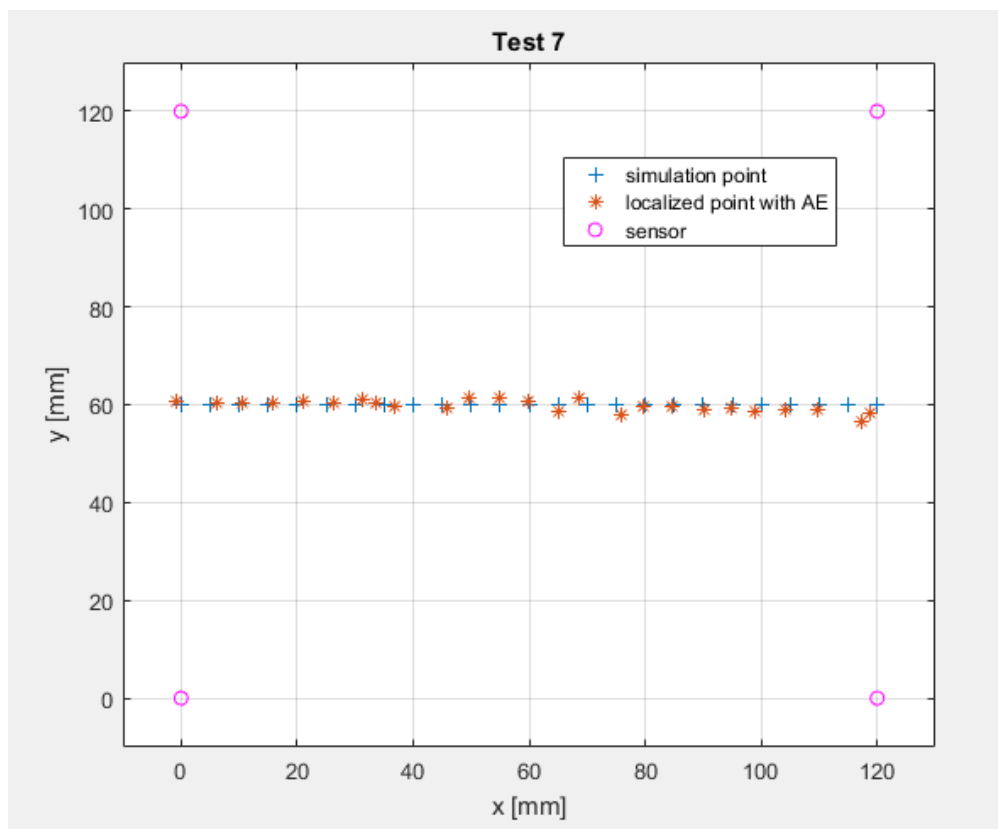
Figure 4.12: Test HEM200, 120 mm x 120 mm, sensors'side
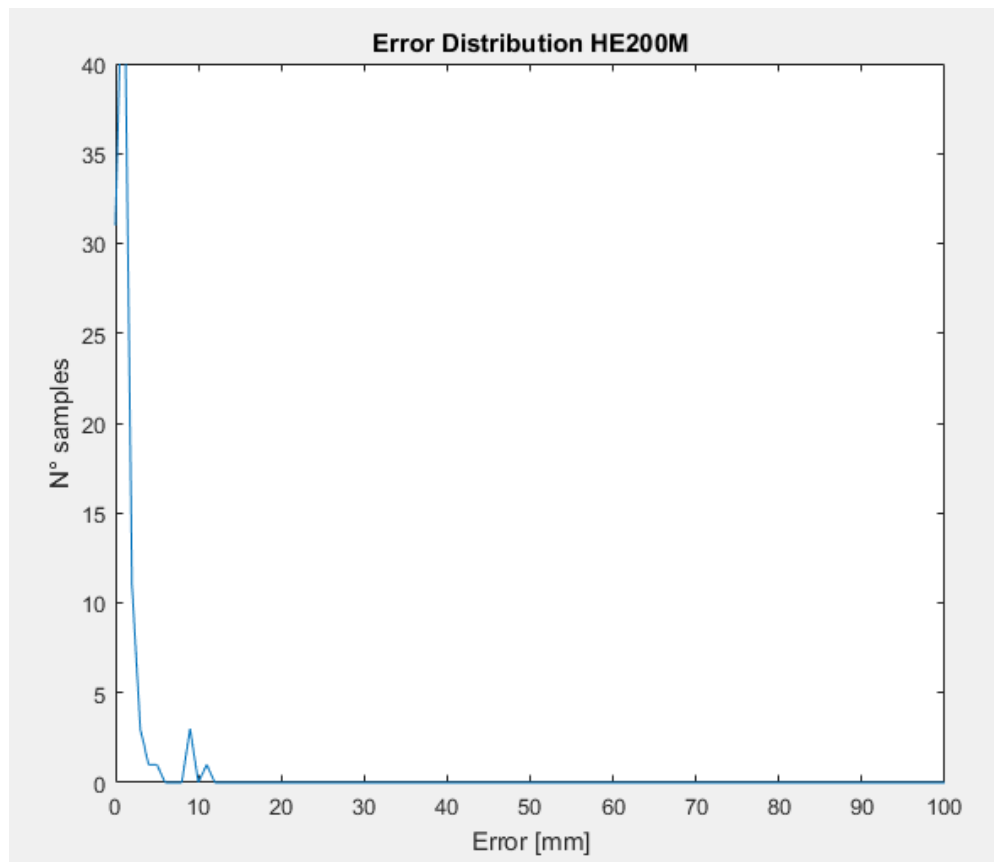
Figure 4.13: Error Distribution in HEM200, 120 mm x 120 mm, sensors'side

space, even if there are two predominant dimensions. In fact, for all the tests performed, the work surface has been approximated to an ideal 2-D surface, without taking into account its thickness. All simulations of AE waves with the pencil lead break, were performed on the same surface on which the sensors were applied. One must now ask oneself how the precision of the location changes, if the source of acoustic emission is not exactly on the surface of the sensors, but occurs in the thickness.

Physically, the phenomenon should not change because the Lamb waves formed, by definition, involve the whole thickness. The energy impulse due to the breaking of the carbon mine in the pencil, generates only Lamb waves if the thickness is sufficiently small. In fact, these develop in a symmetrical or anti-symmetrical way with respect to the axis of the plate, without referring to one of the two faces. However, the localization scheme set in the software is that of a flat surface, and small delays in arrival times due to thickness can decrease the accuracy of the location.

For this reason the same test, as the previous one, was performed but with the emission of AE waves, through pencil lead break, on the opposite side of the beam's core on which the sensors are applied. In this way, it can be understood how the location, due to the thickness, worsens and how much is in the case of maximum thickness (worst case, that is on the face opposite to the sensors).

4.3.2 Sensor Layout Check on HEM200 Beam Opposite Side to Sensors'one

Fig. 4.14 shows one of the tests conducted with the pencil lead break on the opposite side to the sensors. Localization is always very good. The localized points have good position and the same behavior as those on the face of the sensors. The average error is 2.71 mm which is slightly higher than the previous one, as expected. However it remains very low and content, and more than sufficient for our application.

Parameter	opposite side to sensors'one
μ [mm]	2.71
σ [mm]	1.9

Table 4.2: Error Localization μ, 120 mm x 120 mm monitored area, opposite side to sensors'one
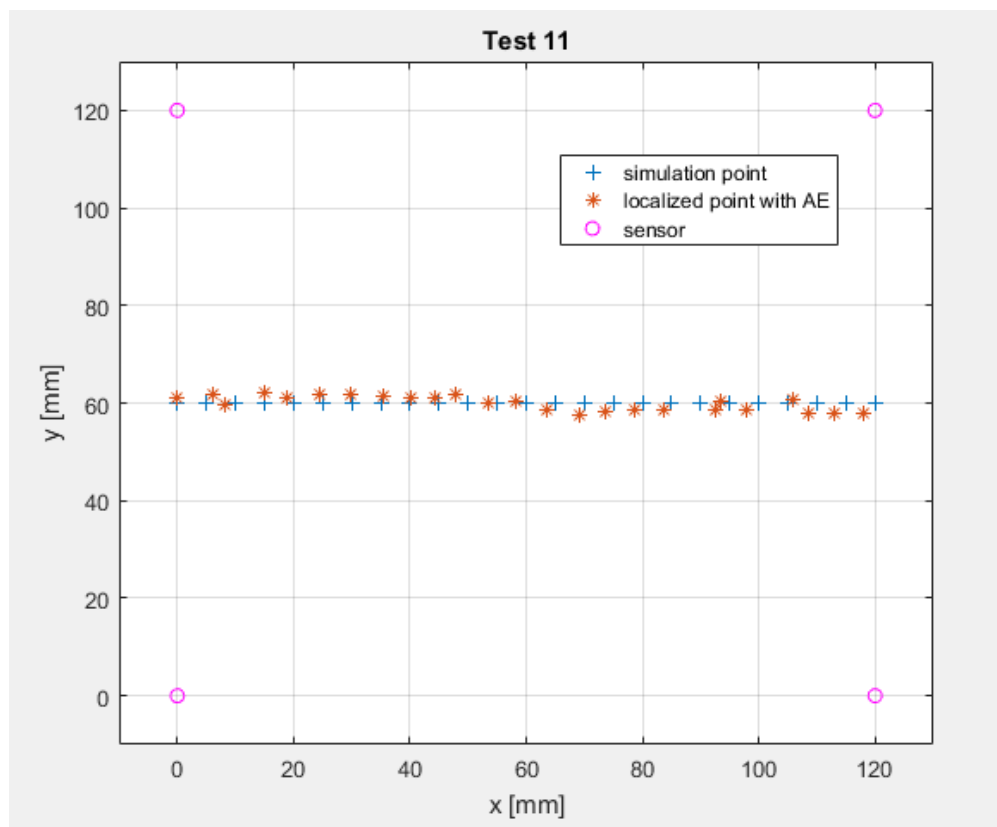
Figure 4.14: Test HEM200, 120 mm x 120 mm, opposite side to sensors'one

Fig. 4.15 shows the variation of the localization error on the tests carried out on the face opposite to that of sensors. The peak of the samples is always very sharp and flattened on the left, at low error values. This, further confirms that tests are good with low data dispersion.
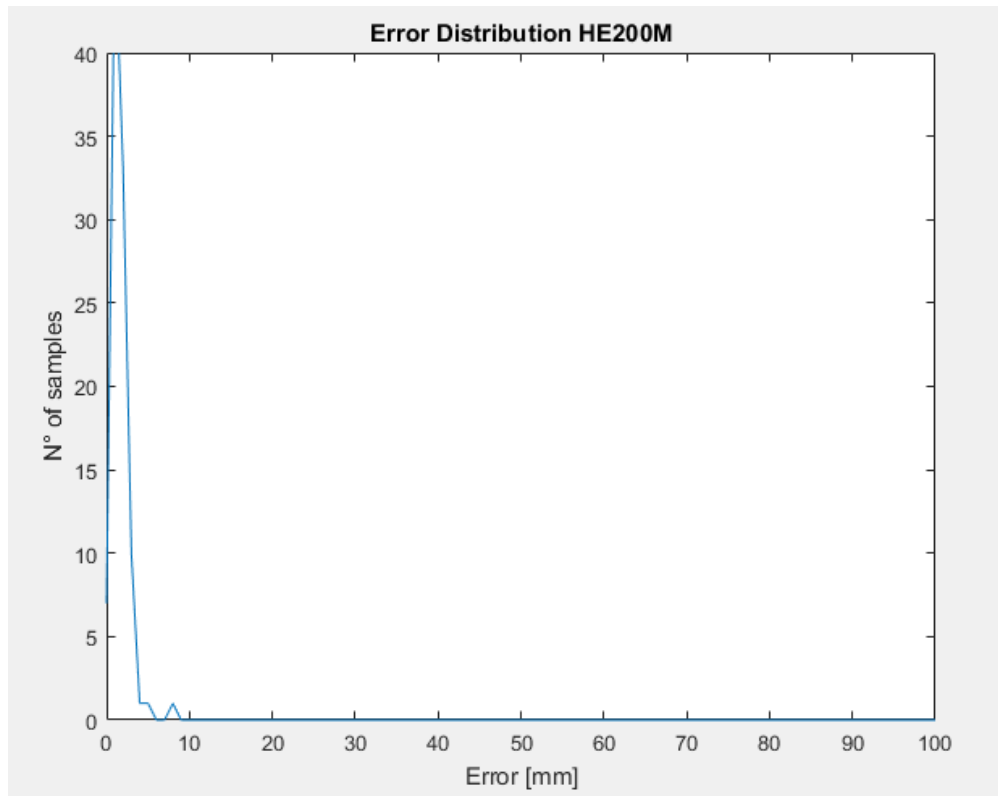
Figure 4.15: Error Distribution in HEM200, 120 mm x 120 mm, opposite side to sensors'one

The quantity and quality of the data obtained until now, can be considered sufficient. The configuration identified and tested on the steel beam, therefore with the same conditions and parameters of the fatigue test, has given satisfactory results. The measurement system arranged for the AE and its setup have reached a very good level of accuracy. The research part of the best sensors'configuration for monitoring of fatigue crack propagation with the AE can therefore be considered completed.

4.3.3   Preparation of Specimen for Test

Before being assembled for testing, the HEM200 beam requires further processing to decrease the angle of the notch tip. In fact this, for a technological limit of machining, is still too smooth to induce quickly a crack. More acute is the angle, shorter is the crack nucleation period. A special blade, with a diamond paste applied on it, was used to create a notch. The combination of blade and diamond paste, through movement, produces an incision with a much smaller radius, creating an overall sharper notch. In Fig. 4.16 it can be seen the processing with the blade. In Fig.4.17 can be seen the different sharpness of notch tip, before and after machining.
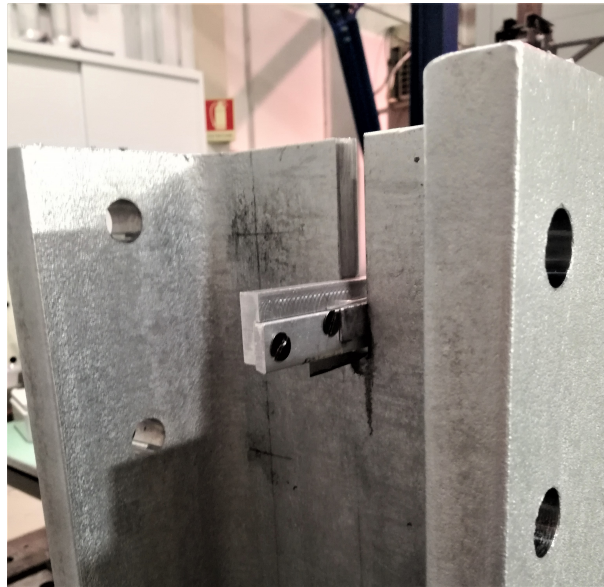
Figure 4.16: Notch machining with blade and diamond paste

4.4   Test Execution

Sensors have been mounted on the HEM200 beam as in the previous tests. The tip of the notch has held at the edge of the sensor layout. As the crack advances, crossing the whole area useful for monitoring, sensors will also be moved. Sensor cables must be fixed with the tape so that:

- They don't move during the test (if they bend, they create elettrical noise).

Figure 4.17: Left part: notch not machining yet. Right part: notch after blade machining

- They don't obstruct the view of the crack because a visual inspection must be carried out periodically.

Before starting the test, it must be checked that everything is connected correctly and functioning with the laed pencil break. Be sure that sensors are well coupled to the beam with grease, that they all receive the signal correctly, that the contact of the cables is perfect ... before starting the test. If the points where the pen lead is broken are correctly located by the software, then it means that everything has been assembled correctly and the test can be started.

As calculated, the optimal load for obtaining tests with sufficient useful data but with a reasonable duration, is a sinusoid that oscillates between a maximum value of 100 KN and a minimum of 10 KN with a frequency of 1Hz.

Every 10000 cycles, the test was stopped to inspect the beam. In fact, it is necessary to have certain information on the position of the crack's tip to be able to compare it with the data obtained from the location of the Vallen Systeme. The only way to know exactly where is the source of acoustic events, is by performing a visual check: a simple Visual Testing (VT) is not enough, it is needed to use a Magnetic Testing (MT). Considering the accuracy to be achieved and the characteristics of our specimen, MT with fluorescent liquids is the most suitable non-destructive testing.

4.4.1   Magnetic Testing

The examination with magnetic particles (also known as magnetoscopy) exploits the phenomenon of ferromagnetism. It is suitable for identifying surface and sub-surface defects such as cracks in ferromagnetic materials. During the inspection, a magnetic field is induced in the piece. A discontinuity has magnetic permeability different from ferromagnetic materials, therefore, in correspondence of a defect, a dispersed flow is created, capable of attracting suitable magnetic powders sprayed on the surface of the piece and used as a detector. Magnetic particles are:

- *Fluorescent*: maximum color contrast which however requires a dark environment and an ultraviolet LED light to be seen.

- *In liquid suspension* made up of magnetite (Fe_3O_4) chopped: grain size which guarantees maximum sensitivity.

An electromagnet was used to magnetize the beam. It is a portable and handy equipment. It consists of segments in soft iron magnetically excited by an electrical circuit. Magnetization is localized between and around the contact regions of the poles. Magnetic induction is directed from one pole to another, making it suitable for identifying defects perpendicular to the joining point of contact of the poles. Although it is already known the orientation of the crack, it is still indicated to magnetize the inspection surface twice, with the two directions of the poles perpendicular to each other. In Fig. 4.18 it can be seen how a defect changes the magnetic field in the material.
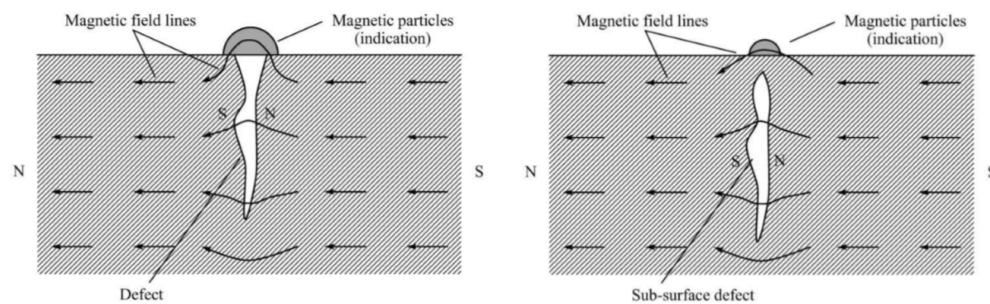
Figure 4.18: Interaction between magentic filed and a defect

4.4.2 Inspection Technique

- *Workpiece preparation*
  The external surface galvanization of the workpiece hinders the
  Magneting Testing method because Zinc is not ferromagnetic and
  prevents the magnetization of the underlying steel. Furthermore,
  the galvanizing surface has a too high roughness and therefore does
  not allow magnetic particles to move easily. They remain trapped
  between the valleys of the surface, unable to follow the magnetic field.
  With a grinding wheel the external galvanization is removed and the
  surface made smooth, then it is cleaned with a rag and solvent to
  remove all the dust (Fig. 4.19, Fig.4.20, Fig. 4.21).

Figure 4.19: Removal of the zinc layer with the grinding wheel

- *Application of magnetic particles*
  The liquid suspension with fluorescent magnetic particles is applied
  to the surface with a spray can (Fig. 4.22).

- *Magnetization*
  The piece is magnetized with the electromagnet. The connecting line
  of the two poles must be perpendicular to the crack (Fig. 4.23).

- *Observation and measurement*
  Through an ultraviolet LED light, the crack and its tip can be
  perfectly identified. It is necessary that there is no light intensity
  greater than 20 lux in the environment. In fact, only in a dark
  room fluorescent particles can be seen with ultraviolet light. Using a

Figure 4.20: Application of cleaner remover

Figure 4.21: Cleaning the surface with a cloth

Figure 4.22: Application of fluorescent magnetic particles

Figure 4.23: Piece magnetization

magnetic ruler that is simply placed on the beam, the length of the crack is measured and photographed (Fig. 4.24 anf Fig. 4.25).
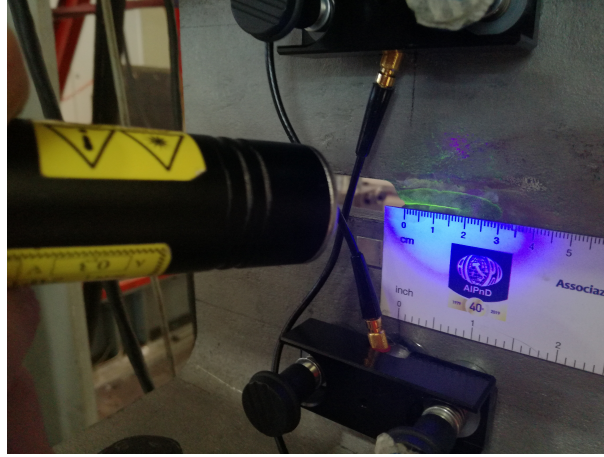
Figure 4.24: Observation and measurement
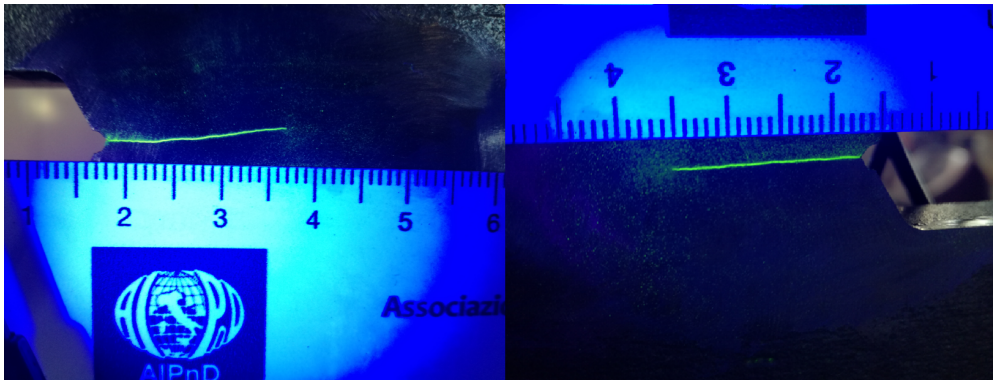
Figure 4.25: Crack length measurement with ultraviolet light, 71108 cycles

The procedure is carried out each time on both sides of the beam.

4.4.3   Test Evolution

Fig. 4.26 shows how the length of the crack, measured from both sides, changes with the number of cycles: its length increases exponentially, Cf.[3]. This occurs because during the test, the control of the actuator was set on the force, which was kept constant between $100\,KN$ and $10\,KN$. So, with

the same load, the crack length increases with time and consequently the *Strees Intenisty Factor K* increases according to the law:

$$K_I = Y\sigma\sqrt{\pi a}$$
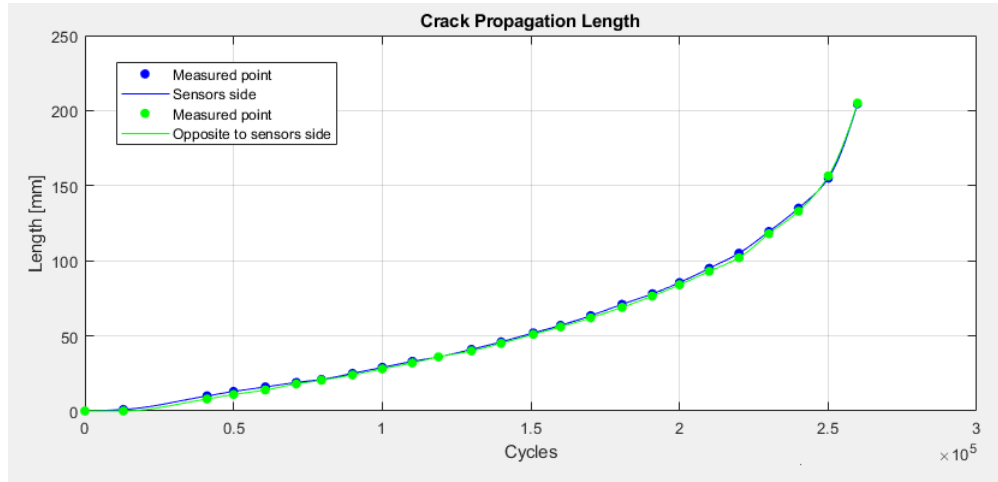
Figure 4.26: Crack length according to the number of cycles, Test

Crack has not propagated perfectly horizontally but obliquely upwards. At a length of about $120 - 130\ mm$ it has deviated sharply upwards leaving the sensor layout, arriving under the flange (see Fig. 4.27). During the design phase, it was expected that the crack would advance horizontally because there are only traction forces and the direction of the crack occurs transversely to the main major stress. This evidently hasn't happened and deviated upwards.

One possible explanation is that the constraints used have not behaved like ideal constraints. In fact, the tolerance between pin and joints, under the beam, was very tight. It is likely that joint generated friction during its rotation, introducing stresses in the beam that had not been foreseen.

In this way, crack has advanced upwards, leaving the monitoring area, arriving at a critical zone, from the point of view of the integrity of the HEM200 beam. At the same time, the crack was spreading very quickly and has entered in the *Instability Propagation Zone*. So at this point, i.e. at 259885 cycles, the test of the specimen was stopped and deemed concluded.

Fig. 4.27 shows crack and its path in the HEM200 beam at the end of the test.
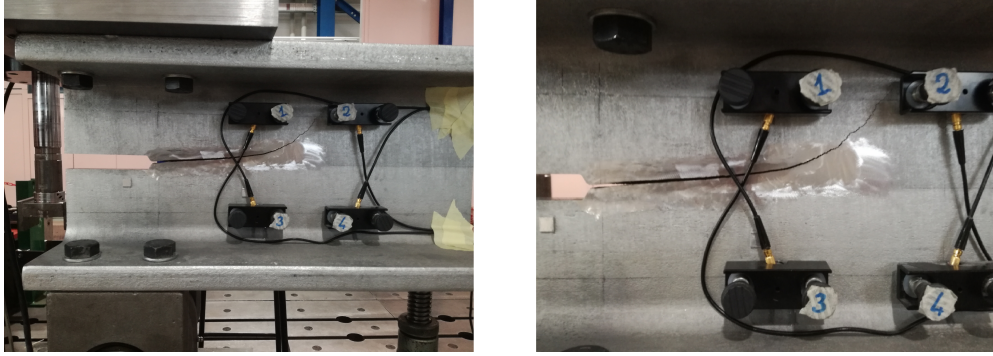
Figure 4.27: Crack path at the end of the test

4.5 Test Raw Results

The Vallen Systeme software acquires the acoustic waves arriving at the PZT sensors, only when they exceed a fixed threshold set at $1\,mV$. When at least three of the four sensors, record a wave in a very limited time interval, the software recognizes these recordings as waves emitted by a single acoustic source. The instant in which the wave passed the threshold for the first time is taken as the arrival time of the wave to the relative sensor. Knowing the arrival times and the position of the sensors, the software reconstructs the position of the acoustic source and places it in the layout map.

Fig. 4.28 shows the "rough" results of the test provided by the Vallen Systeme: the position of the sensors is indicated with red crosses. They are six but only four sensors have been used: initially only those at the vertices of the left cell were turned on. Once the crack tip has passed this monitoring area, those that make up the right cell have been turned on. Each blue dot represents an acoustic source, in this graph no filter has been applied, it is sufficient that the acoustic wave has exceeded the $1\,mV$ threshold at least one time.

Since most of the signals are not impulses due to the propagation of the crack but due to external noise (friction, external sources . . .) it is necessary to be able to distinguish signals due to the phenomenon of interest from false indications. In the Vallen Systeme software it is possible
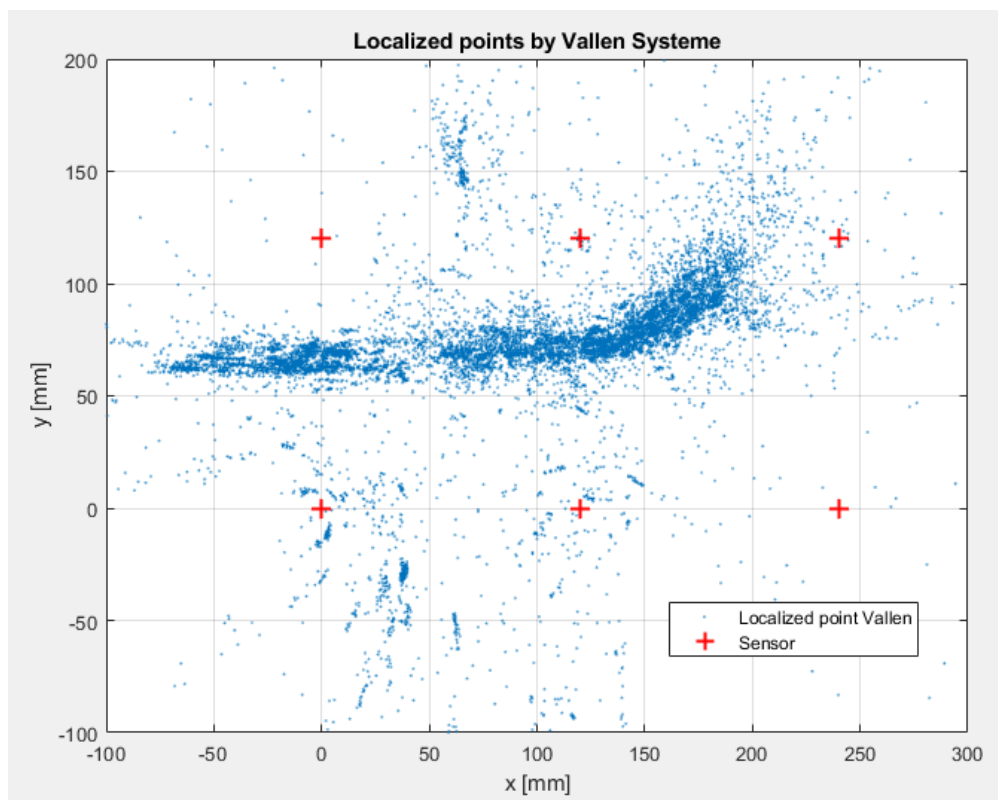
Figure 4.28: Vallen Systeme test results

set some filters on the waveform parameters to eliminate some acoustic signals. The following filters have been set:

- Energy $E > 1000 \ eu = 1 \cdot 10^{-15} \ J$

- Rise Time $R < 400 \ \mu s$

- Duration $D > 300 \ \mu s$

It consists of a first "raw" skimming, but signals that are clearly due to external noise and do not concern the propagation of the crack are eliminated. Fig. 4.29 shows the same graph above, but with these filters applied on the waveform parameters.
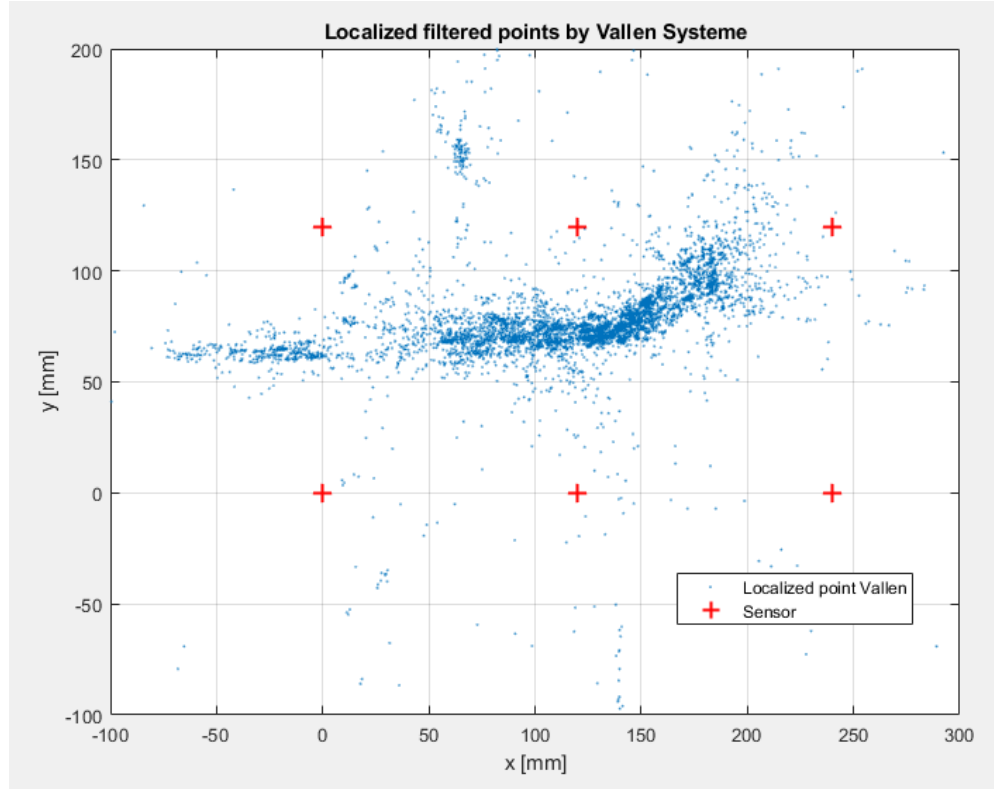
Figure 4.29: Vallen Systeme test results with filtered waveform parameters

At first sight it's easy see a group of points that retraces the path made by the crack. However, it is also easily noted that the accuracy of the localized points is much lower than those simulated with the lead pencil break. This is due to several explanations:

- HEM200 beam is not stationary but moves: this generates background noise which makes it difficult to understand the exact moment in which the acoustic wave arrives

- Acoustic wave generated by the crack is much less intense than one simulated with the leadpencil break, so the arrival of the wave is less pronounced (also due to the presence of high background noise)

- Generation of acoustic waves of the crack is not as stable and repeatable as that of the lead pencil break, a certain degree of uncertainty is always present

The results of the localization of Fig. 4.29 provided by the Vallen Systeme are summarized in the following table (Tab. 4.3):

Parameter	Vallen results
μ [mm]	52.1
σ [mm]	34.1

Table 4.3: Localization accurcy of Vallen Systeme, with a fixed threshold set on 1 mV

The histogram in Fig. 4.30 helps to better understand the error distribution. It illustrates how the localized points are distributed in relation to their error of localization. As mentioned earlier, a good location should have a sharp and flattened curve to the left.

This result is not satisfactory enough, although an increase in error was natural, given the complexity of the real phenomenon. An accurate analysis of the data collected is required to try to achieve greater accuracy. Post processing data is necessary to better explain these results and try to increase the final result.
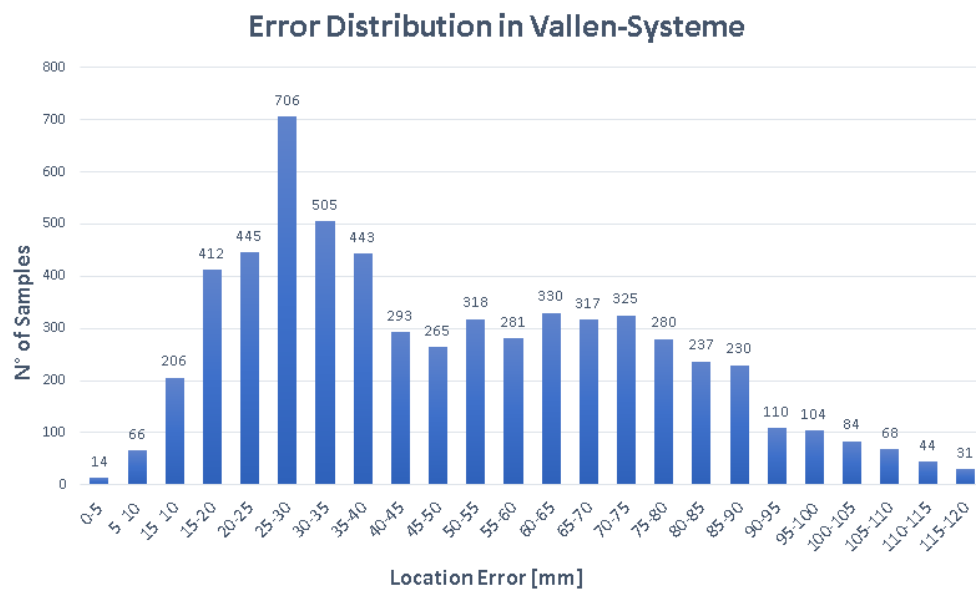
Figure 4.30: Error distribution of Vallen results

Chapter 5

Post Processing Data and Comments

The Vallen Systeme has many filters and settings on the acquisition parameters. However, it is not possible to change the arrival time of the acoustic wave once it has been recorded. In this software, the arrival time corresponds to the instant in which the signal exceeds a fixed threshold set before recording. This threshold cannot be changed during post processing data and therefore also the arrival time cannot be changed. Furthermore, it is not possible to understand how the software calculates the position of the acoustic source starting from the arrival times. This is because the Vallen Systeme is a commercial software, and therefore it is conceived as a "closed package": it is possible to set only some input parameters and it is not possible to see algorithms and logical steps it carries out.

To carry out an effective post processing data, it is necessary to have a greater possibility to manipulate the recorded data, to modify the arrival time, identifying the best one. Consequently, a software capable of calculating the position of the acoustic source will be needed, starting from the arrival times. Therefore, it is necessary perform post processing data independently from the Vallen Systeme, with autonomous Matlab algorithms.

From this point, an additional filter in Matlab has been applied to those already listed of energy, rise time and duration. Only signals that have a signal-to-noise ratio $S/N > 20$ will be considered. S is the maximum absolute amplitude of the entire recorded signal, and N is the maximum absolute amplitude of the first $20\,\mu s$ of the recorded noise (first $20\,\mu s$ of the recorded signal). For the acoustic emissions recorded during the HEM200 destructive test, the ratio was required to be $S/N > 20$ to consider the

transient signal "pulsive" enough.

The first step was to program a localization algorithm.

5.1 Localization Algorithm

Generally localization methods are applied as described in the following. The arrival time is measured at each sensor and is used as the reference value for a calculated arrival time. The calculated arrival time is computed from a trial or a "guesse" location and a user-defined velocity model. The location guess is corrected using the residuals (or difference) between the measured and calculated arrival time. The calculated arrival time t_i^c can be written as:

$$t_i^c = t(x_i, y_i, z_i, x_0, y_0, z_0) + t_0 \qquad (5.1)$$

The calculated arrival time is composed of the travel time t, which is a function of the location of the sensors (x_i, y_i, z_i) and the hypocenter (x_0, y_0, z_0), and the source time t_0. Since this equation consists of four unknowns, at least four arrival times are needed to determine the hypocenter and the origin time; three arrival times are necessary if only the epicenter and the arrival time are to be calculated. If n arrival times from n sensors are measured the system is over-determined because there are more knowns than unknowns. The over-determined system has to be solved in a way that the residuals ri between calculated and measured arrival time, at each sensor, are minimized.

$$r_i = t_i^0 - t_i^c = Min \qquad (5.2)$$

Several methods to solve this nonlinear problem exist but an iterative algorithm was used because it is the same method used by Vallen Systeme for localization. The various steps of the algorithm are explained in the next section.

5.1.1 Iterative Algorithm for Localization

An already existing localization algorithm and explained in Cf. [4], has been adopted by us. Its functioning is shown below.

The standard technique for localization is to linearize the problem. The equations used to calculate a location (hypocenter or source of an acoustic emission) are based on the assumptions that the material is homogeneous and isotropic and that the AE source resembles a point source. If this is

not the case, the following approach is not valid and another one has to be choosen.

Two dimensional localization requires the onset times from at least 3 sensors. The most common approach is to use an iterative localization algorithm, which requires the linearization of the problem. To do this, a "first guess" or trial hypocenter (x_0, y_0, t_0) is required. This first guess hypocenter must lie relatively close to the true hypocenter, which is not known. The travel time residuals ri of the first guess hypocenter are then a linear function of the correction in hypocentral distance .

For smaller specimens, the middle of the specimen is an adequate choice for the first guess hypocenter. For larger specimens, the sensor which recorded the event first can be chosen.

In the case of acoustic emission analysis of steel beam, the material can be assumed to be homogeneous and isotropic. The travel times for localization can then be calculated using (see also Eq. 5.1):

$$t_i = \frac{\sqrt{(x - x_i)^2 + (y - y_i)^2}}{v} + t_0 \tag{5.3}$$

The coordinates (x, y) represent the point at which the travel time to each sensor (x_i, y_i) is calculated, i.e. the first guess of the hypocenter. The body wave velocity of the material is denoted by v and t_0 is the first guess origin time, which is taken as the centre point of the specimen. Due to the first guess hypocenter being a trial solution, the calculated travel times differ from the measured ones. A correction $(\Delta x, \Delta y, \Delta t)$ of the first guess hypocenter is needed to minimize the travel time residuals (see also Eq. 5.2). If the necessary corrections are relatively small, the travel time function (Eq. 5.3) can be linearized. Therefore, Eq. 5.3 can be approximated by a Taylor series, from which only the first term is used. Eq. 5.2 can be rewritten as:

$$r_i = \left(\frac{\partial t}{\partial x_i} \cdot \Delta x \right) + \left(\frac{\partial t}{\partial y_i} \cdot \Delta y \right) + \Delta t \tag{5.4}$$

In matrix form this is:
$$r = G \cdot \Delta x \tag{5.5}$$

G is the matrix of partial derivatives and Δx is the correction vector. Due to the source time correction term, the last column of this matrix is always 1. The partial derivatives of one component of Eq. 5.3 is:

$$\frac{\partial t_i}{\partial x} = \frac{(x - x_i)}{v} \cdot \frac{1}{\sqrt{(x - x_i)^2 + (y - y_i)^2}} \tag{5.6}$$

To calculate the correction vector, Eq. 5.5 is solved via matrix inversion, e.g. by calculating the Moore-Penrose generalized matrix inverse:

$$\Delta x = (G^T G)^{-1} \, G^T r \tag{5.7}$$

If more than four sensors are used, this procedure is repeated and the correction vector is minimized iteratively. Convergence criteria can be set for terminating the iteration when a particular desired accuracy has been reached, or if the procedure is diverging. The diagram of the algorithm is represented below in Fig. 5.1, showing how the equations just explained are related.

$$\vec{x} = \{x, y, t_0\}$$

$$\vec{r} = t^{\vec{m}} - t^{\vec{c}} \qquad \xrightarrow{\text{if } r \leq N} \qquad \vec{x} = \{x, y, t\} \text{ epicenter}$$

$$\text{if } r > N$$

$$G = \begin{bmatrix} \frac{(x-x_1)}{v} \cdot \frac{1}{\sqrt{(x-x_1)^2+(y-y_1)^2}} & \frac{(y-y_1)}{v} \cdot \frac{1}{\sqrt{(x-x_1)^2+(y-y_1)^2}} & 1 \\ \frac{(x-x_2)}{v} \cdot \frac{1}{\sqrt{(x-x_2)^2+(y-y_2)^2}} & \frac{(y-y_2)}{v} \cdot \frac{1}{\sqrt{(x-x_2)^2+(y-y_2)^2}} & 1 \\ \vdots & \vdots & \vdots \\ \frac{(x-x_4)}{v} \cdot \frac{1}{\sqrt{(x-x_4)^2+(y-y_4)^2}} & \frac{(y-y_4)}{v} \cdot \frac{1}{\sqrt{(x-x_4)^2+(y-y_4)^2}} & 1 \end{bmatrix}$$

$$\Delta x = (G^T G)^{-1} \, G^T r$$

$$\vec{x} = \vec{x} + \vec{\Delta x}$$
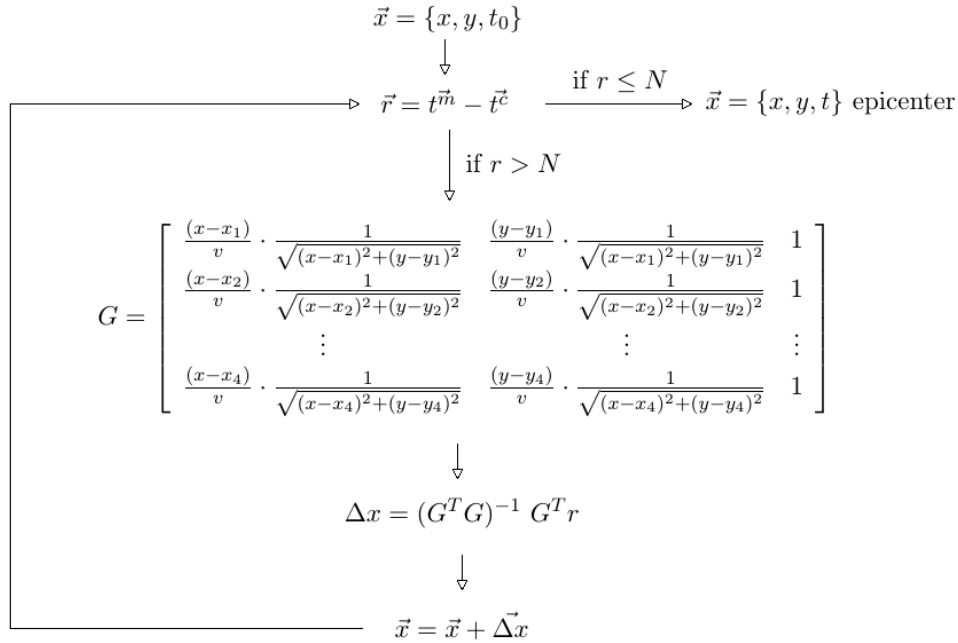
Figure 5.1: Software algorithm scheme for localization

5.1.2   Localization Algorithm Validation

Once has been written the Matlab code just explained, it is needed to check that it works correctly. Some data of the tests made previously with the lead pencil break were taken: the arrival times of the recorded data by the Vallen Systeme have been provided at the entrance to the Matlab code. For the same input (arrival time and sensors position), the

acoustic sources calculated by Matlab are compared with those of Vallen. In this way it can be possible quantify the difference error between the two algorithms and validate this location code written independently.

Fig. 5.2 shows one of the tests performed with the lead pencil break, with points located by Vallen and the same but localized by the Matlab code: the points are almost coincident.
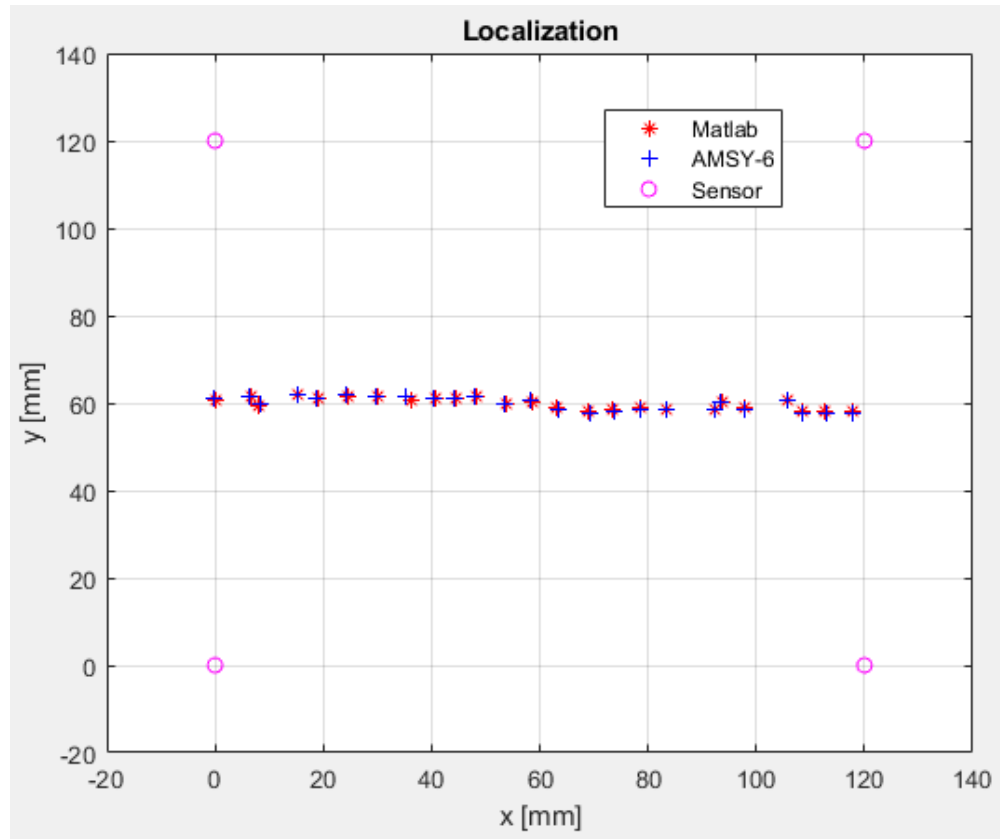
Figure 5.2: Comparison of points located by Vallen and the Matlab algorithm

As can be seen from the Tab. 5.1, the mean difference of error between the two methods is $0.1\,mm$. It is very low and can be considered negligible compared to other factors that have much greater incidence on the error (a few tens of millimeters), as will be seen below. The localization error of the Matlab is slightly lower: probably the constraint on the residue to exit the iteration cycle is lower than that of the Vallen. It can therefore, consider this localization algorithm reliable and equivalent, like the one used by the Vallen Systeme.

Localization Error	Vallen Systeme	Matlab algorithm
μ [mm]	2.22	2.12
σ [mm]	1.49	1.53

Table 5.1: Error Localization μ, Vallen Systeme compared with Matlab algorithm

5.2 Methods for Acquiring the Arrival Time

Understanding the exact moment when the acoustic wave reaches the sensor is not easy. In the Vallen Systeme, the fixed threshold method is easy to use but has a low flexibility. If the threshold is too low, some oscillations of the background noise could be recognized by the software as arrival time. On the other hand, if the threshold is too high, differences in time dt between the various sensors compared to the real arrival time can be accumulated. In both cases, the arrival time is not the correct one and could be improved.

Precisely because the propagation of a fatigue crack is not a repeatable and constant phenomenon, it is difficult to choose an optimal threshold value. A certain threshold may be fine for some signals and not for others. These reasonings, born observing signal by signal, have prompted us to investigate alternative methods to that of the fixed threshold, to understand how the accuracy of the localization changes and whether it can be improved, Cf. [2].

5.2.1 AIC picking

The AIC (*Akaike Information Criterion*) function, as used in Cf. [10] and for an AE test on a concrete specimen and in Cf. [7], is a method for identifying the arrival time of the p-waves.

AIC window was defined and positioned symmetrically around ariival time t_a of Vallen Systeme. The AIC values for the signal within this window were subsequently determined according to

$$AIC(k) = k \cdot log(Var(x[1,k])) + (n-k-1) \cdot log(Var(x[k+1,n])) \quad (5.8)$$

In Eq. 5.8 n denotes the width of the AIC window and k denotes a point inside the AIC window ($1 \leq k \leq n$). The time corresponding to the lowest point of the resulting AIC value graph was selected as the final arrival time of the p-wave denoted as t_a. For the recorded signal visualized in Fig. 5.3 (a), t_a is very likely a satisfactory estimation of the real arrival time of the p-wave.

In order to estimate the accuracy of t_a, two criteria were used. The first criterion included verifying the signal-to-noise ratio S/N. Generally, for acoustic emissions the ratio was required to be $S/N > 20$. The artificial pencil lead breaks generate loud and clear AE signals. Therefore, a highervalue can be adopted, such as $S/N > 50$. In any case, this filter has already been applied previously for all registered signals.

The second criterion concerned the shape of the AIC-value graph. The picked arrival time was expected to be an accurate estimation of the actual arrival time of the p-wave if the lowest point of the AIC-value graph (almost) coincided with the first low point of the graph. If that was the case, the AIC picking result was denoted as *good*, like for the example visualized in Fig. 5.3 (a).

If the two points did not coincide, it was checked whether the time difference between the first low point and the lowest point of the AIC-value graph was less than $50\,\mu s$. Additionally, it was confirmed that the difference in the AIC value between the first high point and the first low point was no greater than $1/50$ of the difference between the lowest and the highest determined AIC value. In that case, the AIC picking result was denoted as *okay*, like for the example visualized in Fig. 5.3 (b). In an *okay* result, the determined arrival time t_a still represents a reasonable estimation of the p-wave arrival time, but is most probably less accurate than that of a *good* AIC picking result.

If the AIC picking result did not fulfill the two mentioned criteria it was denoted as *bad*, as for the example visualized in Fig. 5.3 (c).

A transient recorded (green line) belonging to an acoustic event of fatigue test, is shown in the Fig. 5.4 below. The Vallen systeme assumes as arrival time t_a when the signal amplitude exceeds $1\,mV$ and that corresponds to $40\,\mu s$ in the image. The AIC function (blue line) is calculated symmetrically with respect to this time instant of $40\,\mu s$. The red line is a vertical line positioned in the minimum of the AIC function and highlights, compared to the recorded transient, where the new arrival time $t_{a,AIC}$ is assumed. The S/N ratio values and the shapes of the AIC function are *good* for the signal: this means that the coordinates of the acoustic source using the arrival times calculated through the AIC function is reliable. In
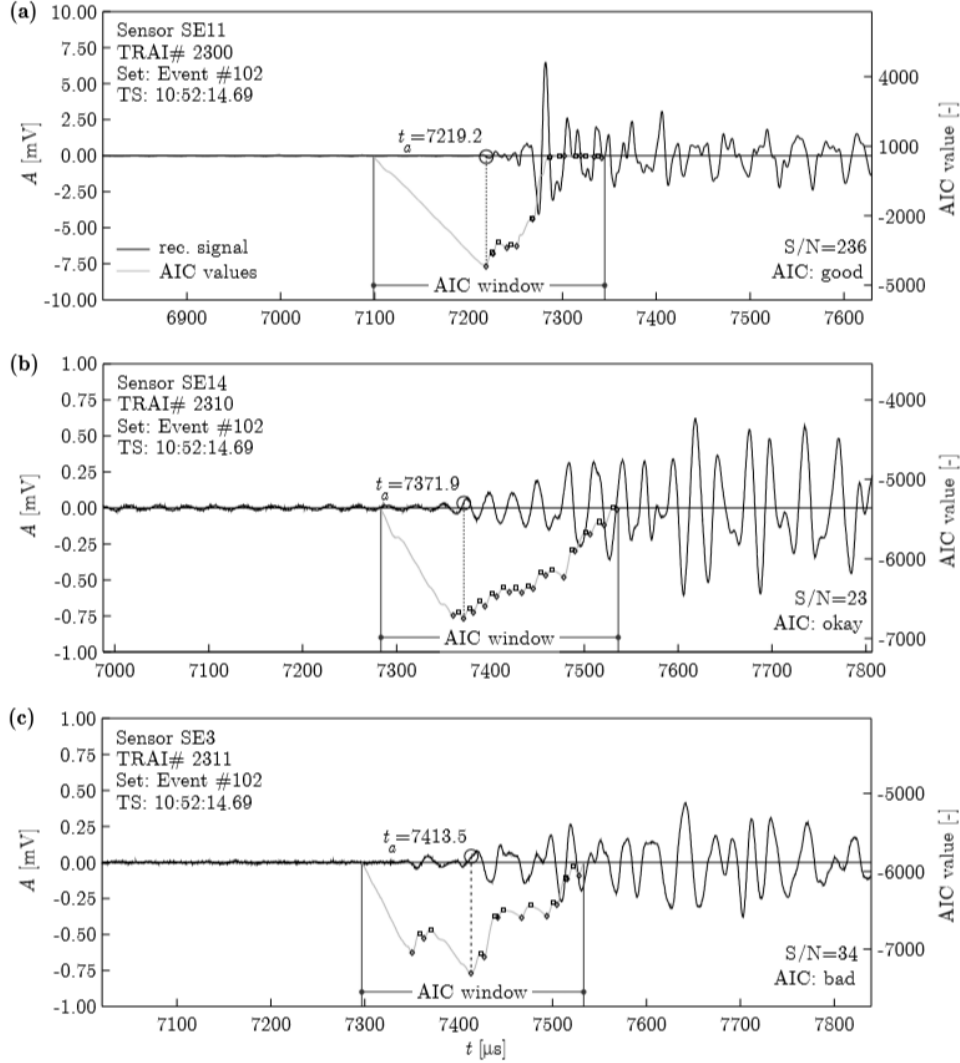
Figure 5.3: Visualization of three recorded wave signals. (a) Signal with per-
missible S/N ratio and verified *good* AIC-picking result; (b) signal
with AIC-picking result verified as *okay*. The global low point is
not the first low point but the two low points do not differ by much.
The S/N ratio is impermissibly low. (c) Signal with AIC-picking
result verified as *bad*. The global low point is not the first low
point, and the two low points differ too much. The S/N ratio is
impermissibly low

the AIC function method, a threshold value is not assigned for the arrival time, but is determined by the minimum of the AIC function.
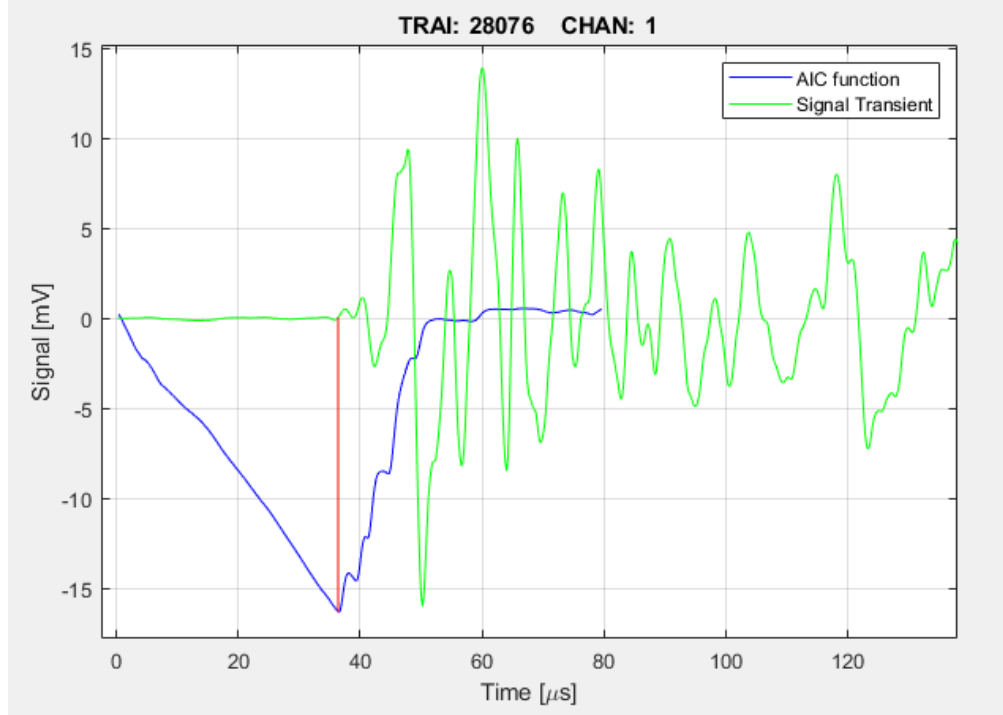
Figure 5.4: AIC function calculated for a recording of an acoustic event

5.2.2 Ranking of Arrival Time

The determined arrival times were ranked with respect to their AIC-function shape. Firstly, signals with S/N ratio less than 20 have been excluded, as to be considered as noise. In fact, signals that have low max amplitude compared to background noise, are not indicative of implusive phenomena such as acoustic emission. Signals which did not fulfill this criteria have been excluded from the source localization process and therefore not included in the ranking.

In addition, signals have also been ranked based on the shape of their AIC function. Arrival times with an *okay* AIC-based arrival-time picking result were always ranked behind arrival times with a *good* and ahead *bad* AIC-based arrival-time picking result. Each localized point is composed by at least three signals.

For each signal recorded by a sensor, a score from 0 (worst) to 1 (best) is assigned based on the form of its AIC-function:

- Score = 1 if the AIC function shape is classified as *good*

- Score = 0.5 if the AIC function shape is classified as *okay*

- Score = 0 if the AIC function shape is classified as *bad*

The final ranking of a localized point is defined as the average of the scores of the individual signals recorded by each sensor. This number is translated into a chromatic scale: blue means low score, so the point has been located but it is not very reliable since the AIC function has hardly identified the arrival time. Green means that the score is high, the acoustic source has produced impulsive signals (burst), the localized position is reliable.

Furthermore, if all four sensors have recorded a signal of the same acoustic event, the point located in the graph is larger. Therefore the location should be more reliable than points with a smaller diameter, which means that only three sensors of four, have recorded the event. Fig. 5.5 shows the location using the AIC function to determine the arrival time and results of localization are summarized in Tab. 5.2.

Parameter	AIC results
μ $[mm]$	53.05
σ $[mm]$	115.5

Table 5.2: Localization accurcy with AIC-function

Fig. 5.6 shows the error distribution with AIC-function.

The location with the AIC-function is not precise, especially in the second cell (on the right), points do not reflect the path of the crack at all. In fact, almost all the points in the last part are blue, which means that they are very unreliable. Instead in the first cell, there are many more green points that are associated enough with the crack path.

This happens because AIC-function works with the p-waves, which are the first acoustic waves that reach the sensor but also those with less amplitude. Probably in the first cell, where the propagation is stable and there is little actuator stroke, the background noise is quite low and the p-waves can still be detected, but with little precision. In the second cell, however, propagation is unstable, where large movements produce more noise. This reaches a higher intensity, such as to cover p-waves and making their detection impossible.
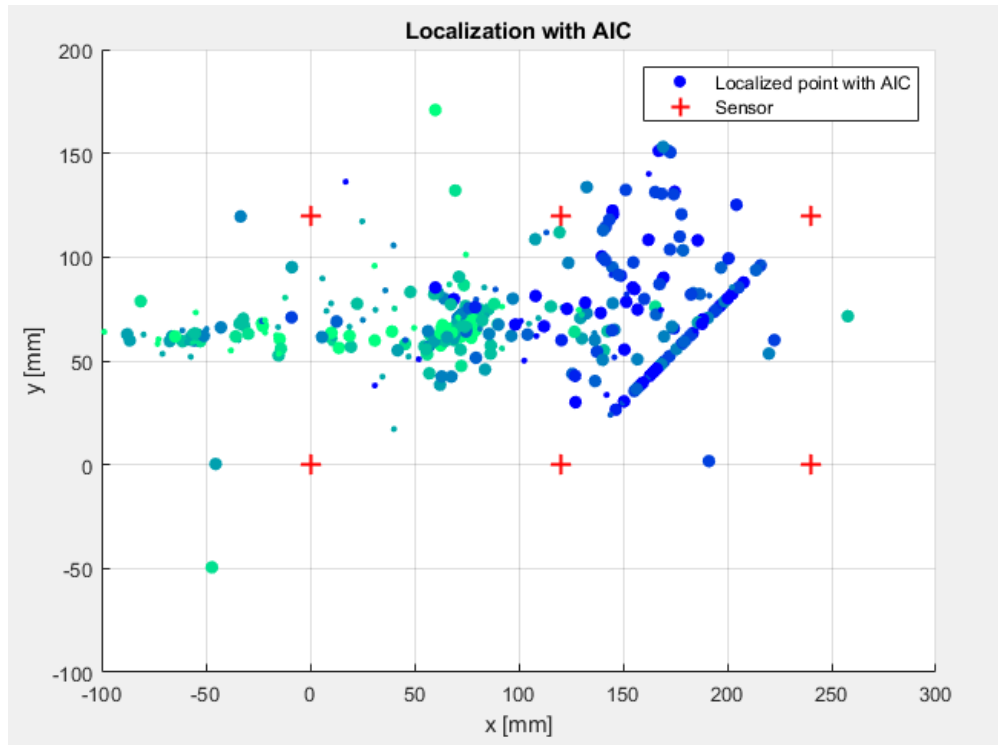
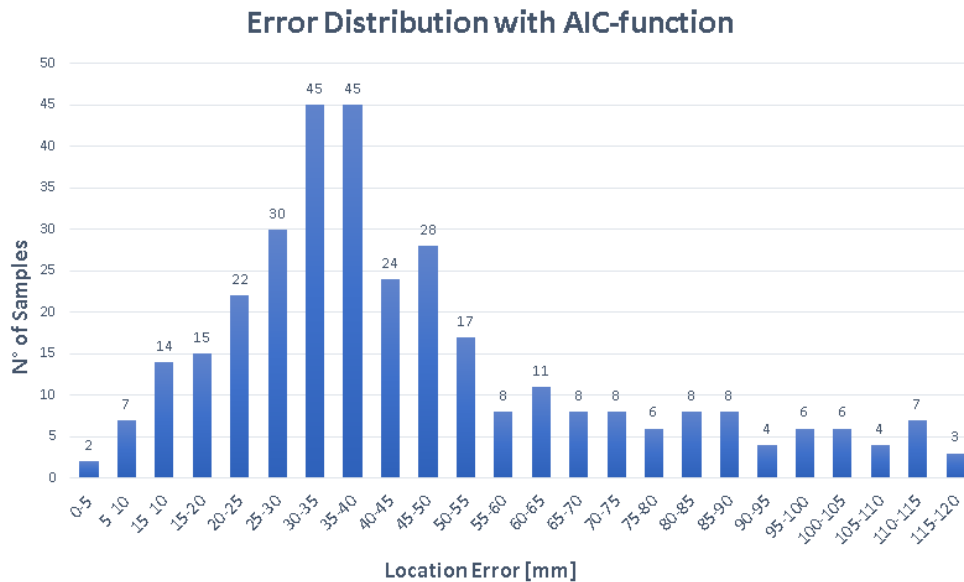**Figure 5.5:** Localization of crack tip calculated with AIC function

Figure 5.6: Error distribution with AIC function

However this method, unlike all the others, is able to independently provide us an estimate of the accuracy through the signal ranking, translated into chromatic scale. We know that blue points have a low ranking value and should not be taken into account because they are calculated with little certainty. We remake the location analysis using an additional filter: only points whose ranking is> 0.75 (i.e. light green points). The results is shown in Fig. 5.7, is the same on the graph before, selecting pionts with high ranking. In Tab. 5.3 are shown the relative results.

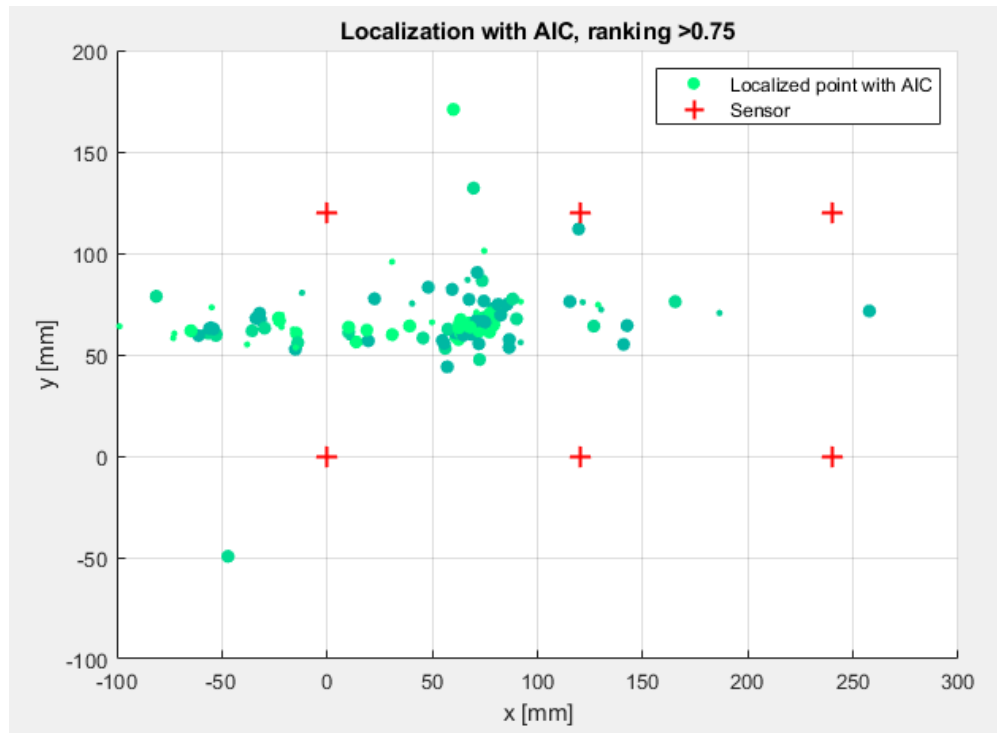**Figure 5.7:** Localization of crack tip calculated with AIC function with $ranking > 0.77$

Parameter	AIC results, ranking>0.75
$\mu \; [mm]$	50.2
$\sigma \; [mm]$	33.4

Table 5.3: Localization accurcy with AIC-function

Localization improves only slightly. In the second cell there is almost no point, which means that the AIC-function is not able to locate points

in the unstable propagation zone. In any case, also in the first cell the accuracy is almost worse than that provided by the Vallen Systeme (set to use the s-waves). It is deduced that locating using p-waves is wrong, or in any case not suitable for our case, because they are too difficult to detect due to noise.

Two other simpler but effective methods have been developed that use s-waves. The following are now illustrated.

5.2.3 Threshold Adapted to Maximun Amplitude Signal

Another method of identifying the arrival time is to exploit the maximum amplitude of the signal. So, set the threshold at a value calculated as a fraction of the maximum amplitude signal, as in Fig. 5.8. In this case, the arrival time is not at low signal values, similar to noise, but far from it. It is looked for the moment when a packet of waves arrives and causes a strong alteration of the signal. In this case, the arrival time is no longer calculated with the acoustic waves S0 (p-waves), but with the A0 (s-waves). Therefore, it has been used the speed of sound of the s-waves, which is $3012\,m/s$.

Before proceeding with the calculation, it is necessary to understand what is the optimal value of the threshold, 20%, 30%, 40%...of the maximum amplitude signal? So data have been analyzed with different threshold values and the localization has been calculated.

Fig. 5.9 shows how the localization error varies with different threshold values. For threshold values that are too high, the arrival time is taken too late compared to the real arrival of the s-waves. Time lag dt are formed which affect the accuracy of localization. Too low threshold values, on the other hand, interfere with the p-waves or noise, anticipating the arrival time of the s-waves. The graph shows that the optimal value is 0.05, so 5% of the maximum amplitude signal value. Once the optimal threshold value has been identified, this will be used to calculate the location of acoustic events.

Once found the optimal value, it has been calculated the location with a threshold set on 5% of maximum signal amplitude. Fig. 5.10 shows the location using a 5% of maximum signal amplitude to determine the arrival time and results of localization are summarized in Tab. 5.4.
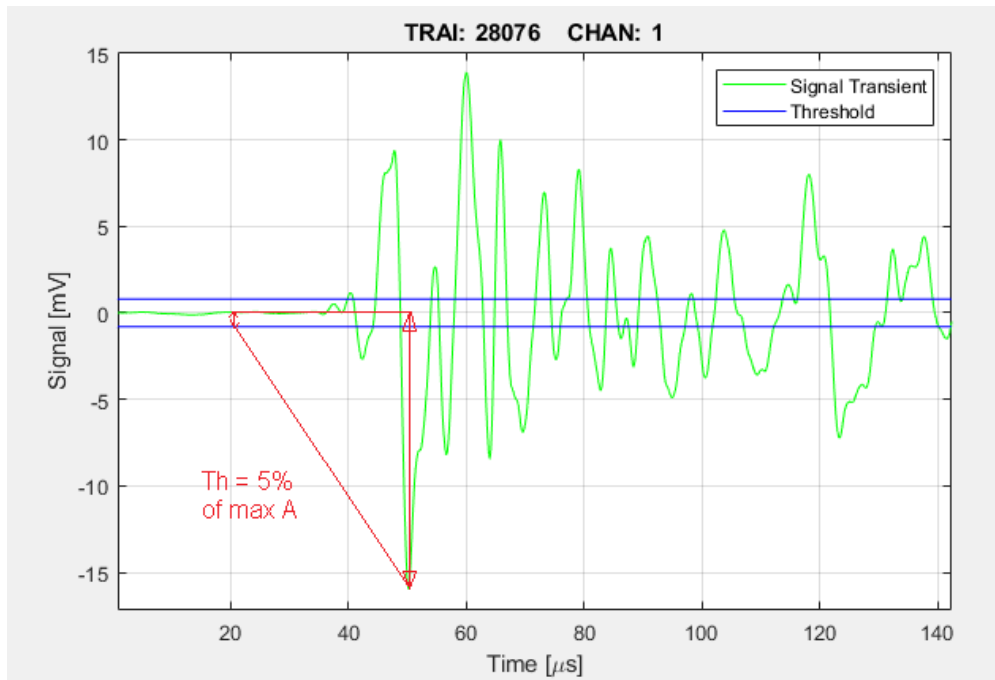
Figure 5.8: Threshold calculated as 5% of max amplitude signal on the four recordings of an acoustic event
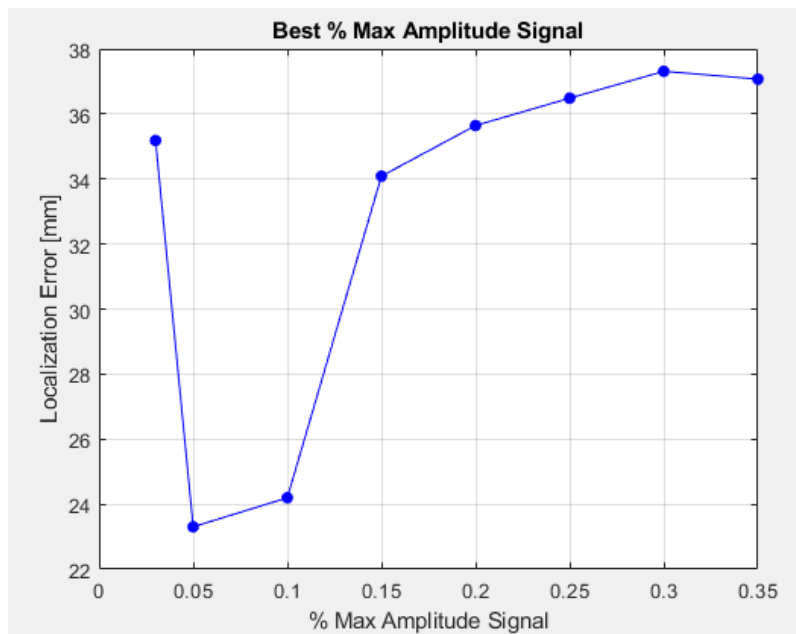
Figure 5.9: Localization accuracy with different threshold values
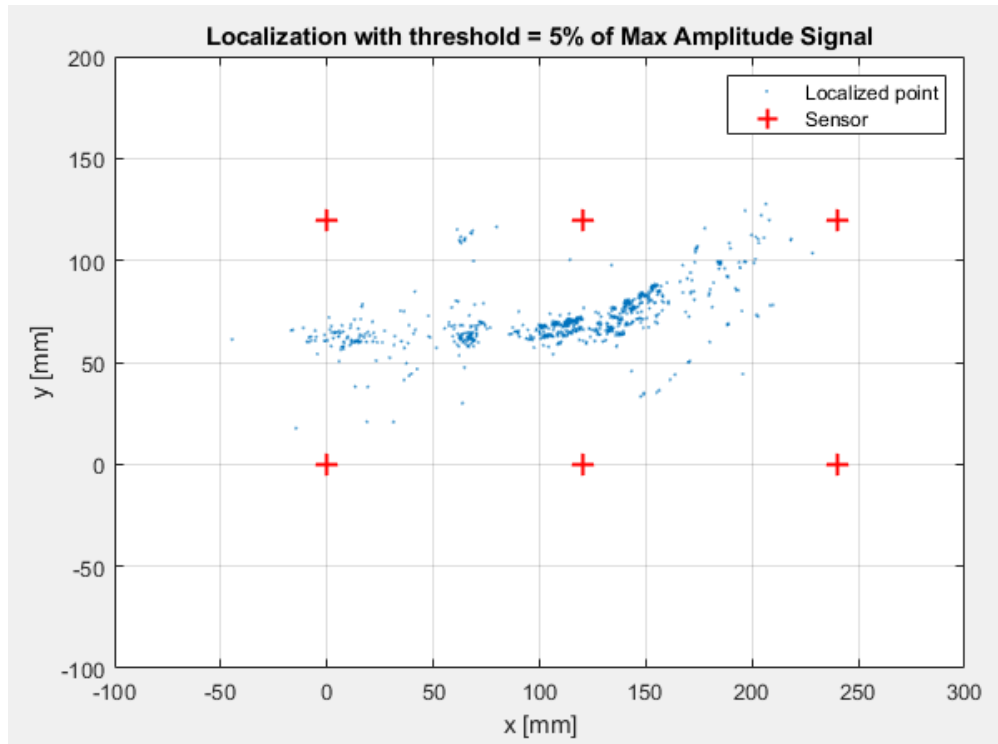
Figure 5.10: Localization accuracy with a threshold equal to 5% of maximum signal amplitude

Parameter	threshold = 5% max signal Amp.
μ $[mm]$	23.3
σ $[mm]$	16.3

Table 5.4: Localization accurcy with a threshold equal to 5% of maximum signal amplitude

Fig. 5.11 shows the error distribution with a threshold equal to 5% of maximum signal amplitude.
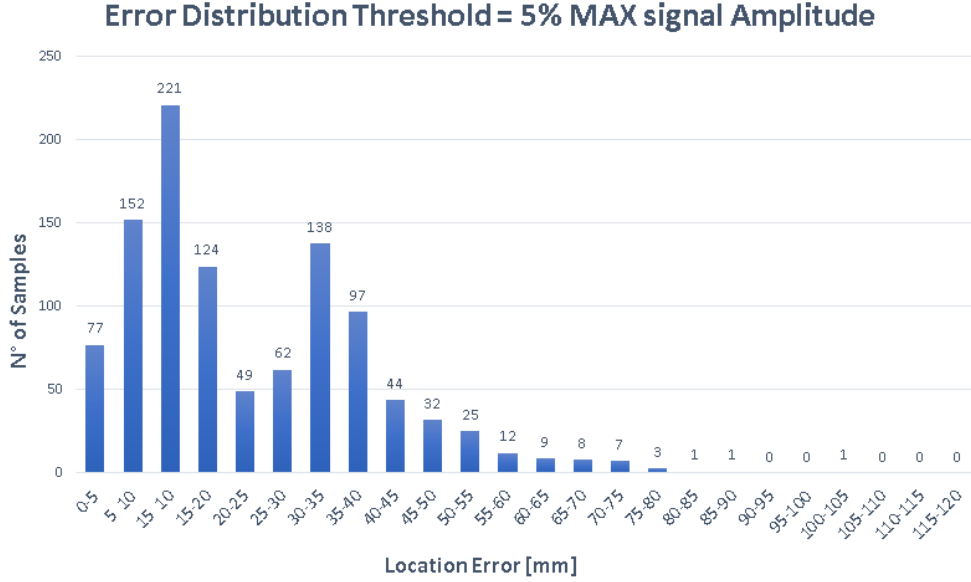
Figure 5.11: Error distribution with a threshold equal to 5% of maximum signal amplitude

The location is better than Vallen. There are fewer points (most of them due to the filter $S/N > 20$), but they are much more reliable and precise. The localized points faithfully reproduce the path of the crack. They are not distributed homogeneously, but it does not necessarily mean that: the production of acoustic waves is not necessarily a constant phenomenon over time, both in terms of periodicity and in the signal shape. Points obtained with a threshold set in this way are reliable. This is demonstrated by the graph of the error distribution which is concentrated on low values and statistical parameters.

5.2.4   Threshold Set on a Fixed Value

Another method that can be used is the one adopted by the Vallen Systeme: set the threshold to a fixed value for all the signals. Unfortunately, Vallen uses the acquisition threshold to record a transient signal also as a threshold to calculate the arrival time and then the location. In this way,

the threshold must obviously be set before run the test. So, it is difficult to know what the background noise intensity will be and what is the optimal value to set the threshold.

Instead, once the signals have been acquired, it is possible in Matlab to set the threshold after the acquisition, to identify the arrival time from which then calculate the location. Also in this case, as in Vallen, it works with the s-waves, and therefore, the set sound speed must be that relative to this type of waves: 3012 m/s. Fig. 5.12 shows how the threshold is independent of the signal and is the same for everyone.
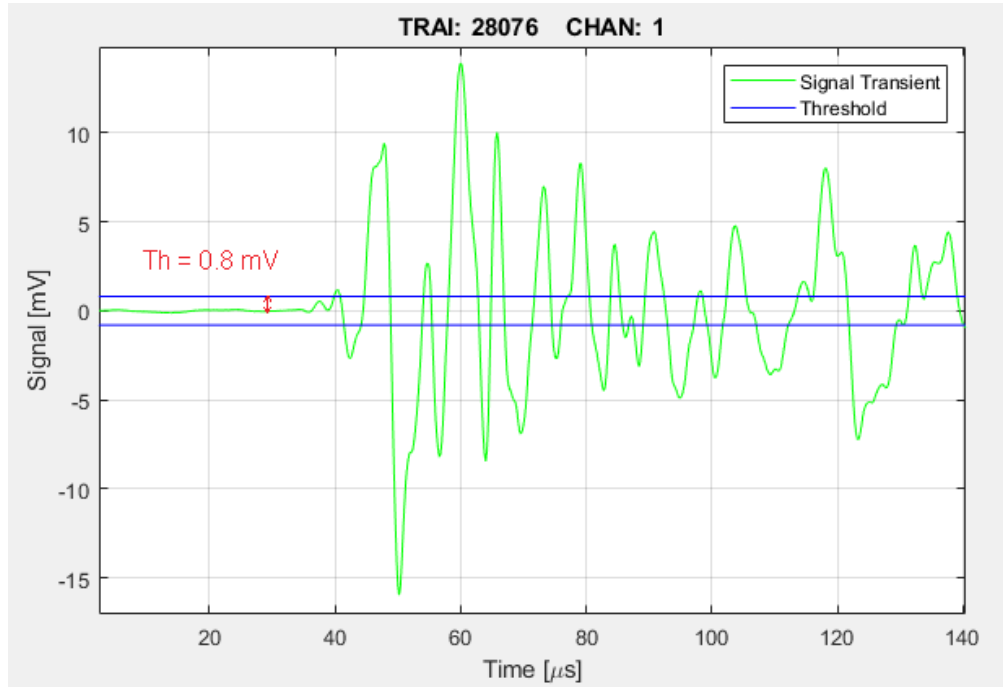
Figure 5.12: Threshold set on fixed value for all recordings of an acoustic event

Also in this case, it should be asked at what value set the threshold, 0.6 mV, 1 mV, 1.2 mV...? Therefore, the location has been calculated with different threshold values to find the optimal one. Fig. 5.13 shows that the best threshold is 0.6 mV. Once the optimal threshold has been found, the location can be calculated with a threshold equal to 0.6 mV, as in Fig.5.14. The relative results are reported in Tab. 5.5. Fig. 5.15 shows the error distribution with a threshold equal to 0.6 mV.

Also in this way the localization is better than that of Vallen. However, this is the same method used by Vallen Systeme . It means that setting
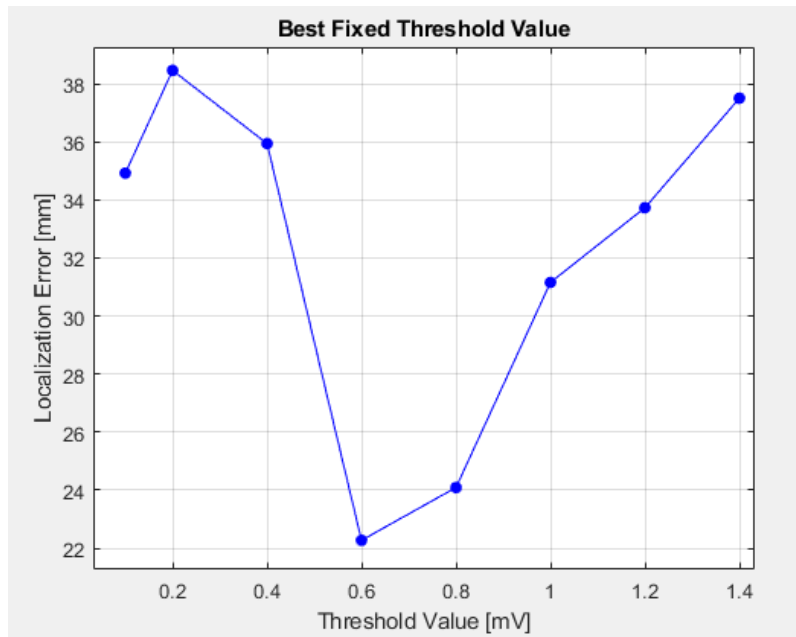
Figure 5.13: Localization accuracy with different threshold values

Parameter	threshold = 0.6 mV
μ [mm]	22.2
σ [mm]	22.1

Table 5.5: Localization accurcy with a threshold set on 0.6 mV

Figure 5.14: Localization accuracy with a threshold equal to 0.6 mV

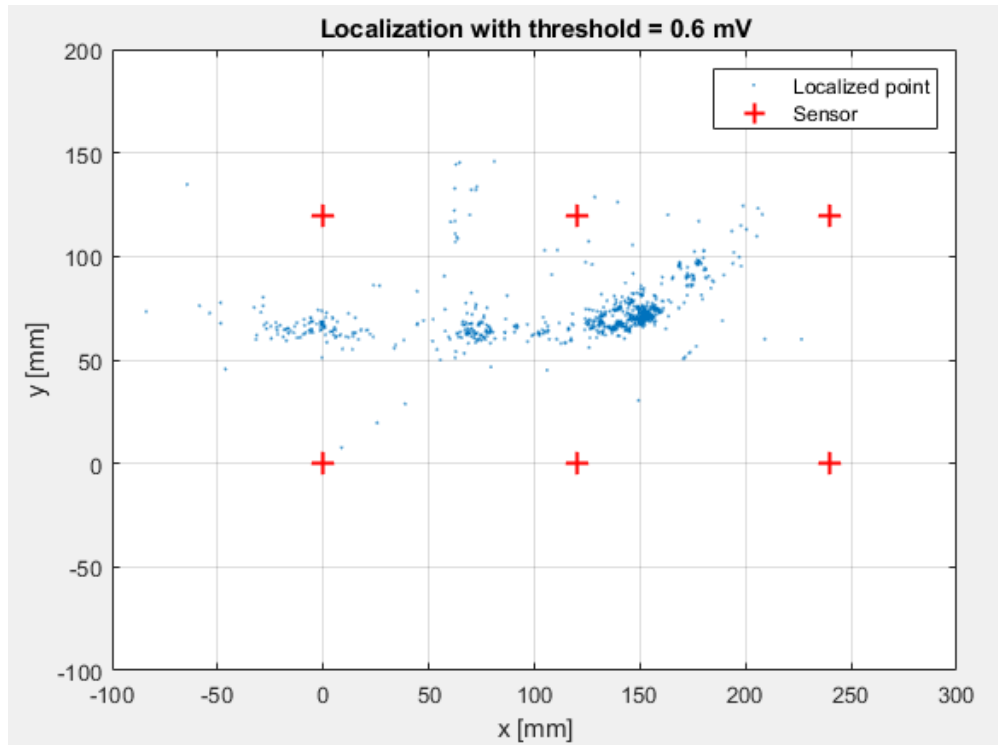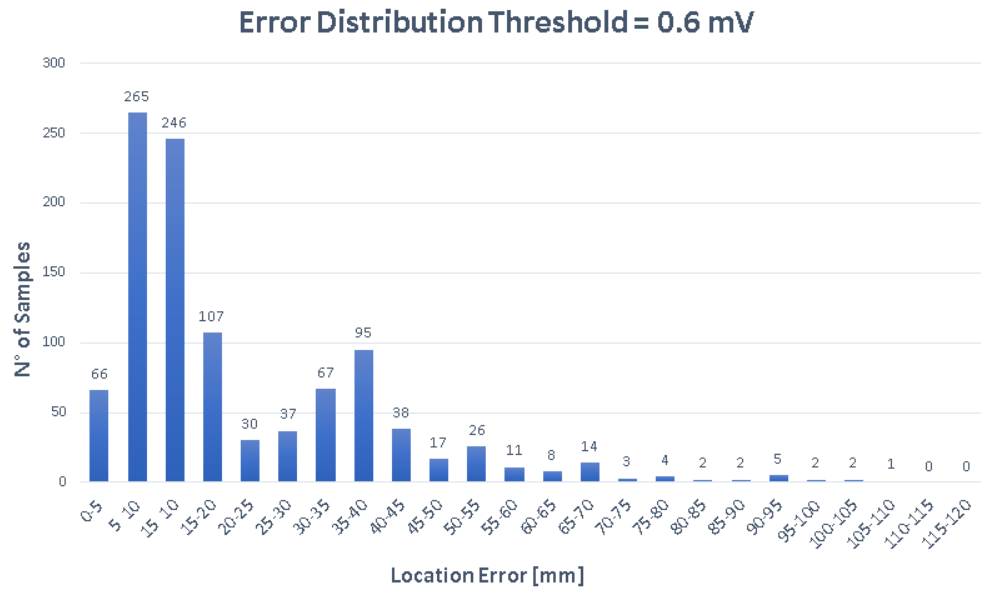**Figure 5.15:** Error distribution with a threshold equal to 0.6 mV

the Vallen with an optimal threshold value (which was possible to calculate only after the test), and with further filters inserted in Matlab (i.e. $S/N > 20$), a similar result could be obtained. The localized points closely follow the path of the crack and the graph of the error distribution also indicates good accuracy.

5.3   Comments on the Results

The location provided by the Vallen is not bad, because the points clearly reproduce the path of the crack. However, there are many points that have a considerable error and therefore, even if it is clear at the macroscopic level the area where the crack tip is, the localized points can have a poor reliability and the accuracy of localization is too low.

The AIC-method is the one that gives the worst results. This method is very elaborate and is not based on the value of a threshold, but depends on the signal shape. In theory, it should be the most precise method, because it recognizes the moment when an acoustic wave arrives with respect to the noise, regardless of the signal intenisty. Initially, after implementing it in Matlab, it had been tested on the signals produced by the lead pencil break and located them precisely. This is because the signals simulated with the pencil are more impulsive and much cleaner from noise. Also the Vallen located precisely, in this case. However, this strong point is at the same time its weak point. If the background noise is too high, it covers the p-waves signal, making it impossible to recognize the arrival time. The AIC-function is a good algorithm for identifying the arrival time, but not in our case, and therefore it must be discarded as a method.

The other two methods, the one with the threshold set on a fixed value and the one as a fraction of the maximum amplitude, provide good results in localization. Both work with the s-waves (A0) which are slower but have greater amplitude, and therefore it is easier to identify the arrival time of this type of acoustic waves. The results of both methods are satisfactory.

During the test progress, it was noted that many localized points were shifted to the left with respect to the sensors, especially those of the first cell. Going to analyze the data point by point, we have realized that sometimes two or three points had been located at the same number of

cycles of the test. This means that these points have been localized with signals belonging to the same acoustic event. Some of these "multiple" points had just this characteristic of being moved to the left. The most likely explanation for this phenomenon is due to the rebound of the acoustic waves on the edge, in particular on the notch, which are reflected and trigger the threshold on the sensors (i.e. four yellow signals in the figure), as in Fig. 5.16. Moreover signals from different reflections could be associated by the software as belonging to the same event causing localization to fail (i.e. in the figure two red and two yellow signals)
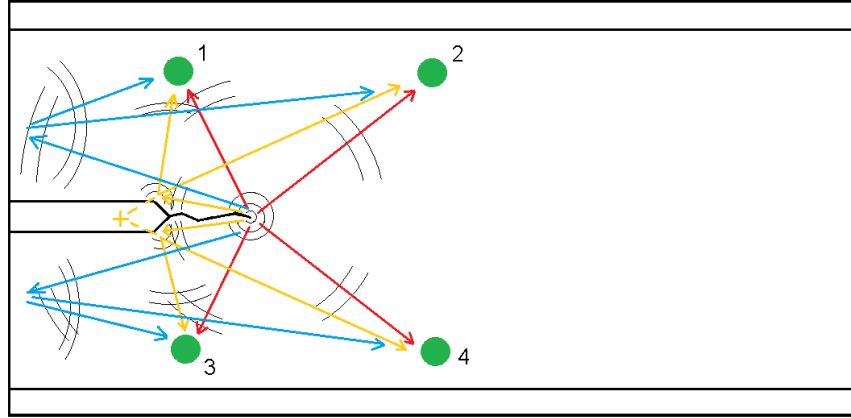
Figure 5.16: Possible acoustic waves reflections

These points constitute false indications that are probably not due to real acoustic sources but simply to reflection on a geometric constraints. This also explains the fact that this phenomenon was not present during the tests on the HEM200 with the lead pencil break: the notch had not yet been made. As the crack moves away from this, towards the right cell, this phenomenon becomes less pronounced. Furthermore, it is much more evident in the Vallen localization graph (Fig 4.28 and Fig. 4.29), and not in those of the other methods, probably due to the $S/N > 20$ filter: acoustic waves refected could lose intensity and not exceed the value of this filter, coming thus excluded from the analysis. This phenomenon cannot be eliminated, we only need to understand problems of edge like this and be able to identify them, so as not to give importance to these false indications.

Chapter 6

Conclusions and Future Developments

The position of a fatigue crack tip, that propagates along the core of a steel beam, has been monitored. The most suitable SHM method for this case is Acoustic Emission. The objective was to locate its position in real time, through a network of PZT sensors applied to the surface of the beam.

Initially, tests were carried out on an aluminum plate to find the best number and distance of the sensors. Once the best sensor layout to optimize localization was identified, the specimen was chosen. Respecting the constraints given, the specimen used for the test is an H-section beam in carbon steel externally galvanized, with a core thickness of 15 mm. It has been made similar to a compact specimen for only traction loads. The fatigue test and its setup has been designed and the specimen was then prepared and sensorized.

The acoustic waves emitted from the crack tip during propagation are recorded by the sensors and collected by the acquisition unit. Knowing the flight times and the position of the sensors, and triangulating signals, the coordinates of the acoustic source can be calculated. During the test, the crack was inspected several times with Magnetic Testing to have certain information on the position of the crack, to be compared with the AE data. The data provided by Vallen are not very accurate. Therefore, several methods were sought during post processing to improve localization. An algorithm has been implemented in Matlab to manage localization and different methods for acquiring the arrival time of acoustic waves.

Threshold set at fixed value and threshold set as fraction of maximum signal amplitude, are the only methods which provided satisfactory local-

ization accuracy of the crack tip. AIC function method does not work, or at least not in our specific case. Vallen localization can be improved but still remains difficult to manage and requires operator experience. Instead with post processing, we have the possibility to do more data analysis, looking for optimal values.

In Tab 6.1 are summarized localization results of different methods.

Location Method	μ [mm]	σ [mm]
Vallen	52.1	34.1
AIC	53.0	36.8
Th= 5% max Amp.	23.3	16.3
Th = 0.6 mV	22.2	22.1

Table 6.1: Localization accuracy of different methods

6.1   Further Improvements

Other tests must be carried out to validate the results and confirm our deductions. We could already set the value of the Vallen threshold to 0.6 mV to see if it actually improves localization. Forces and setup are correct; some precautions could be adopted to reduce the friction in the pin and prevent the crack path from bending upwards, as in the second cell.

A clustering analysis could help a lot to decrease the dispersion of the data and therefore the variance. The filters we set on energy, duration, rise time and S/N eliminate most of the signals due to noise, but few disturbing signals may still be present. Clustering analyzes all signals via neural networks, identifying which signals are related to each other and with which waveforms parameters, Cf. [2]. In this way the signals that would be analyzed would be only those effectively due to a crack. Signal filtering, like ours, is effective but cannot be as precise as clustering analysis.

Another interesting point could be to repeat the test but with different types of PZT sensors. The model used is the VS150-M, which are characterized by a specific resonance curve for detection of acoustic events produced by cracks in metal structures. They have 150 kHz resonance, flattening signals with frequency out of the 100-300 kHz range. There are other types of PZT sensors that Vallen supplies, with different resonance curves.
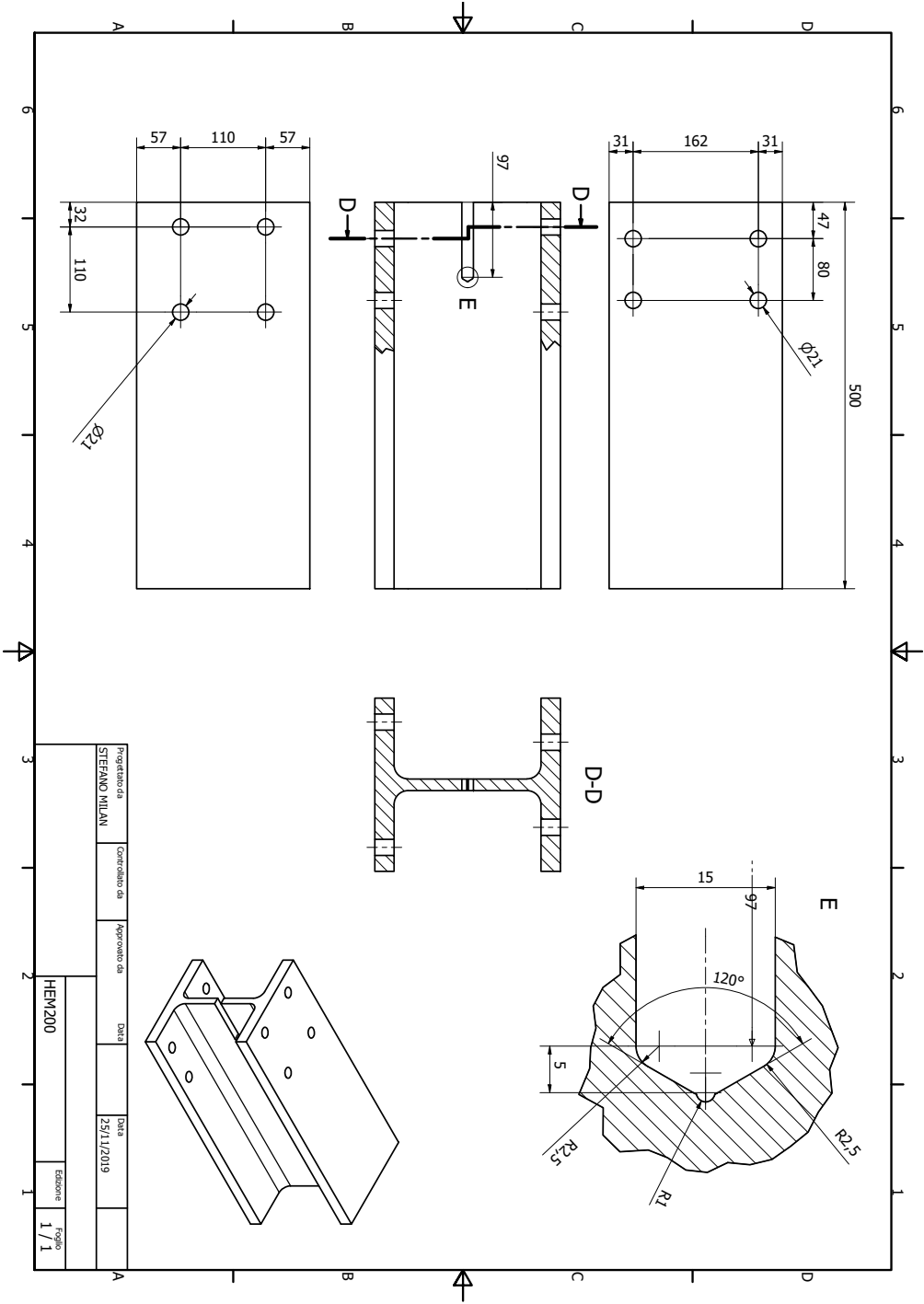
Repeating the test with sensors with different characteristics could help us understand if the resonance flattens perhaps useful signals or effectively cancels only unnecessary signals and noise.

As has been shown with the lead pencil break, acoustic emission monitoring can reach high levels of precision. However, in a real test, and especially in-field environment, many disturbance phenomena are present and make its use difficult. Although we have managed to achieve satisfactory results, much remains to be understood and worked on, to improve this technology. Nowadays, monitoring with AE remains a support tool for NDT methods, whose level of precision and reliability has not yet been achieved, and therefore cannot be replaced yet.

Appendix A

Technical Drawings of Test Setup

Technical drawings of the components designed for the fatigue test are shown below. The *Assembly* indicates how the various parts were assembled and the types of joints that bind the components together.

57 110 57

32

110

Ø21

97

D–D

D

E

D

31 162 31

47

80

500

Ø21

15

97

120°

5

R2,5

R2,5

R1

E

Progettato da
STEFANO MILAN

Controllato da

Approvato da

Data

HEM200

Data
25/11/2019

Edizione

Foglio
1 / 1

300

184,2

110

A

300

184,2

110

A-A

A

M 20

M 24

30

Progettato da
MILAN STEFANO

Controllato da

Approvato da

Data

Data
25/11/2019

PLATE 1

Edizione

Foglio
1 / 1

A-A

230

150

54

230

80

150

20

30

Ø34
Ø21
Ø21
Ø21

A

A

STEFANO MILAN
Progettato da
Controllato da
Approvato da
Data

PLATE 2

Data
25/11/2019

Edizione

Foglio
1 / 1

60,00

52

A-A

M20

20

80

20

A

A

100

Progettato da
STEFANO MILIAN

Controllato da

Approvato da

Data

Data
25/11/2019

JOINT 249XX.M340

Edizione

Foglio
1 / 1

280

⌀60

Progettato da
STEFANO MILAN

Controllato da

Approvato da

Data

PIN

Data
25/11/2019

Edizione

Foglio
1 / 1

Ø62

Ø70

2

ELENCO PARTI		
ELEMENTO	QTÀ	NUMERO PARTE
1	1	Actuator MTS 244.31
2	2	Plate 1
3	4	M24 - 8.8
4	1	HEM200
5	8	M20 - 8.8
6	4	Joint 249xx.M340
7	1	Pin
8	2	Bushing
9	1	Plate 2
10	4	M20 - 8.8
11	4	M20 - 8.8 socket head
12	4	Nut M20
13	1	HEB300 x 2100

Progettato da
STEFANO MILAN

Controllato da

Approvato da

Data

Assembly View

Data 1/12/2019

Edizione

Foglio 1 / 1

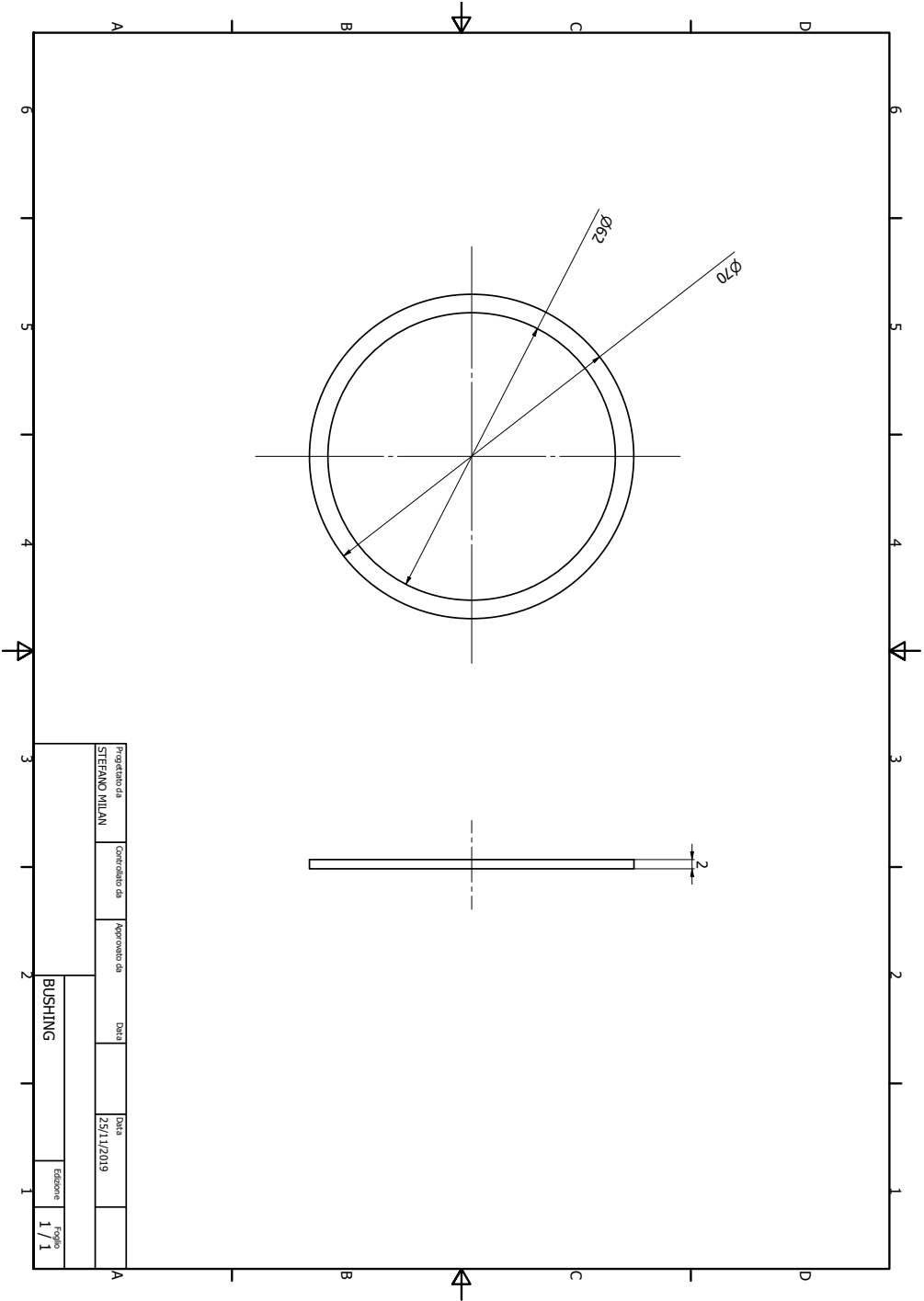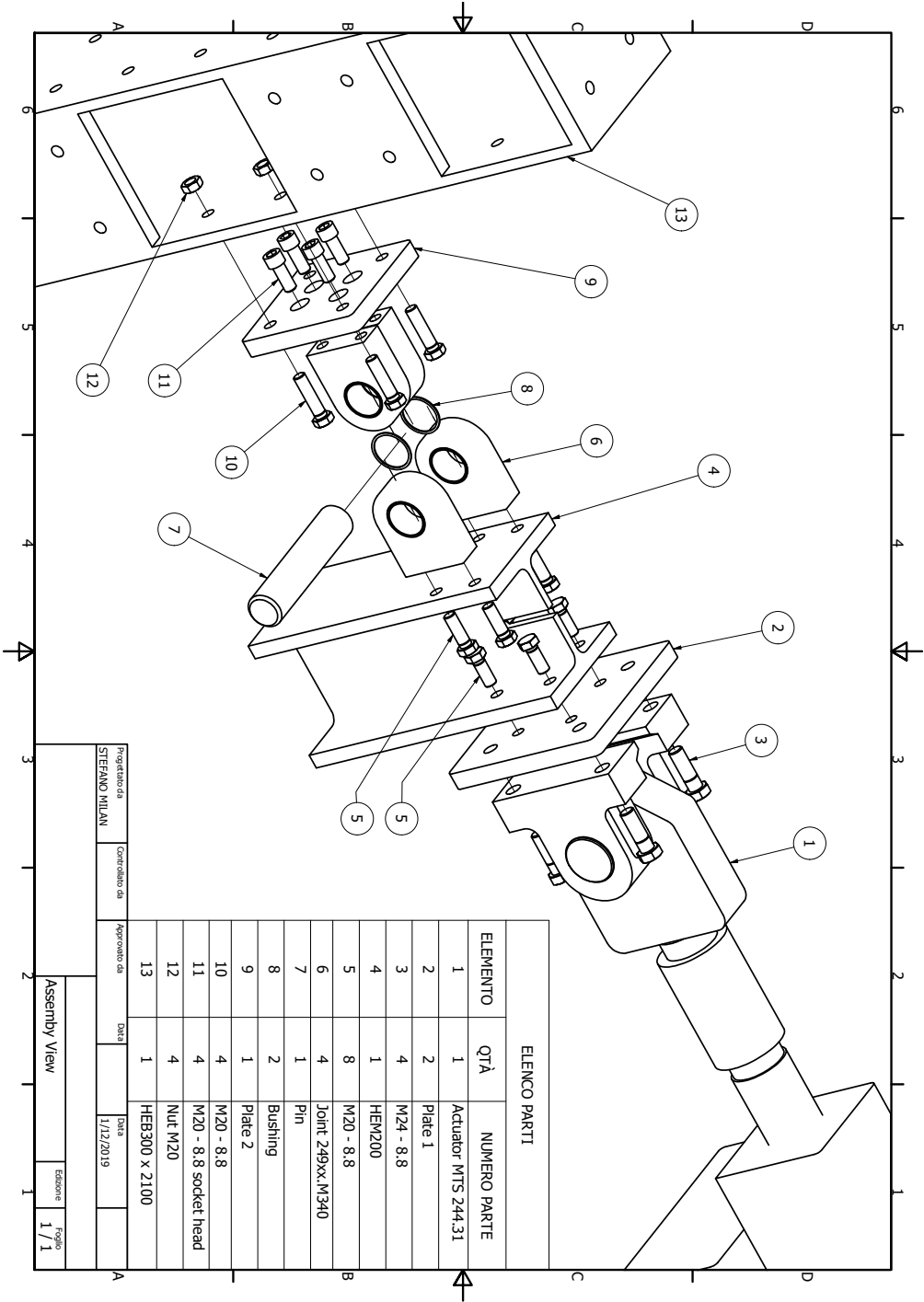# Bibliography

[1] Hiroshi Tada, Paul C. Paris, George R. Irwin. *The stress analysis of cracks handbook.* ASME press New York, 2000.

[2] Sengupta, Sanjay and Datta, Aloke Kumar and Topdar, Pijush. *Structural damage localisation by acoustic emission technique: A state of the art review.* SciELO Brasil, 2015.

[3] Jianguo Yu, Paul Ziehl. *Stable and unstable fatigue prediction for A572 structural steel using acoustic emission.* Journal of constructional steel research, 2012.

[4] Grosse, Christian U and Ohtsu, Masayasu. *Acoustic Emission Testing.* Springer Science & Business Media, 2008.

[5] The Japanese Society for Non-Destructive Inspection. *Practical Acoustic Emission Testing.* Springer.

[6] Chen, Yongguang and Kobayashi, Hisashi. *Signal strength based indoor geolocation.* IEEE, 2002.

[7] Ohtsu, Masayasu. *Acoustic emission and related non-destructive evaluation techniques in the fracture mechanics of concrete: fundamentals and applications.* Woodhead Publishing, 2015.

[8] Luca Martinelli. *Ultrasonic lamb wave detection by coherent fiber optic sensor.* 2016.

[9] Stephens, RI and Lee, SG and Lee, HW. *Constant and variable amplitude fatigue behavior and fracture of A572 steel at 25 C (77 F) and- 45 C (- 50 F).* Springer, 1982.

[10] Gollob, Stephan. *Source localization of acoustic emissions using multisegment paths based on a heterogeneous velocity model in structural concrete.* ETH Zurich, 2017.